Eastward-propagating planetary wave in the polar middle atmosphere

Liang Tang[1], Sheng-Yang Gu[1*], Xian-Kang Dou[1]

[1] Electronic Information School, Wuhan University, Wuhan, China.

*Corresponding author: Sheng-Yang Gu, (gushengyang@whu.edu.cn)

Abstract. We presented the global variations of the eastward propagating wavenumber 1 (E1), 2 (E2), 3 (E3), and 4 (E4) planetary waves (PWs) and their diagnostic results in the polar middle atmosphere, using MERRA-2 temperature and wind datasets in 2019. It is clearly shown that the eastward wave modes exist during winter periods with westward background wind in both hemispheres. The maximum wave amplitudes in the southern hemisphere (SH) are slightly larger and lie lower than those in the northern hemisphere (NH). It is also found that the wave perturbations peak at lower latitudes with smaller amplitude as the wavenumber increases. The period of the E1 mode varies from 3 to 5 days in both hemispheres, while the period of E2 mode is slightly longer in the NH (~48 h) than in the SH (~40 h). The periods of the E3 are ~30 h in both SH and NH, and the period of E4 is ~24 h. Though the wave periods become shorter as the wavenumber increases, their mean phase speeds are relatively stable, which are ~53, ~58, ~55, and ~52 m/s at 70° latitudes for W1, W2, W3, and W4, respectively. The eastward PWs occur earlier with increasing zonal wavenumber, which agrees well with the seasonal variations of the critical layers generated by the background wind~~seasonal variations of the background zonal wind through the generation of critical layers~~. Diagnostic analysis also shows that the mean flow instability in the upper stratosphere and upper mesosphere may both contribute to the amplification of the eastward PWs.

1 Introduction

Large amplitude planetary waves are dominant in the stratosphere, mesosphere, and lower thermosphere region and their interaction with zonal mean winds is the primary driving force of atmospheric dynamics. In addition, sudden stratospheric warmings (SSWs) and quasi-biennial oscillation (QBO) events can dynamically couple the entire atmosphere from the lower atmosphere to the ionosphere ~~(~~(Li et al., 2020; Yamazaki et al., 2020; Yadav et al., 2019; Matthias and Ern, 2018; Stray et al., 2015)~~Li et al., 2020; Yamazaki et al., 2020; Yadav et al., 2019; Matthias and Ern, 2018; Stray et al., 2015)~~. Westward propagating planetary wave is one of the prominent features during austral and boreal summer~~ periods~~. Westward quasi-2-day waves (Q2DWs) are the most obvious representative waves and one of the most investigated phenomena by planetary wave observations. Most previous studies focused on westward propagating Q2DWs, including zonal wavenumbers of 2 (W2), 3 (W3), and 4 (W4) modes (Lainer et al., 2018; Gu et al., 2018b; Wang et al., 2017; Pancheva et al., 2016; Gu et al., 2016a; Gu et al., 2016b; Lilienthal and Jacobi, 2015; Gu et al., 2013; Limpasuvan and Wu, 2009; Salby, 1981)~~(Lainer et al., 2018; Gu et al., 2018c; Wang et al., 2017; Pancheva et al., 2017; Gu et al., 2016a; Gu et al., 2016b; Lilienthal and Jacobi, 2015; Gu et al., 2013; Limpasuvan and Wu, 2009; Salby, 1981)~~. ~~The s~~Seasonal variations of the occurrence date, peak amplitude, and wave period for eastward Q2DWs are rarely studied (Gu et al., 2017; Lu et al., 2013; Alexander and Shepherd, 2010; Sandford et al., 2008; Palo et al., 2007; Merzlyakov and Pancheva, 2007; Manney and Randel, 1993; Venne and Stanford, 1979)~~(Gu et al., 2017; Lu et al., 2013; Alexander and Shepherd, 2010; Venne and Stanford, 2010; Merzlyakov and Pancheva, 2007; Palo et al., 2007; Sandford et al., 2007; Manney et al., 1993)~~.

Q2DWs usually maximize after the summer solstice in middle latitudes. The largest wave amplitudes are observed near the mesopause in January–February in the Southern Hemisphere (SH), while in the Northern Hemisphere (NH) in July–August (Tunbridge et al., 2011)~~(Tunbridge et al., 2011)~~. ~~The~~ W3 and W4 Q2DWs reach ~~a maximum~~ amplitudes during austral and boreal summer~~ periods~~ in the mesosphere and lower thermosphere, respectively. The westward Q2DWs activity has an obvious seasonal variation (Liu et al., 2019; Gu et al., 2018b; Rao et al., 2017)~~(Liu et al., 2019; Gu et al., 2018d; Rao et al., 2016)~~. ~~Tunbridge et al. (2011)~~Tunbridge et al. (2011) have~~ long-term~~ observed long-term Q2DW in the NH and SH, and found that~~ the~~ W3 is generally stronger than~~ those of~~ the other two modes in the SH, reaching ~~an~~ the amplitude of ~12~~-~~K, while ~~the~~ W4 is stronger than W3 in the NH, ~~and can~~ reaching ~4~~-~~K. In addition, W4 is generally longer lived than W3, and W4 is still observed after W3 has ended. The results of Liu et al. (2004)~~Liu and H.-L. (2004)~~ show that ~~the~~ wave source, instability, critical layer, and mean zonal wind

~~structure~~ are the primary reasons for the seasonal variation of Q2DWs. Gu et al. (2019)~~Gu et al. (2018d)~~ have the long-term observation of satellite datasets in the SH and found that the strongest events of W2, W3, and W4 are delayed with increasing the zonal wavenumber and would be indistinguishable~~confused~~ during ~~the~~ SSWs~~ period~~. Then wave periods of W4, W3 and W2 vary between ~41-56 h, ~45-52 h, and ~45-48 h, respectively.~~Then the wave period of W3 primarily fluctuated in 45-52 h, while the W4 varies is concentrated between 41-56 h, and the W2 is primarily distributed in 45-48 h.~~ In addition, W2 can be observed in global satellite datasets, showing weaker amplitude than W3 and W4 in the NH and SH (Meek et al., 1996)~~(Meek et al., 1996)~~. The propagation and amplification of Q2DWs are primarily modulated~~dominated~~ by instability, refractive index, and critical layer, while the variation of background wind may cause different zonal wavenumber events (Gu et al., 2016a; Gu et al., 2016b)~~(Gu et al., 2016a; Gu et al., 2016b)~~. ~~Xiong et al. (2018)~~Xiong et al. (2018) studied variations in Q2DWs activity during ~~the~~ SSWs~~ period~~ and found that W1 is~~was~~ generated by the nonlinear interaction between SPW2 and W3. ~~Gu et al. (2018c)~~Gu et al. (2018b) found that the coupling between the NH and SH enhanced the summer easterly during SSWs and promoted the nonlinear interaction between W3 and SPW1 during ~~the~~ SSWs~~ period~~.

Recent studies have found significant eastward planetary waves ~~activity~~ in the polar stratosphere and mesosphere regions, with periods of nearly 2 and 4 days~~with near 2 and 4 days in the wave periods~~ (Gu et al., 2017; Sandford et al., 2008; Merzlyakov and Pancheva, 2007; Coy et al., 2003; Manney and Randel, 1993)~~(Gu et al., 2017; Venne and Stanford, 2010; Merzlyakov and Pancheva, 2007; Sandford et al., 2007; Coy et al., 2003; Manney et al., 1993)~~. Planetary waves with zonal wavenumbers -1 (E1) and -2 (E2) correspond to 4- and 2-day waves, respectively. In addition, planetary waves of 1.2-day with wavenumber -3 (E3) and 0.8-day with wavenumber -4 (E4) have been found to have the same phase speeds as E1 and E2~~In addition, the planetary waves of 1.2-day with wavenumber -3 (E3) and 0.8-day with wavenumber -4 (E4) have been found same phase speeds as the 2- and 4-day waves~~ (Manney and Randel, 1993)~~(Manney et al., 1993)~~. This series of eastward ~~propagating~~ planetary wave~~s~~ ha~~ve~~s a significant effect on the thermal and dynamic structure of the polar stratosphere, resulting in significant changes in the wind and temperature ~~variations in~~of the polar stratosphere (Coy et al., 2003; Venne and Stanford, 1979)~~(Venne and Stanford, 2010; Coy et al., 2003)~~. ~~Palo et al. (1999)~~Palo et al. (1999) demonstrated a series of nonlinear interactions between ~~the~~ migrating tides and Q2DWs. Further research, ~~Palo et al. (2007)~~Palo et al. (2007) presented evidence that ~~the eastward~~E2 Q2DW is~~was~~ coupled by ~~the~~ nonlinear planetary wave and ~~the~~ tides in the mesosphere and lower thermosphere.

~~Merzlyakov & Pancheva. (2007)~~Merzlyakov and Pancheva. (2007)

analyzed and studied satellite datasets and ~~they observed~~found that the wave periods of ~~the eastward propagating wave with the zonal wave numbers -1 and -2 in February 2004, while~~ E1 and E2 events is ~~with wave periods~~ within 1.5-5 days. They found that ~~the direction of~~ EP flux~~es for eastward planetary waves~~ is from the upper layer to the lower atmosphere, suggesting that the upper atmosphere has a dynamic influence on the lower atmosphere. Sandford et al. (2008)~~Sandford et al. (2007)~~ reported ~~a~~ significant ~~Q2DW~~ fluctuations of E2 Q2DW in the polar mesosphere ~~with a zonal wavenumber of -2 (E2)~~. They found that changes~~variations of~~ in mean zonal winds during a major SSW ~~period can~~ influenced the propagation of polar E2~~affect the propagation of polar E2~~. In addition, they believe that E2 fluctuation is representative in the mesosphere and caused by the instabilities in the polar night jet. Gu et al. (2017)~~Gu et al. (2017)~~ found~~proposed~~ that the amplitude of E2 can reach ~10K, ~20 m/s, and ~30 m/s in temperature, zonal wind, and meridional wind in the austral winter ~~period~~, while the amplitude of E2 decreases by near two-thirds in the boreal winter ~~period~~. ~~Lu et al. (2013)~~Lu et al. (2013) found that ~~the propagation height of~~ eastward planetary wave propagation~~s~~ was limited to ~~the~~ winter high latitudes, which may be because negative refractive indices equatorward of ~45°S result in evanescent wave characteristics~~caused by the negative refractive index of 45°S at the equator~~, thus preventing the propagation of planetary wave ~~propagation~~ to ~~the~~ low latitudes. They believe that the instability region at ~50-60°S may be induced by the stratospheric polar night jet and/or the "double-jet" structure.

The second modern retrospective research and application analysis (MERRA-2) datasets are used to investigate the eastward propagating~~propagation~~ wave characteristics in the polar stratospheric and mesospheric region during 2019~~ in the polar stratospheric and mesospheric region~~, including ~~zonal wavenumbers -1 (~~E1~~)~~, ~~-2 (~~E2~~)~~, ~~-3 (~~E3~~)~~ and ~~-4 (~~E4~~)~~. Particularly, we~~our~~ investigate ~~study is to explore~~ the variation of the occurrence date, peak amplitude, and wave period ~~for~~ of eastward waves, ~~and~~ as well as the role of instability, background wind structure, and critical layer ~~for~~ in the propagation and amplification of eastward waves ~~propagation and amplification~~. The remaining parts of this paper are organized as follows. In Section 2, the data and methods used in our study are described. In Section 3 analyzes the global latitude-temporal variation structure of eastward waves in the 2019 winter~~ of 2019~~. The amplification and propagation features of the eastward planetary waves ~~different wavenumber events for eastward planetary waves~~ in the NH and SH with different wavenumber events are investigated in Section 3.1 and 3.2, respectively. In Section 3.3 compares and analyzes~~will compare and analyze~~ eastward waves in the NH and SH. In Section 4 summarizes our research results.

2 Data and Analysis

The least-square method is applied to each time window to extract the E1-, E2-, E3-, and E4-wave, with 10-day, 6-day, 4-day, and 4-day, and is used by us to determine the amplitude (Gu et al., 2013)~~(Gu et al., 2013)~~. This method has previously been used successfully to identify planetary waves from satellite measurements (Gu et al., 2019; Gu et al., 2018a; Gu et al., 2018b; Gu et al., 2018c; Gu et al., 2013)~~(Gu et al., 2018a; Gu et al., 2018b; Gu et al., 2018c; Gu et al., 2018d)~~.

$$y = A\cos[2\pi(\sigma \cdot t + s \cdot \lambda)] + B\sin[2\pi(\sigma \cdot t + s \cdot \lambda)] + C \qquad (1)$$

The least-squares method is used to fit the parameters of ($A, B,$ and C). Where ($\sigma, t, s,$ and λ) are the frequency, UT time, zonal wavenumber, ~~,~~ ~~UT time,~~ and longitudes. The amplitude of wave R ~~of wavenumber~~ could be expressed as $R = \sqrt{A^2 + B^2}$.

The second modern retrospective research and application analysis (MERRA-2) data is a set of long-term atmospheric reanalysis datasets started by NASA in 1980, and now using an upgraded version of the Goddard Earth Observing System Model, Version 5 (GEOS-5) data assimilation system. MERRA-2 includes updates to the model (Molod et al., 2014; Molod et al., 2012)~~(Molod et al., 2015; Molod et al., 2012)~~ and the Global Statistical Interpolation (GSI) analysis scheme of Wu et al. (2002)~~Wu et al. (2002)~~. The MERRA-2 data includes various meteorological variables such as net radiation, temperature, relative humidity, wind speed, etc. The MERRA-2 data covers the world, with a spatial resolution of 0.5°*0.625° and a temporal resolution of 1 hour. This kind of meteorological data is widely used to detect the middle atmosphere such as the planetary wave in the polar atmosphere, global thermal tides, climate variability, and aerosol (Ukhov et al., 2020; Sun et al., 2020; Bali et al., 2019; Lu et al., 2013)~~(Sun et al., 2020; Ukhov et al., 2020; Bali et al., 2019; Lu et al., 2013)~~. These studies indicate that MERRA-2 data can be used in our research with high authenticity. The MERRA-2 datasets are used to obtain the variation in background wind, instability, refractive index, and critical layer, and explore the rules of eastward planetary waves propagation and amplification through diagnostic analysis.

The critical layer will absorb or reflect planetary waves during upward propagation from the lower atmosphere. Planetary waves that gain sufficient energy in the instability region will be amplified during reflection.~~The planetary wave will be amplified from the reflection process after gaining sufficient energy in the instability region.~~ This shows that the critical layer plays an important role in regulating the amplification and propagation of planetary waves (Gu et al., 2016a; Gu et al., 2016b; Liu et al., 2004)~~(Gu et al., 2016a; Gu et al., 2016b; Liu and H.-L., 2004)~~. ~~The baroclinic/barotropic instability in the atmospheric space structure is caused by the simultaneous equalization of the negative latitude gradient and the quasi-geostrophic potential vorticity (~~ $\cancel{\overline{q_{\varphi}}}$ ~~). Where (~~ $\cancel{\Omega}$ ~~) denote the angular speed of the Earth's rotation, and the latitude and zonal mean zonal~~

~~wind are represented by (φ and $\overline{u}$), in the second part, the (a) represents the Earth radius, in the last part, (ρ, f , and N) denote the background air density, Coriolis parameter, and buoyancy frequency, respectively. The vertical and latitudinal gradients are represented by subscripts (z and φ).~~

$$\overline{q_\varphi} = 2\Omega\cos\varphi - \left(\frac{\left(\overline{u}\cos\varphi\right)_\varphi}{a\cos\varphi}\right)_\varphi - \frac{a}{\rho}\left(\frac{f^2}{N^2}\rho\overline{u}_z\right)_z \quad (2)$$

The baroclinic/barotropic instability in the atmospheric space structure is caused by the simultaneous equalization of the negative latitude gradient and the quasi-geostrophic potential vorticity ($\overline{q_\varphi}$). w~~W~~here (Ω) denote the angular speed of the Earth's rotation, and the latitude and zonal mean zonal wind are represented by (φ and $\overline{u}$), in the second part, the (a) represents the Earth radius, in the last part, (ρ, f , and N) denote the background air density, Coriolis parameter, and buoyancy frequency, respectively. The vertical and latitudinal gradients are represented by subscripts (z and φ).

~~Andrews et al. (1987)~~Andrews et al. (1987) define the Eliassen-Palm (EP) flux vectors (F) to show the properties of planetary wave propagation, calculated as follows:

$$F = \rho a\cos\varphi \begin{bmatrix} \dfrac{\overline{u}_z\overline{v'\theta'}}{\overline{\theta}_z} - \overline{v'u'} \\ \left[f - \dfrac{\left(\overline{u}\cos\varphi\right)_\varphi}{a\cos\varphi}\right]\dfrac{\overline{v'\theta'}}{\overline{\theta}_z} - \overline{w'u'} \end{bmatrix} \quad (3)$$

w~~W~~here u' and v' are the planetary wave perturbations in the zonal and meridional wind, θ' and w' represent potential temperature and vertical wind, respectively. The planetary wave propagation is only favorable where the square of refractive index m^2 was positive:

$$m^2 = \frac{\overline{q_\varphi}}{a\left(\bar{u}-c\right)} - \frac{s^2}{\left(a\cos\varphi\right)^2} - \frac{f^2}{4N^2H^2} \tag{4}$$

w~~W~~here (s) denote the zonal wavenumber, the phase speed is represented by (c), and the (H) represents the scale height. The square of the refractive index is taken as the waveguide of planetary waves.

$$c = -\upsilon_0 \cos\left(\frac{\varphi\pi}{180}\right) \Big/ sT \tag{5}$$

where (c) denote the phase speed, the equatorial linear velocity is represented by (υ_0), and the (φ) represents the latitude, s and T represent zonal wavenumber and wave period, respectively.

3 Results and Discussion

The global temporal-latitude variation structures of E1, E2, E3, and E4 extracted from the 2019 MERRA-2 temperature datasets using time windows of 10-, 6-, 4- and 4-days respectively are shown in Figure 1. The mean temperature amplitudes of E1, E2, E3, and E4 at 55.4km during periods of 3~5-, 1.5~2.5-, 1~1.5-, and 0.9~1.1-days are shown in Figure1a, 1b, 1c, and 1d. Eastward waves are characterized by obvious seasonal variations in the SH and NH.~~The eastward wave modes during winter periods in the SH and NH are characterized by obvious seasonal variations.~~ In addition, ~~the~~ E1, E2 (E3), and E4 reach their maximum amplitude~~s~~s at

50-80°(S/N). In the SH, the strongest E1 and E2 events ~~of E1 and E2~~ occur on days 209-218 and 167-172, while ~~those of~~ E3 and E4 events occur on days 151-154 and 139-142~~ days~~. This shows that their occurrence date of maximum amplitude occurs earlier with increasing zonal wavenumber. In addition, the maximum amplitudes of E1, E2, E3, and E4 are ~6.0K, ~4.2K, ~3.6K, and ~2.4K, indicating that their peak amplitudes decrease with increasing zonal wavenumber. In the NH, the strongest E1, E2, E3 and E4 events occur on days 41-50, 69-74, 35-38 and 63-66, and the corresponding peak amplitudes are ~5.5K, ~3.8K, ~2.8K and ~1.2K.~~the occurrence dates of the strongest events of E1, E2, E3, and E4 are days 41-50, 69-74, 35-38, and 63-66, and the corresponding peak amplitudes are 5.5K, 3.8K, 2.8K, and 1.2K.~~ The results show~~It is found~~ that the peak amplitude ~~also~~ decreases with increasing zonal wavenumber in the NH, but the occurrence date is irregular~~their occurrence dates vary irregularly~~. In addition,~~ the~~ E4 is weak in the NH and almost impossible to find, so W4 is out of the discussion in the NH. Figure 2 shows the changes in zonal mean zonal wind at 70°S and 70°N in 2019~~that the 2019 zonal mean zonal wind variations at 70°S and 70°N~~. It is found that the background wind on days 90-240 (70°S) is dominated by westward wind, and reached ~80 m/s at ~50km on days 210, while it is dominated by eastward wind in late and early 2019, and reaches ~-40 m/s at ~60km. Meanwhile, the background wind is primarily westerly wind in late and early 2019 (70°N), and reaches ~90 m/s at ~ 60km on days 50, while on days 120-240, the background wind is primarily easterly wind, and the amplitude reaches -40 m/s on days 200. Compared with Figure 1, the results show that the eastward wave modes exist during winter periods with westward background wind in both hemispheres.~~It is clearly shown that the eastward wave modes exist during winter periods with westward background wind in both hemispheres.~~

3.1 In the Southern Hemisphere

Figure 3 shows that maximum amplitude is observed to be ~48.2km and ~70-80°S for E1, and E2 and E3 at ~48.2km and ~60-70°S, while E4 at ~48.2km and ~50-60°S~~the E1, E2 (E3), and E4 are distributed in ~70-80˚S, ~60-70˚S, and ~50-60˚S at ~48.2km, respectively~~. The maximum perturbation observed for E1 occur on days 211-220 with an amplitude of ~8.5K, and the remaining fluctuations occur on days 161-170, 187-196 and 231-240, while the E2 maximizes at days 219-224 with an amplitude of ~7.8K, and also shows three peaks at days 139-144, 173-178, and 187-192. Besides, the strongest E3 occurs on days 151-154 with an amplitude of ~5.2K, and the rest are distributed on days 141-144, 201-204, 209-202. E4 perturbations are distributed on days 127-130, 145-148, 161-164, 213-216, with weak amplitude of ~3K. According to previous studies, the wave period of the eastward wave varies. Therefore, periodic variability of E1, E2, E3, and E4 has also been investigated. The results show that the period corresponding to the maximum perturbation of E1 falls between ~106 (days 187-196) and ~69 h (days 211-220), and their wave periods vary greatly. However, the wave period of E2 gradually changes from ~42 h (days 139-144) to ~38 h (days 219-224), and its stability is stronger than that of E1. In addition, the wave periods of E3 and E4 are about ~39 h and ~24 h, respectively. Thus, E2, E3, and E4 wave periods are more stable than E1. ~~E1 events occur on days 161-170, 187-196, 211-220, and 231-240, respectively, and the maximum fluctuation on days 211-220 is ~8.5K, as shown in Figure 3a. In addition, the wave period of E1 decreased from the maximum ~106 h (days 187-196) to ~69 h (days 211-220), indicating the instability of the E1 wave period. E2 events occur on days 139-144, 173-178, 187-192, and 219-224, and the maximum amplitude of ~7.8K occurs on days 219-224, and the wave period of E2 is stable approximate 40 h (Figure 3b). The strongest E3 event occurs on days 151-154, and the rest are distributed on days 141-144, 201-204, 209-202, and shows E3 wave period approximate 29 h, as shown in Figure 3c. From Figure 3d, E4 events are distributed on days 127-130, 145-148, 161-164, 213-216, with a weak amplitude of about ~3K, while the wave period is stable at near 24 h. In addition, we found that the planetary waves E1, E2, E3, and E4 have similar phase speeds.~~

The spectra, spatial (vertical and latitudinal) structures of temperature, zonal and meridional wind, and diagnostic analysis of E1 are extracted from the corresponding two representative events, as shown in Figure 4.

Figure 4a, 4b shows the least-squares fitting spectra for MERRA-2 temperature on days 187–196, 211-220 at ~48.2km and ~70-80°S, when and where the E1 maximizes. An eastward wavenumber -1 signal with the period of ~106 h and ~69 h clearly dominates the whole spectrum. The temperature spatial structure corresponding to these E1 is shown in Figure 4c, 4d. The temperature spatial structure of E1 presents an obvious amplitude bimodal structure at ~70-80˚S and ~50km, and ~70-80˚S and ~60km, with the maximum at ~70-80˚S and ~50km. The strongest temperature amplitude of E1 occurs at ~50km and ~70-80˚S with an amplitude of ~10K on the days 211-220, and the other peak is ~9K (~70-80˚S and ~60km). The temperature amplitude of ~9K occurs at ~50km and ~70-80˚S during days 187-196, and the rest is ~7K (~70-80˚S and ~60km). The corresponding spatial structures of zonal wind and meridional wind of these E1 is shown in Figures 4e, 4f, 4g, and 4h. The maximum zonal wind amplitude of E1 occurs at ~60-70˚S and ~60km with an amplitude of ~14 m/s on days 187-196, and ~20 m/s at ~50-60˚S and ~60km on days 211-220. The amplitude of E1 meridional wind reaches ~10 m/s at ~70-80˚S and ~55km (days 187-196) and ~17 m/s at ~70-80˚S and ~60km (days 211-220), respectively.

~~The E1 planetary wave has a wave period of ~106 h and ~69 h on days 187-196 and 211-220 (Figures 4a and 4b). The temperature spatial structure of E1 events presents an obvious dual structure of amplitudes at~~

~~~50km and ~60km, as displayed in Figures 4c and 4d. The strongest temperature amplitude of E1 occurs at ~50 km and ~70-80˚S with an amplitude of ~10K on the days 211-220, and the other peak is ~9K (60km). The temperature amplitude of ~9K occurs on days 187-196, and the rest is ~7K (60km). The spatial structures of zonal wind and meridional wind of E1 are shown in Figures 4e, 4f, 4g, and 4h. The maximum amplitudes of zonal and meridional winds occur at ~60˚S and ~60km, and ~80˚S and ~60km. The amplitude of zonal and meridional wind reaches ~14 m/s and ~20 m/s, and ~10m/s and ~17m/s on days 187-196 and 211-220, respectively.~~ Figure 4i, 4j shows the diagnostic analysis results for the E1 events during days 187–196, 211–220. It is clear that the EP flux vectors is more favorable to propagate in the SH winter and is dramatically amplified by the mean flow instabilities and appropriate background winds at polar and between ~40 and ~80km, with EP flux propagating into the upper atmosphere (Figure 4i). Meanwhile, there is an EP flux at mid-latitudes and ~60-80km, which propagates into the lower atmosphere. The wave-mean flow interactions near its critical layer (106 h) of the green curve amplifies E1, and the positive refractive index region surrounded by the yellow curve also enhances E1 propagation. In addition, the strong instability and weak background wind at ~70-80˚S and ~40-60km provide sufficient energy for the upward EP flux to propagate and amplify. However, the downward propagating EP flux is amplified by weak instability and strong
~~~

background wind at ~50-60˚S and ~60-70km. Besides, both upward and downward EP flux eventually propagate toward the equator at ~50km. Figure 4j shows that EP flux on days 211-220 propagates downward and amplifies after the interaction of the critical layer (~69 h), facilitated by the positive refractive index region, which strong instability and weak background wind at ~50-60˚S and ~60-70km provide sufficient energy, and ultimately point towards the equator at ~50km. The results show that the weak background wind and strong instability in the polar promote the upward propagation and amplification of the EP flux. Meanwhile, the appropriate background wind and instability in mid-latitude are also conducive to the downward propagation and amplification of EP flux.~~From Figure 4i, E1 EP flux presents two directions of propagation. It is clear that the E1 is more favorable to propagate in the winter hemisphere and is dramatically amplified by the mean flow instabilities and appropriate background winds at polar and middle latitudes between ~40 and ~80 km, where the former propagate to the upper atmosphere and the latter to the lower atmosphere. In addition, E1 is amplified by wave-mean flow interactions near its critical layer (106 h). The strong instability and weak background wind and positive refractive index region provide sufficient energy for the upward EP flux to propagate and amplify. However, the downward EP flux is propagated and amplified by the interaction of the critical layer in the positive refractive index region, where the strong~~

~~background wind and weak instability provide sufficient energy. In addition, both upward and downward EP fluxes eventually propagate toward the equator at ~50km. Figure 4j shows that EP flux propagates downward and amplifies after the interaction of the critical layer (~69 h), which strong instability and strong background wind provide energy, and ultimately point towards the equator. We believe that the weak background wind and strong instability in the polar region promote the upward propagation and amplification of the EP flux. In addition, the strong background wind and weak instability in the middle latitudes are not conducive to the downward propagation and amplification of the EP flux.~~ In other words, instability and appropriate background wind play a dominant role in the propagation and amplification of the E1.

The spectra are observed at ~48.2km and ~60-70°S on days 173-178, 219-224 for E2, when the eastward wavenumber -2 becomes the primary wave mode with the wave period of ~38 h and ~39 h, as shown in Figure 5a, 5b. The temperature spatial structure corresponding to these E2 is shown in Figure 5c, 5d. The temperature spatial structure of E2 shows an obvious amplitude bimodal structure at ~60-70˚S and ~50km, and ~60-70˚S and ~60km, with the maximum at ~60-70˚S and ~50km. The maximum temperature amplitude of E1 occurs at ~50km and ~60-70˚S with an amplitude of ~7.5K on the days 173-178, and the other peak is ~6K (~70˚S and ~60km). The temperature amplitude of ~10K occurs at ~50km and ~60-70˚S during days 219-224, and the rest is ~6K (~70˚S and ~60km). The corresponding spatial structures of zonal wind and meridional wind of these E2 is shown in Figures 5e, 5f, 5g, and 5h. The zonal wind spatial structure of E2 shows an obvious amplitude bimodal structure at ~50-60˚S and ~60km, and ~70-80˚S and ~60km, with the maximum at ~50-60˚S and ~60km. The maximum zonal wind amplitudes of E2 occur at ~50-60˚S and ~60km with an amplitude of ~10 m/s on days 173-178, and the other peak is ~9 m/s (~70-80˚S and ~60km). The zonal wind amplitude of ~20 m/s occurs at ~50-60˚S and ~60km on days 219-224, and the rest is ~15 m/s (~70-80˚S and ~60 km). The amplitude of E2 meridional wind reaches ~13 m/s at ~70-80˚S and ~60km (days 173-178) and ~27 m/s at ~70-80˚S and ~60km (days 219-224), respectively.

~~From Figures 5a and 5b, the wave periods of E2 planetary waves are 38 h and 39 h on days 173-178 and 219-224. The temperature spatial structure of E2 events shows an obvious amplitude dual structure (Figures 5c and 5d). The maximum temperature amplitude of the E2 event on days 219-224 and 173-178 is ~9K (~50km) and ~7K (~50km). The spatial structures of zonal wind and meridional wind of E2 are shown in Figures 5e, 5f, 5g, and 5h. The maximum amplitudes of zonal and meridional winds occur at ~60˚S and ~60km, and ~80˚S and ~60km. The maximum amplitude of zonal wind reaches ~10 m/s and ~20 m/s, while the meridional wind is slightly stronger than the zonal wind, which reaches~~

~~~13 m/s and ~27 m/s on days 173-178 and 219-224.~~ The results in Figures 5i and 5j show diagnostic analysis during days 173-178, 219-224 for E2. It is clear that E2 is more favorable to propagate in the SH winter and is dramatically amplified by the mean flow instabilities at middle-high latitudes between ~40km and ~80km, with EP flux propagating into the lower atmosphere, and EP flux eventually propagate toward the equator at ~50km. Besides, E2 is amplified and propagated by the wave-mean flow interactions near its critical layer (~38 h) of the green curve, and the promoting effect of the positive refractive index region surrounded by the yellow curve. Meanwhile, the weak instability and strong background wind at ~50-60˚S and ~50-70km provide energy for the propagation and amplification of EP flux into the lower atmosphere during days173-178 (Figure 5i). In the diagnostic analysis of days 219-224, it is found that E2 obtains sufficient energy from strong instability and strong background wind at ~50-60˚S and ~60-70km, and is amplified and propagated into the lower atmosphere through the critical layer and positive refractive index action, as shown in Figure 5j. The results show that the background wind at ~50-60˚S and ~50-70km is weaker on days 173-178 than on days 219-224, and the instability at ~50-60˚S and ~60-70km is stronger on days 219-224 than on days 173-178. According to Figure 5a, 5b results shows that E2 has absorbed sufficient energy to be amplified under the background conditions during days 219-224.~~From Figures 5i and 5j, it is clear that the~~
~~~

~~E2 is more favorable to propagate in the SH winter and is dramatically amplified by the mean flow instabilities at middle-high latitudes between ~40km and ~80km. Then turns to the equator at ~50km. We find that the background wind in Figure 5j is weaker than that in Figure 5i, but the instability is stronger. This finding indicates that E2 has absorbed sufficient energy to be amplified under the background conditions during days 219-224 (Figure 5j).~~

Figures 6a and 6b show the observed spectra of E3 at ~48.2km and ~60-70°S on days 151-154 and 201-204, and the wave period of locked wavenumber -3 is ~29 h and ~29 h, respectively. The corresponding temperature spatial structures of these E3 is shown in Figure 6c, 6d. The temperature spatial structure of E3 shows an obvious amplitude bimodal structure at ~60-70˚S and ~50km, and ~60-70˚S and ~60km, with the maximum at ~60-70˚S and ~50km. Besides, E3 also has a weak peak at ~60-70˚S and ~70km. The strongest temperature amplitude of E3 occurs at ~50km and ~60-70˚S with an amplitude of ~6K on the days 151-154, and the other peak is ~5K (~60-70˚S and ~60km). The temperature amplitude of ~5K occurs at ~50km (~60km) and ~60-70˚S during days 201-204. The corresponding spatial structures of zonal wind and meridional wind of these E3 is shown in Figures 6e, 6f, 6g, and 6h. The zonal wind spatial structure of E3 shows an obvious amplitude bimodal structure at ~70-80˚S and ~60km, and ~50-60˚S and ~60km. The zonal wind amplitudes of E3 occur at ~70-80˚S and ~60km (~50-60˚S and ~60km) with an amplitude of ~9 m/s on days 151-154, and ~9 m/s at ~70-80˚S and ~60km (~50-60˚S and ~60km) on days 201-204. The amplitude of E3 meridional wind reaches ~13 m/s at ~60-70˚S and ~55km (days 151-154) and ~16 m/s at ~60-70˚S and ~55km (days 201-204), respectively.

EP flux of E3 is similar to that of E2. The instability and appropriate background wind at mid-high latitudes between ~50 and ~70km dramatically amplify the propagation of E3, which is enhanced by the interaction near the critical layer (~29 h) and the positive refractive index region. (Figures 6i and 6j). It is worth noting that the strong instability and weak background wind at ~50-60˚S and ~60-70km on days 151-154 provide sufficient energy for the propagation and amplification of EP flux into the lower atmosphere, and ultimately point towards the equator at 50km. The EP flux propagate to the lower atmosphere during days 201-204, and is amplified by interaction at the critical layer (~29 h). In addition, weak instability and weak background wind at ~50-60˚S and ~60-70km provide the energy to amplify E3 propagation. Combine with Figure 6c, 6d, the stronger the instability at ~50-60˚S and ~60-70km, the stronger the temperature amplitude of E3. We believe that the background wind and instability at ~50-60˚S and ~60-70km are the primary reasons for the propagation and amplification of EP flux into the lower atmosphere.

The spectra are observed to be at ~48.2 km and ~50-60°S on days

127-130, 213-216 for E4, when the eastward wavenumber -4 signal with the wave period of ~25 h and ~21 h, as shown in Figure 7a, 7b. The corresponding temperature spatial structures of these E4 is shown in Figure 7c, 7d. The temperature spatial structure of E4 shows an obvious amplitude bimodal structure at ~50-60˚S and ~50km, and ~50-60˚S and ~60km, with the maximum at ~50-60˚S and ~50km. The maximum temperature amplitude of E4 occurs at ~50km and ~50-60˚S with an amplitude of ~4K on the days 127-130, and the other peak is ~3K (~60-70˚S and ~60km). The temperature amplitude of ~3K occurs at ~50km (~60km) during days 213-216. The corresponding spatial structures of zonal wind and meridional wind of these E4 is shown in Figures 7e, 7f, 7g, and 7h. The zonal wind spatial structure of E4 shows an obvious amplitude bimodal structure at ~50-60˚S and ~55km, and ~60-70˚S and ~55km, with the maximum at ~50-60˚S and ~55km. The maximum zonal wind amplitude of E4 occurs at ~50-60˚S and ~55km with an amplitude of ~9 m/s on days 127-130, and the other peak is ~5K (~60-70˚S and ~55km). The zonal wind amplitude of ~5m/s occurs at ~50-60˚S (~60-70˚S) and ~55km on days 213-216. The amplitude of E4 meridional wind reaches ~8 m/s at ~60-70˚S and ~55km (days 127-130) and ~10 m/s at ~60-70˚S and ~55km (days 213-216), respectively. ~~Figures 6a and 6b show that the E3 planetary waves have wave periods of ~29 h on days 151-154 and 201-204. The temperature spatial structure of E3 events presents a dual structure, as shown in Figures~~

~~6c and 6d. The maximum temperature amplitude of E3 is ~7K (~50km) on days 151-154, and the other peak is ~5K (~60km). The temperature amplitude of E3 is ~5K (~50, ~60km) on days 201-204. The spatial structures of zonal wind and meridional wind of E3 are shown in Figures 6e, 6f, 6g, and 6h. The maximum amplitudes of zonal and meridional winds occur at ~50˚S and ~60km, and ~60˚S and ~60km. The maximum zonal wind is ~10 m/s, while the meridional wind is slightly stronger than the zonal wind at ~15 m/s. The EP flux of E3 is similar to that of E2. We find that instability at mid-high latitudes between ~50 and ~70km dramatically amplifies the E3 propagation and that the interaction near the critical layer enhances the process (Figures 6i and 6j). It is worth noting that the region of background wind at ~50-60˚S and ~60-70km is similar during days 151-154 and 201-204, while the former is strong instability and the latter is weak instability. This finding indicates that the strong instability provides sufficient energy for the amplification for E3 propagation on days 151-154.~~

Figures 7i and 7j show diagnostic analysis on days 127-130, 213-216 for E4. The results show that E4 is dramatically amplified by the mean flow instabilities at middle-high latitudes between ~50km and ~70km, with EP flux propagating into the lower atmosphere, and EP flux eventually propagate toward the equator at ~50km. E4 is amplified and propagated by the wave-mean flow interaction near the critical layer (~25 h, ~21 h), and the positive refractive index region provides the promoting effect. The strong instability and weak background wind at ~50-60˚S and ~60-70km provide sufficient energy for the propagation and amplification of EP flux into the lower atmosphere during days127-130. Besides, E4 obtains energy from weak instability and weak background wind at ~50-60˚S and ~60-70km on days 213-216, and is amplified and propagated into the lower atmosphere. The background wind at ~50-60˚S and ~60-70km on days 127-130 is similar to on days 213-216, and the instability at ~50-60˚S and ~60-70km is stronger on days 127-30 than on days 213-216. According to Figure 7a, 7b results shows that E4 has absorbed sufficient energy to be amplified under the background conditions on days 127-130. The temperature amplitude on 127-130 days is stronger.

~~The wave period of E4 reaches ~25 h and ~21h during days 127-130 and 213-216 in Figures 7a and 7b. The maximum temperature amplitude of E4 occurs on days 127-130, reaching ~4K (~50km), the other peak is ~3K (~60km). The temperature amplitude is ~3K (~50, ~60 km) on days 213-216, as displayed in Figure 7d. The spatial structures of zonal wind and meridional wind of E4 are shown in Figures 7e, 7f, 7g, and 7h. The maximum amplitudes of zonal and meridional winds occur at ~50˚S and ~60km, and ~60˚S and ~60km. The maximum zonal wind is ~8 m/s, while the meridional wind is slightly stronger than the zonal wind at ~10 m/s. We find that the instability in the mid-high latitudes between ~50 and ~70km~~

~~and the interaction near the critical layer greatly enhance the propagation and amplification of E4 EP flux, as shown in Figures 7i and 7j. The weak background wind and strong instability appear on days 127-130, while the strong background wind and weak instability appear on days 213-216. This finding indicates that E4 is difficult to obtain sufficient energy to be amplified under background conditions during days 213-216. The amplitude on 127-130 days is stronger.~~

3.2 In the Northern Hemisphere

Figure 8 shows that maximum amplitude is observed to be ~59.2 km and ~70-80°N for E1, and the E2 and E3 peaks at ~59.2 km and ~60-70°N. The maximum perturbation of E1 is observed to be at days 41-50 with an amplitude of ~8K, and the remaining fluctuation occur on days 25-34, 339-348. Besides, the strongest E2 occurs on days 69-74 with an amplitude of ~7K, and the rest are distributed on days 25-30, 317-322, and 341-346, while the E3 maximizes at days 35-38 with an amplitude of ~3K, and also shows one peaks at days 53-56. Based on the study of the wave period in the SH for eastward wave, the periodic variability in the NH for E1, E2, and E3 is also investigated. The wave periods of E1 decreased from a maximum of ~118 h (days 25-34) to ~80 h (days 41-50), indicating that the wave period of E1 is unstable in the NH. The E2 events occur on days 25-30, 69-74, 317-322, and 341-346, of which the corresponding wave periods are ~36, ~53, ~52, and ~48 h, which are stronger stable than E1. Besides, the wave period of E3 is relatively stable at ~29 h and ~27 h. Thus, E2 and E3 wave periods are more stable than E1.

~~Figure 8 shows that the E1 and E2 (E3) are distributed at ~70-80°N, and ~60-70°N at ~59.2km, respectively. E1 events occur on days 25-34, 41-50, and 339-348 respectively, in which the maximum temperature amplitude of days 41-50 reaches ~8K, as shown in Figure 8a. In addition, the wave periods of E1 decreased from a maximum of ~118 h (days 25-34) to ~80 h (days 41-50), indicating that the wave period of E1 is unstable in the NH. Clearly, the E2 events occur on days 25-30, 69-74, 317-322, and 341-346, of which the corresponding wave periods are ~36, ~53, ~52, and ~48 h, and the maximum temperature amplitude reaches ~7K on days 69-74, as shown in Figure 8b. Figure 8c shows two E3 events. The strongest temperature amplitude of E3 occurs on days 35-38 and reaches ~3K, and the other one occurs on days 53-56. The wave period of E3 is relatively stable at ~29 h and ~27 h. We did not study the E4 event in the NH, because E4 is weak.~~

The spectra, spatial (vertical and latitudinal) structures of temperature, zonal and meridional wind, and diagnostic analysis of E1 are extracted from the corresponding representative events, as shown in Figure 9. Figures 9a and 9b show the observed spectra of E1 at ~59.2km and ~70-80°N on days 25-34 and 41-50, and the wave period of locked wavenumber -1 is ~118 h and ~80 h, respectively. The corresponding temperature spatial structures of these E1 is shown in Figure 9c, 9d. The temperature spatial structure of E1 shows an obvious amplitude bimodal structure during days 25-34 at ~60-70˚N and ~60km, and ~40-50˚N and ~70km, with the maximum at ~60-70˚N and ~60km. Besides, E1 also has bimodal structure on days 41-50 at ~60-70˚N and ~60km, and ~60-70˚N and ~70km. The strongest temperature amplitude of E1 occurs at ~60-70˚N and ~60km with an amplitude of ~7K on the days 25-34, and the other peak is ~4K (~40-50˚N and ~70km). The temperature amplitude of ~10K occurs at ~60km and ~60-70˚N during days 41-50, and the rest is ~8K (~60-70˚N and ~70km). The corresponding spatial structures of zonal wind and meridional wind of these E1 is shown in Figures 9e, 9f, 9g, and 9h. The zonal wind spatial structure of E1 shows an obvious amplitude bimodal structure at ~70-80˚N and ~70km, and ~50-60˚N and ~70km. The zonal wind amplitude of ~13 m/s occurs at ~70-80˚N and ~70km on days 25-34, and the rest is ~10 m/s (~50-60˚N and ~70 km). In addition, there is a weak peak of 9K during days 25-34 (~30-40˚N and ~70 km). The maximum zonal wind amplitude of E1 occurs at ~70-80˚N and ~70km with an amplitude of ~19 m/s on days 41-50, and the other peak is ~13K (~50-60˚N and ~70km). The amplitude of E1 meridional wind reaches ~14 m/s at ~70-80˚N and ~70km (days 25-34) and ~22 m/s at ~70-80˚N and ~70km (days 41-50), respectively. ~~From Figures 9a and 9b, the wave periods of planetary E1 waves on days 25-34 and 41-50 are ~118 h and ~80 h, respectively. The~~

~~temperature spatial structure of the E1 event presents an obvious dual amplitude structure (~60km, ~70km). From Figure 9d, the strongest temperature amplitude of E1 appears at ~60km on days 41-50, with an amplitude of ~10K, and the rest peak is ~8K (~70km). The temperature amplitude of ~7K appears on days 25-34, and the rest is ~4K (~70km), as shown in Figure 9c. The spatial structures of zonal wind and meridional wind of E1 are shown in Figures 9e, 9f, 9g, and 9h. The maximum amplitudes of zonal and meridional winds occur at ~50˚N and ~70km, and ~80˚N and ~70km. The maximum zonal wind is ~14 m/s, while the meridional wind is slightly stronger than the zonal wind at ~18 m/s.~~

The diagnostic analysis results for E1 in Figures 9i and 9j show that E1 is dramatically amplified by the mean flow instabilities at middle-high latitudes between ~50km and ~70km, with EP flux propagating into the polar lower atmosphere, and EP flux eventually propagate toward the equator at ~50km. The wave-mean flow interaction near the critical layers (~118 h, ~80 h) amplifies and propagates E1, and the promoting effect of the positive refractive index region amplifies E1. Besides, the weak instability and strong background wind at ~40-50˚N and ~60-70km provide energy for the propagation and amplification of EP flux into the polar lower atmosphere during days 25-34. The E1 obtains sufficient energy from weak instability and suitable background wind on days 41-50 at ~40-50˚N and ~60-70km, and is amplified and propagated into the polar lower atmosphere through the critical layer and positive refractive index action. The background wind at ~40-50˚N and ~60-70km is stronger on days 25-34 than on days 41-50, but their instability is similar, indicating that stronger background winds may be unfavorable to E1 propagation and amplification at mid-northern latitudes. According to Figure 9a, 9b results shows that E1 has absorbed sufficient energy to be amplified under the background conditions during days 41-50, showing a stronger temperature amplitude.~~The results show that E1 is more conducive to the propagation in winter in the NH, and the instability at mid-latitude between ~60 and ~80 km and the interaction near the critical layer dramatically amplify the propagation of E1, which eventually turns toward the equator in the Arctic (Figures 9i and 9j). Obviously, the instability on days 25-34 and 41-50 is relatively weak, but the former has stronger background winds. This finding indicates that the background condition on days 41-50 is conducive to the propagation and amplification for E1.~~

The spectra are observed to be at ~59.2 km and ~60-70°N on days 25-30, 69-74 for E2, when the eastward wavenumber -2 signal with the period of ~36 h and ~53 h, as shown in Figure 10a, 10b. The corresponding temperature spatial structures of these E2 is shown in Figure 10c, 10d. The temperature spatial structure of E2 shows an obvious amplitude bimodal structure at ~60-70˚N and ~60km, and ~60-70˚N and ~70km, with the maximum at ~60-70˚N and ~60km. The maximum temperature amplitude of E2 occurs at ~60-70°N and ~60km with an amplitude of ~5K on days 25-30, and the other peak is ~4K (~60-70°N and ~70km). The temperature amplitude of ~9K occurs on days 69-74 at ~60°S and ~60km, and the other peaks are ~7K (~60-70°N and ~70km), ~5K (~60-70°N and ~50km). The corresponding spatial structures of zonal wind and meridional wind of these E2 is shown in Figures 10e, 10f, 10g, and 10h. The zonal wind spatial structure of E2 shows an obvious amplitude bimodal structure at ~60-70°N and ~60km, and ~40-50°N and ~60km, with the maximum at ~40-50°N and ~60km. The maximum zonal wind amplitude of E2 occurs at ~60-70°N and ~60km (~40-50°N and ~60km) with an amplitude of ~6 m/s on days 25-30. Zonal wind amplitude occurs at ~40-50°N and ~60km with an amplitude of ~18 m/s on days 41-50, and the other peak is ~16K (~60-70°N and ~60km). The amplitude of E2 meridional wind reaches ~7 m/s at ~60-70°N and ~70km (days 25-30) and ~18 m/s at ~60-70°N and ~60km (days 41-50), respectively.

Figures 10i and 10j show diagnostic analysis on days 25-30, 69-74 for E2. It is clear that E2 is dramatically amplified by the mean flow instabilities at middle-high latitudes between ~40km and ~70km, with EP flux propagating into the polar lower atmosphere, and EP flux eventually propagate toward the equator at ~50km. E2 is amplified and propagated by the wave-mean flow interaction near the critical layers (~36 h, ~53 h), and the positive refractive index region provides the promoting effect. The weak instability and strong background wind at ~50-60˚N and ~60-70km provide energy for the propagation and amplification of EP flux into the polar lower atmosphere during days 25-30. Besides, E2 obtains sufficient energy from strong instability and suitable background wind at ~50-60˚N and ~60-70km on days 69-74, and is amplified and propagated into the polar lower atmosphere. The background wind at ~50-60˚N and ~60-70km on days 127-130 is similar to on days 213-216, and the instability at ~50-60˚S and ~60-70km is stronger on days 127-30 than on days 213-216. The background wind at ~50-60˚N and ~60-70km is stronger on days 25-30 than on days 69-74, but the instability at ~50-60˚N and ~60-70km is stronger on days 69-74 than on days 25-30. According to Figure 10a, 10b temperature amplitude results shows that E2 has absorbed sufficient energy to be amplified under the background conditions on days 69-74, with the temperature amplitude on days 69-74 is stronger.

Figures 11a and 11b show the observed spectra of E3 at ~59.2km and ~60-70°N on days 35-38 and 53-56, and the wave period of locked wavenumber -3 is ~29h and ~27h, respectively. The corresponding temperature spatial structures of these E3 is shown in Figure 11c, 11d. The temperature spatial structure of E3 shows an obvious amplitude bimodal structure at ~50-60˚N and ~60km, and ~50-60˚N and ~70km, with the maximum at ~50-60˚N and ~60km. The strongest temperature amplitude of E3 occurs at ~60km and ~50-60˚N with an amplitude of ~6K on the days 35-38, and the other peak is ~5K (~50-60˚N and ~70km). The temperature amplitude of ~4K occurs at ~60km (~70km) and ~50-60˚N during days 53-56. The corresponding spatial structures of zonal wind and meridional wind of these E3 is shown in Figures 6e, 6f, 6g, and 6h. The zonal wind spatial structure of E3 shows an obvious amplitude bimodal structure at ~40-50˚N and ~70km, and ~60-70˚N and ~70km. The zonal wind amplitudes of E3 occur at ~40-50˚N and ~70km with an amplitude of ~15 m/s on days 35-38, and ~12 m/s at ~60-70˚N and ~70km. The maximum zonal wind amplitude of E3 occurs at ~40-50˚N and ~70km (~60-70˚N and ~70km) with an amplitude of ~7 m/s (~6 m/s) on days 53-56. The amplitude of E3 meridional wind reaches ~22 m/s at ~50-60˚N and ~70km (days 35-38) and ~12 m/s at ~60-70˚N and ~70km (days 53-56), respectively.

Obviously, the instability and appropriate background wind at mid-latitude between ~50 and ~70 km and the interaction near the critical layers (~29 h, ~27 h) dramatically amplify the propagation of E3, as shown in Figures 11i and 11j. The background wind is similar on days 35-38 and 53-56, and the former is more unstable. This finding indicates that the E3 in propagation is more likely to get sufficient energy to be amplified on days 35-38. The instability and appropriate background wind at mid-high latitudes between ~50 and ~70km dramatically amplify the propagation of E3, which is enhanced by the interaction near the critical layers (~29 h, ~27

h) and the positive refractive index region. (Figure 11i, 11j). It is worth noting that the strong instability and weak background wind at ~50-60˚N and ~60-70km on days 35-38 provide sufficient energy for the propagation and amplification of EP flux into the lower atmosphere, and ultimately point towards the equator at 50km. The EP flux propagate to the lower atmosphere during days 35-38, and is amplified by interactions at the critical layer (~29 h). In addition, weak instability and weak background winds on days 53-56 at ~50-60˚N and ~60-70km provide the energy to amplify E3 propagation. Combine with Figure 11c, 11d, the stronger the instability at ~50-60˚N and ~60-70km, the stronger the temperature amplitude of E3. The results show that the instability on days 35-38 at ~50-60˚N and ~60-70km are the primary reasons for the propagation and amplification of EP flux into the lower atmosphere.~~From Figures 10a and 10b, the wave period of E2 on days 25-30 and 69-74 reaches ~36h and ~53h. The maximum temperature amplitude of E2 appears on days 69-74, reaches ~10K (~60km), and the other peak is ~7K (~70km). The maximum temperature amplitude is ~5K (~60km) during days 25-30, and another peak is ~4K (~70km). The spatial structures of zonal wind and meridional wind of E2 are shown in Figures 10e, 10f, 10g, and 10h. The maximum amplitudes of zonal and meridional winds occur at ~50˚N and ~70km, and ~60˚N and ~70km. The maximum zonal and meridional winds are ~7 (~18) m/s on days 35-30 (69-74). Clearly, the instability at a mid-high latitude~~

~~between ~40 and ~80 km and the interaction near the critical layer dramatically amplify the propagation of E2, which eventually turns toward the equator, as displayed in Figures 10i and 10j. Obviously, the temperature amplitude is stronger on days 69-74, which indicates that E2 obtains sufficient energy for amplification under the background condition.~~

~~The E3 planetary waves have wave periods of ~29h and ~27h on days 35-38 and 53-56, as shown in Figures 11a, and 11b. Clearly, from Figures 11c, and 11d, the maximum temperature amplitude of E3 is ~6K (~70km) on days 35-38, and another peak is ~5K (~60km). The peak temperature amplitude is ~4K (~60, ~70 km) on days 53-56. The spatial structures of zonal wind and meridional wind of E3 are shown in Figures 11e, 11f, 11g, and 11h. The maximum amplitudes of zonal and meridional winds occur at ~40°N and ~70km, and ~50°N and ~70km. The maximum zonal and meridional winds are ~15 (~7) and ~22 (~13) m/s on days 35-38 (53-56). Obviously, the instability at mid-latitude between ~60 and ~70 km and the interaction near the critical layer dramatically amplify the propagation of E3, as shown in Figures 11i and 11j. The background wind is similar on days 35-38 and 53-56, and the former is more unstable. This finding indicates that the E3 in propagation is more likely to get sufficient energy to be amplified on days 35-38.~~

3.3 Comparison between SH and NH

~~We find that t~~The observed latitude and maximum amplitude for eastward planetary waves (E1, E2, E3, E4) decrease~~e~~ and weaken with increasing zonal wavenumber in the SH, reaching ~70-80˚S, ~60-70˚S, ~60-70˚S, and ~50-60˚S, and ~10K, ~9K, ~6K, and ~3K, respectively. In addition, the occurrence date is earlier with increasing zonal wavenumber. The temperature spatial structure shows a bimodal~~dual~~-peak structure (~50 and ~60km), primarily located at ~50km. The maximum zonal wind amplitudes of E1 and E2, E3 and E4 are almost the equivalents, which are ~20 m/s and ~10 m/s respectively. The maximum meridional wind amplitudes of E1, E2, E3 and E4 are ~17 m/s, ~27 m/s, ~16 m/s, and ~11 m/s respectively. The wave period of E1 tends to get shorter from 5 to 3 days, while E2 and E3 are close to ~40 h and ~30 h, while E4 remains at ~24 h. E1, E2, E3, and E4 are more favorable to propagation in the SH winter and are dramatically amplified by the mean flow instabilities at middle latitudes between ~40 and ~70~~-~~km, with EP flux propagating into the lower atmosphere, and EP flux eventually propagate toward the equator at ~50km. In addition, the propagation of EP flux for E1 to the upper atmosphere~~E1 upward propagating EP flux~~ may be influenced by the instability and background wind at the Antarctic ~50km.

The observed latitudes of E1, E2 (E3) decrease with increasing wavenumber in the NH, which are ~70-80˚N, ~60-70˚N, and ~60-70˚N. The temperature spatial structure of E1, E2, and E3 presents a bimodal~~dual~~-peak structure, primarily located at ~70km, reaches ~10K, ~9K, and ~6K.

The maximum zonal wind amplitude for E1, E2 and E3 occurs at ~50-80°N and ~70km, and their amplitude is almost equal to ~18 m/s.~~The maximum zonal wind amplitude appears at ~50-80°N and ~60km. E1, E2, E3, and E4 are almost the equivalent, which is ~18 m/s respectively.~~ The maximum meridional wind of E1, E2 and E3 occur at ~50-80°N and ~70km, with amplitudes of ~22 m/s, ~18 m/s and ~22 m/s, respectively.~~The maximum meridional wind amplitude appears at ~50-80°N and ~60km. The maximum amplitudes of E1, E2, and E3 are ~22 m/s, ~18 m/s, and ~22 m/s respectively.~~ The wave period of E1 tends to be shorter from 5-3 days, and E2 and E3 are close to ~48 h and ~30 h. In addition, E1, E2, and E3 are more favorable to propagation in the NH winter and are dramatically amplified by the mean flow instabilities at middle latitudes between ~40 and ~70~~-~~km, with EP flux propagating into the lower atmosphere, and EP flux eventually propagate toward the equator at ~50km.

4 Summary and Conclusions

We present for the first time an extensive study of the global variation for eastward planetary wave activity, including zonal wave numbers of -1 (E1), -2 (E2), -3 (E3), -4 (E4), in the stratosphere and mesosphere using the MERRA-2 temperature and wind observations in 2019. The temperature and wind amplitudes and wave periods of each event were determined by 2-D least-squares fitting. Our study includes the spatial and temporal behaviors of the eastward planetary waves in both hemispheres with a comprehensive diagnostic analysis on their propagation and amplification. The key findings of the study are summarized as follows:

1. The latitudes for the maximum (temperature, zonal and meridional wind) amplitudes of E1, E2, E3, and E4 decrease with increasing wavenumber in the SH and NH. The E1, E2, E3, and E4 events occur earlier with increasing zonal wavenumber in the SH. In addition, eastward wave modes exist during summer periods with westward background wind in both hemispheres.

2. The temperature spatial structures of E1, E2, E3, and E4 present a double-peak structure, which is located at ~50km and ~60km in SH, ~60km, and ~70km in SH. In addition, the lower peak is usually larger than the higher one.

3. The maximum (temperature, zonal and meridional wind) amplitudes of E1, E2, and E3 decrease with increasing zonal wavenumber in the SH and NH. The maximum temperature amplitudes in the SH are slightly larger and lie lower than those in the NH. In addition, the meridional wind amplitudes are slightly larger than the zonal wind in the SH and NH.

4. The wave period of the E1 mode varies from 3 to 5 days in both hemispheres, while the period of E2 mode is slightly longer in the NH (~48 h) than in the SH (~40 h). The periods of E3 are ~30 h in both SH and NH, and the period of E4 is ~24 h.

5. The eastward planetary wave is more favorable to propagate in the

winter hemisphere and is dramatically amplified by the mean flow instabilities and appropriate background winds at polar and middle latitudes between $\sim$40 and $\sim$80~~–~~km. Furthermore, the amplification of planetary waves through wave-mean flow interaction most easily occurs near its critical layer. In addition, the direction of EP flux ultimately points towards the equator.

6. The strong instability and appropriate background wind in the lower layer of the Antarctic region may provide sufficient energy to promote the E1 propagation and amplification to the upper atmosphere~~layer~~.

This study demonstrates how the background zonal wind in the polar middle atmosphere affects the dynamics of eastward planetary waves in the polar middle atmosphere.

Data availability. MERRA-2 data are available at http://disc.gsfc.nasa.gov.

Author contributions. LT carried out the data processing and analysis and wrote the manuscript. SYG and XKD contributed to reviewing the article.

Competing interests. The authors declare that they have no conflict of interest.

Acknowledgements. This work was performed in the framework of the Space Physics Research (SPR). The authors thank NASA for free online access to the MERRA-2 temperature reanalysis.

Acknowledgments. This research work was supported by the National Natural Science Foundation of China (41704153, 41874181, and 41831071).

References

Alexander, S. P. and Shepherd, M. G.: Planetary wave activity in the polar lower stratosphere, Atmos. Chem. Phys., 10, 707-718, 10.5194/acp-10-707-2010, 2010.

Andrews, D., Holton, J., and Leovy, C.: Middle Atmosphere Dynamics, 489 pp.1987.

Bali, K., Dey, S., Ganguly, D., and Smith, K. R.: Space-time variability of ambient PM2.5 diurnal pattern over India from 18-years (2000–2017) of MERRA-2 reanalysis data, Atmos. Chem. Phys. Discuss., 2019, 1-23, 10.5194/acp-2019-731, 2019.

Coy, L., Štajner, I., DaSilva, A. M., Joiner, J., Rood, R. B., Pawson, S., and Lin, S. J.: High-Frequency Planetary Waves in the Polar Middle Atmosphere as Seen in a Data Assimilation System, Journal of the Atmospheric Sciences, 60, 2975-2992, 10.1175/1520-0469(2003)060<2975:Hpwitp>2.0.Co;2, 2003.

Gu, S.-Y., Liu, H.-L., Dou, X., and Jia, M.: Ionospheric Variability Due to Tides and Quasi-Two Day Wave Interactions, Journal of Geophysical Research: Space Physics, 123, 1554-1565, https://doi.org/10.1002/2017JA025105, 2018a.

Gu, S.-Y., Dou, X., Pancheva, D., Yi, W., and Chen, T.: Investigation of the Abnormal Quasi 2-Day Wave Activities During the Sudden Stratospheric Warming Period of January 2006, Journal of Geophysical Research: Space Physics, 123, 6031-6041, https://doi.org/10.1029/2018JA025596, 2018b.

Gu, S.-Y., Liu, H.-L., Pedatella, N. M., Dou, X., and Liu, Y.: On the wave number 2 eastward propagating quasi 2 day wave at middle and high latitudes, Journal of Geophysical Research: Space Physics, 122, 4489-4499, https://doi.org/10.1002/2016JA023353, 2017.

Gu, S.-Y., Liu, H.-L., Pedatella, N. M., Dou, X., and Shu, Z.: The quasi-2 day wave activities during

2007 boreal summer period as revealed by Whole Atmosphere Community Climate Model, Journal of Geophysical Research: Space Physics, 121, 7256-7268, https://doi.org/10.1002/2016JA022867, 2016a.

Gu, S.-Y., Li, T., Dou, X., Wu, Q., Mlynczak, M. G., and Russell Iii, J. M.: Observations of Quasi-Two-Day wave by TIMED/SABER and TIMED/TIDI, Journal of Geophysical Research: Atmospheres, 118, 1624-1639, https://doi.org/10.1002/jgrd.50191, 2013.

Gu, S.-Y., Liu, H.-L., Pedatella, N. M., Dou, X., Li, T., and Chen, T.: The quasi 2 day wave activities during 2007 austral summer period as revealed by Whole Atmosphere Community Climate Model, Journal of Geophysical Research: Space Physics, 121, 2743-2754, https://doi.org/10.1002/2015JA022225, 2016b.

Gu, S.-Y., Ruan, H., Yang, C.-Y., Gan, Q., Dou, X., and Wang, N.: The Morphology of the 6-Day Wave in Both the Neutral Atmosphere and F Region Ionosphere Under Solar Minimum Conditions, Journal of Geophysical Research: Space Physics, 123, 4232-4240, https://doi.org/10.1029/2018JA025302, 2018c.

Gu, S.-Y., Dou, X.-K., Yang, C.-Y., Jia, M., Huang, K.-M., Huang, C.-M., and Zhang, S.-D.: Climatology and Anomaly of the Quasi-Two-Day Wave Behaviors During 2003–2018 Austral Summer Periods, Journal of Geophysical Research: Space Physics, 124, 544-556, https://doi.org/10.1029/2018JA026047, 2019.

Lainer, M., Hocke, K., and Kämpfer, N.: Long-term observation of midlatitude quasi 2-day waves by a water vapor radiometer, Atmos. Chem. Phys., 18, 12061-12074, 10.5194/acp-18-12061-2018, 2018.

Li, H., Pilch Kedzierski, R., and Matthes, K.: On the forcings of the unusual Quasi-Biennial Oscillation structure in February 2016, Atmos. Chem. Phys., 20, 6541-6561, 10.5194/acp-20-6541-2020, 2020.

Lilienthal, F. and Jacobi, C.: Meteor radar quasi 2-day wave observations over 10 years at Collm (51.3° N, 13.0° E), Atmos. Chem. Phys., 15, 9917-9927, 10.5194/acp-15-9917-2015, 2015.

Limpasuvan, V. and Wu, D. L.: Anomalous two-day wave behavior during the 2006 austral summer, Geophysical Research Letters, 36, https://doi.org/10.1029/2008GL036387, 2009.

Liu, G., England, S. L., and Janches, D.: Quasi Two-, Three-, and Six-Day Planetary-Scale Wave Oscillations in the Upper Atmosphere Observed by TIMED/SABER Over ~17 Years During 2002–2018, Journal of Geophysical Research: Space Physics, 124, 9462-9474, https://doi.org/10.1029/2019JA026918, 2019.

Liu, H. L., Talaat, E. R., Roble, R. G., Lieberman, R. S., Riggin, D. M., and Yee, J. H.: The 6.5-day wave and its seasonal variability in the middle and upper atmosphere, Journal of Geophysical Research: Atmospheres, 109, https://doi.org/10.1029/2004JD004795, 2004.

Lu, X., Chu, X., Fuller-Rowell, T., Chang, L., Fong, W., and Yu, Z.: Eastward propagating planetary waves with periods of 1–5 days in the winter Antarctic stratosphere as revealed by MERRA and lidar, Journal of Geophysical Research: Atmospheres, 118, 9565-9578, https://doi.org/10.1002/jgrd.50717, 2013.

Manney, G. L. and Randel, W. J.: Instability at the Winter Stratopause: A Mechanism for the 4-Day Wave, Journal of Atmospheric Sciences, 50, 3928-3938, 10.1175/1520-0469(1993)050<3928:IATWSA>2.0.CO;2, 1993.

Matthias, V. and Ern, M.: On the origin of the mesospheric quasi-stationary planetary waves in the unusual Arctic winter 2015/2016, Atmospheric Chemistry and Physics, 18, 4803-4815,

10.5194/acp-18-4803-2018, 2018.

Meek, C. E., Manson, A. H., Franke, S. J., Singer, W., Hoffmann, P., Clark, R. R., Tsuda, T., Nakamura, T., Tsutsumi, M., Hagan, M., Fritts, D. C., Isler, J., and I. Portnyagin, Y.: Global study of northern hemisphere quasi-2-day wave events in recent summers near 90 km altitude, Journal of Atmospheric and Terrestrial Physics, 58, 1401-1411, https://doi.org/10.1016/0021-9169(95)00120-4, 1996.

Merzlyakov, E. G. and Pancheva, D. V.: The 1.5–5-day eastward waves in the upper stratosphere–mesosphere as observed by the Esrange meteor radar and the SABER instrument, Journal of Atmospheric and Solar-Terrestrial Physics, 69, 2102-2117, https://doi.org/10.1016/j.jastp.2007.07.002, 2007.

Molod, A., Takacs, L., Suarez, M., and Bacmeister, J.: Development of the GEOS-5 atmospheric general circulation model: evolution from MERRA to MERRA2, Geoscientific Model Development Discussions, 7, 10.5194/gmdd-7-7575-2014, 2014.

Molod, A., Takacs, L., Suarez, M., Bacmeister, J., Song, I. S., and Eichmann, A.: The GEOS-5 Atmospheric General Circulation Model: Mean Climate and Development from MERRA to Fortuna, 2012.

Palo, S. E., Roble, R. G., and Hagan, M. E.: Middle atmosphere effects of the quasi-two-day wave determined from a General Circulation Model, Earth, Planets and Space, 51, 629-647, 10.1186/BF03353221, 1999.

Palo, S. E., Forbes, J. M., Zhang, X., Russell Iii, J. M., and Mlynczak, M. G.: An eastward propagating two-day wave: Evidence for nonlinear planetary wave and tidal coupling in the mesosphere and lower thermosphere, Geophysical Research Letters, 34,

https://doi.org/10.1029/2006GL027728, 2007.

Pancheva, D., Mukhtarov, P., Siskind, D. E., and Smith, A. K.: Global distribution and variability of quasi 2 day waves based on the NOGAPS-ALPHA reanalysis model, Journal of Geophysical Research: Space Physics, 121, 11,422-411,449, https://doi.org/10.1002/2016JA023381, 2016.

Rao, N. V., Ratnam, M. V., Vedavathi, C., Tsuda, T., Murthy, B. V. K., Sathishkumar, S., Gurubaran, S., Kumar, K. K., Subrahmanyam, K. V., and Rao, S. V. B.: Seasonal, inter-annual and solar cycle variability of the quasi two day wave in the low-latitude mesosphere and lower thermosphere, Journal of Atmospheric and Solar-Terrestrial Physics, 152-153, 20-29, https://doi.org/10.1016/j.jastp.2016.11.005, 2017.

Salby, M. L.: The 2-day wave in the middle atmosphere: Observations and theory, Journal of Geophysical Research: Oceans, 86, 9654-9660, https://doi.org/10.1029/JC086iC10p09654, 1981.

Sandford, D. J., Schwartz, M. J., and Mitchell, N. J.: The wintertime two-day wave in the polar stratosphere, mesosphere and lower thermosphere, Atmos. Chem. Phys., 8, 749-755, 10.5194/acp-8-749-2008, 2008.

Stray, N. H., Orsolini, Y. J., Espy, P. J., Limpasuvan, V., and Hibbins, R. E.: Observations of planetary waves in the mesosphere-lower thermosphere during stratospheric warming events, Atmos. Chem. Phys., 15, 4997-5005, 10.5194/acp-15-4997-2015, 2015.

Sun, J., Veefkind, J. P., van Velthoven, P., Tilstra, L. G., Chimot, J., Nanda, S., and Levelt, P. F.: Defining aerosol layer height for UVAI interpretation using aerosol vertical distributions characterized by MERRA-2, Atmos. Chem. Phys. Discuss., 2020, 1-36, 10.5194/acp-2020-39, 2020.

Tunbridge, V. M., Sandford, D. J., and Mitchell, N. J.: Zonal wave numbers of the summertime 2 day planetary wave observed in the mesosphere by EOS Aura Microwave Limb Sounder, Journal of Geophysical Research: Atmospheres, 116, https://doi.org/10.1029/2010JD014567, 2011.

Ukhov, A., Mostamandi, S., da Silva, A., Flemming, J., Alshehri, Y., Shevchenko, I., and Stenchikov, G.: Assessment of natural and anthropogenic aerosol air pollution in the Middle East using MERRA-2, CAMS data assimilation products, and high-resolution WRF-Chem model simulations, Atmospheric Chemistry and Physics, 20, 9281-9310, 10.5194/acp-20-9281-2020, 2020.

Venne, D. E. and Stanford, J. L.: Observation of a 4–Day Temperature Wave in the Polar Winter Stratosphere, Journal of the Atmospheric Sciences, 36, 2016-2019, 10.1175/1520-0469(1979)036<2016:Ooatwi>2.0.Co;2, 1979.

Wang, J. C., Chang, L. C., Yue, J., Wang, W., and Siskind, D. E.: The quasi 2 day wave response in TIME-GCM nudged with NOGAPS-ALPHA, Journal of Geophysical Research: Space Physics, 122, 5709-5732, https://doi.org/10.1002/2016JA023745, 2017.

Wu, W.-S., Purser, R. J., and Parrish, D. F.: Three-Dimensional Variational Analysis with Spatially Inhomogeneous Covariances, Monthly Weather Review, 130, 2905-2916, 10.1175/1520-0493(2002)130<2905:TDVAWS>2.0.CO;2, 2002.

Xiong, J., Wan, W., Ding, F., Liu, L., Hu, L., and Yan, C.: Two Day Wave Traveling Westward With Wave Number 1 During the Sudden Stratospheric Warming in January 2017, Journal of Geophysical Research: Space Physics, 123, 3005-3013, https://doi.org/10.1002/2017JA025171, 2018.

Yadav, S., Vineeth, C., Kumar, K. K., Choudhary, R. K., Pant, T. K., and Sunda, S.: Role of the phase of Quasi-Biennial Oscillation in modulating the influence of SSW on Equatorial Ionosphere, 2019 URSI Asia-Pacific Radio Science Conference (AP-RASC), 9-15 March 2019, 1-4, 10.23919/URSIAP-RASC.2019.8738274,

Yamazaki, K., Nakamura, T., Ukita, J., and Hoshi, K.: A tropospheric pathway of the stratospheric quasi-biennial oscillation (QBO) impact on the boreal winter polar vortex, Atmos. Chem. Phys., 20, 5111-5127, 10.5194/acp-20-5111-2020, 2020.

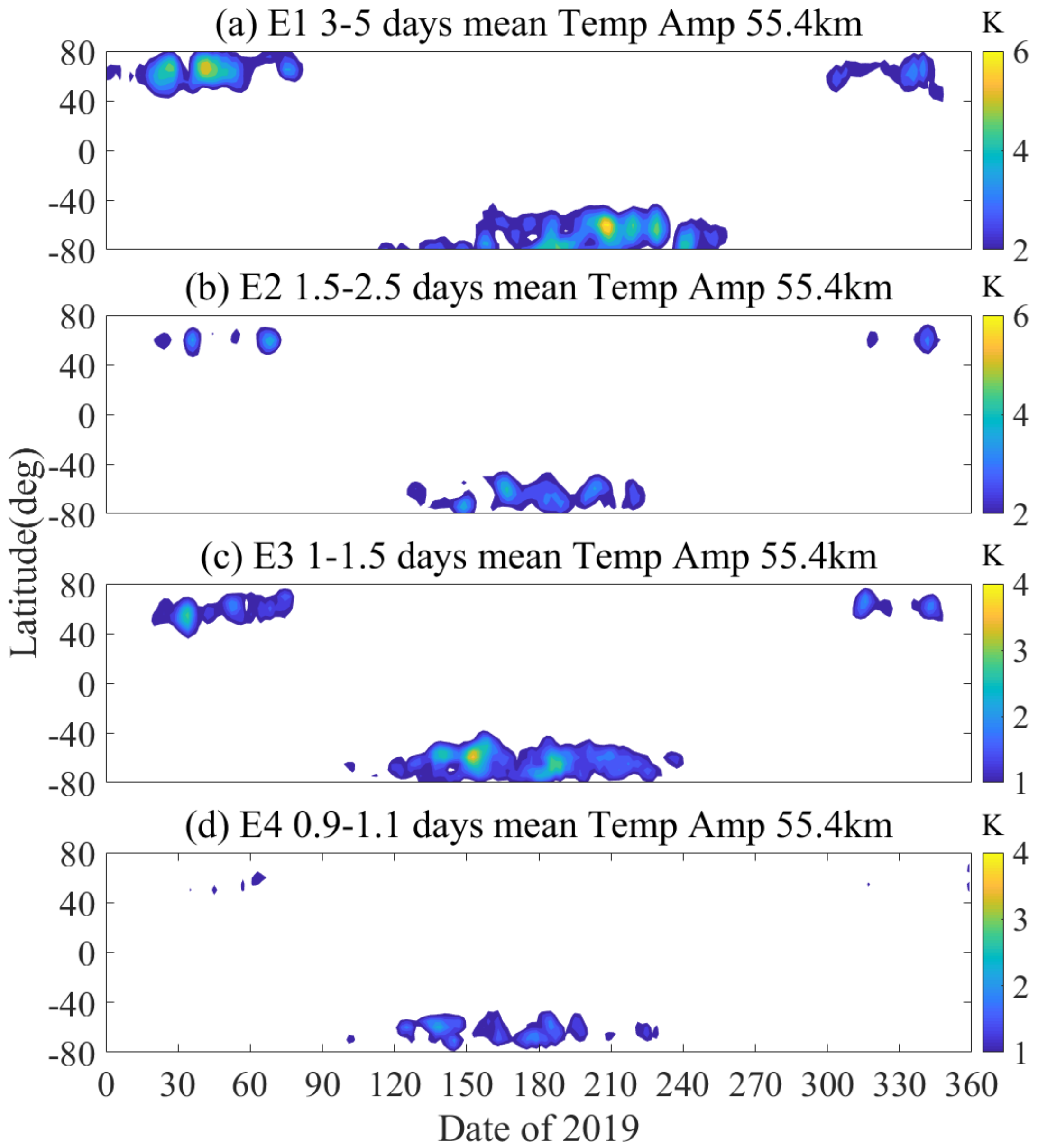

Figure 1. The global latitude-temporal variation structures of the (a) E1, (b) E2, (c) E3, (d) E4 planetary waves during 2019. White areas represent small amplitude data (corresponds to the right color bar). The confidence interval is 0.95.

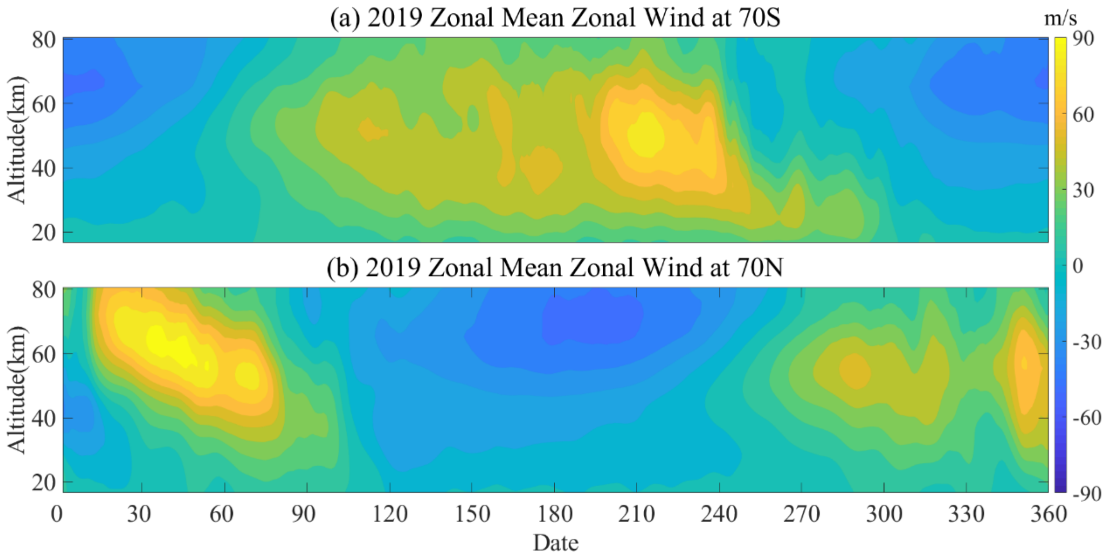

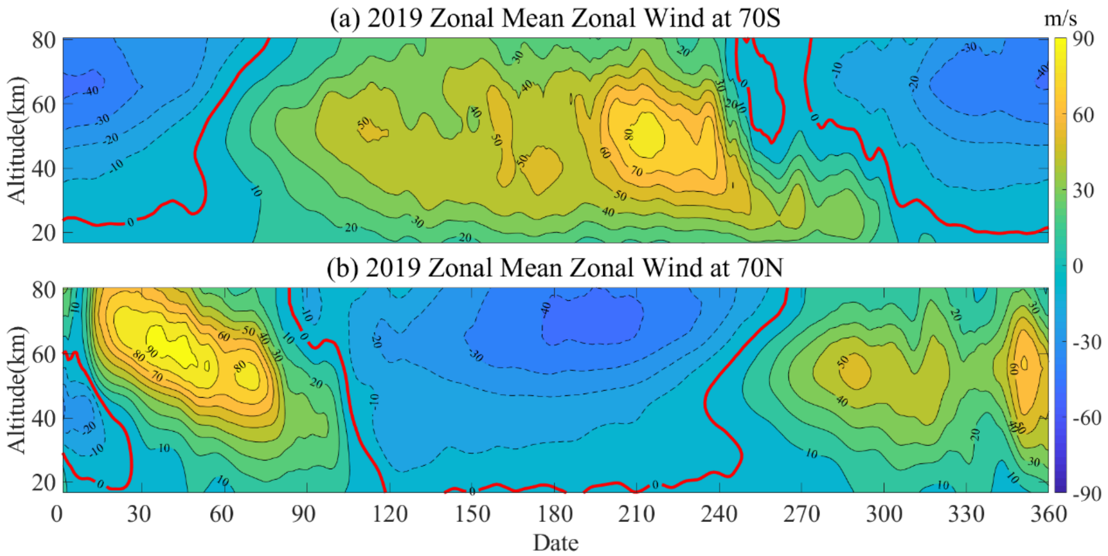

Figure 2. The zonal mean zonal wind variations of the (a) the 70S and (b) 70N during 2019. The dotted line represents east wind, the solid line represents west wind, and the red solid line is 0m/s.

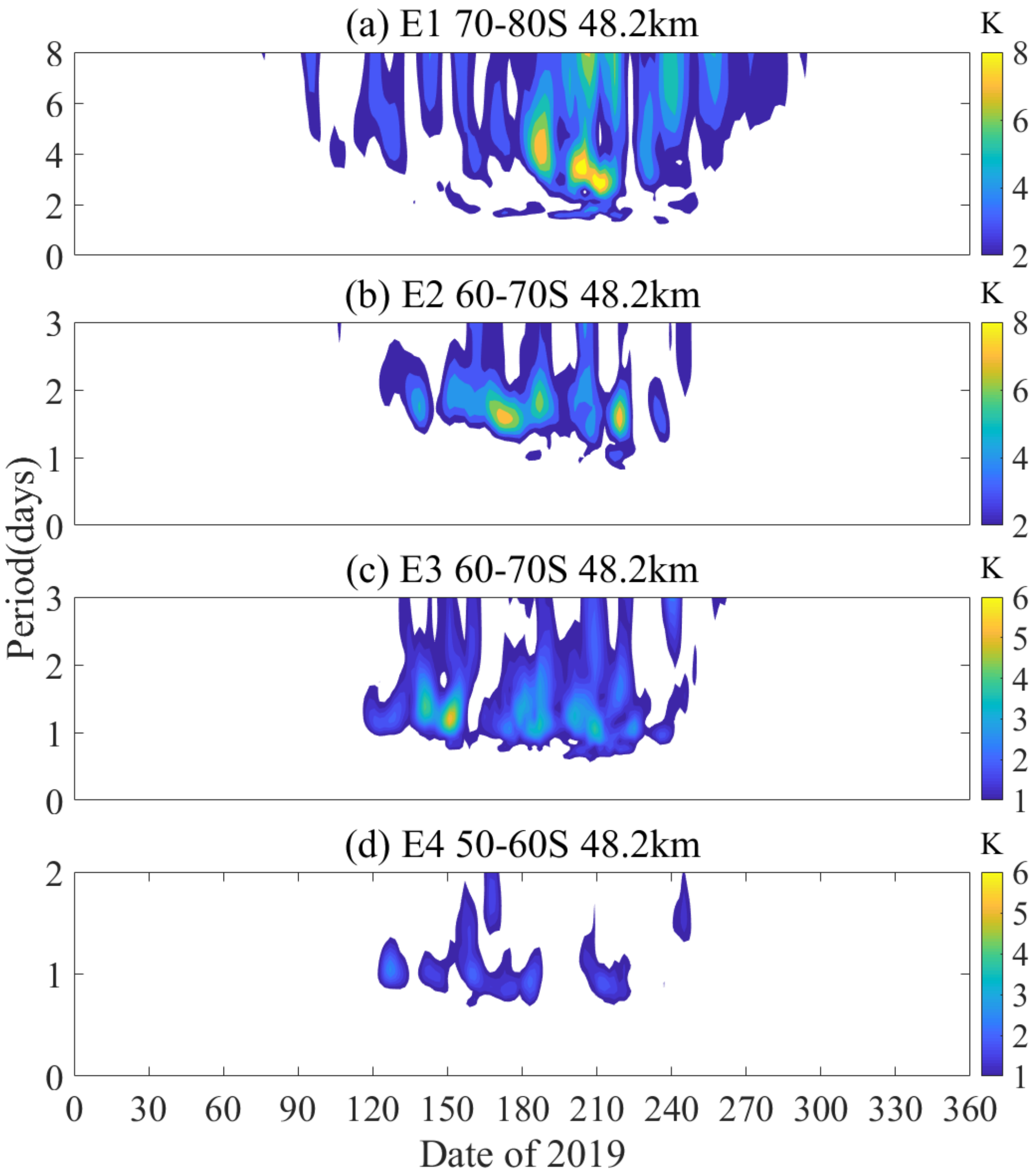

Figure 3. The temporal variations of the (a) E1, (b) E2, (c) E3, (d) E4 QTDWs during 2019 austral winter period.

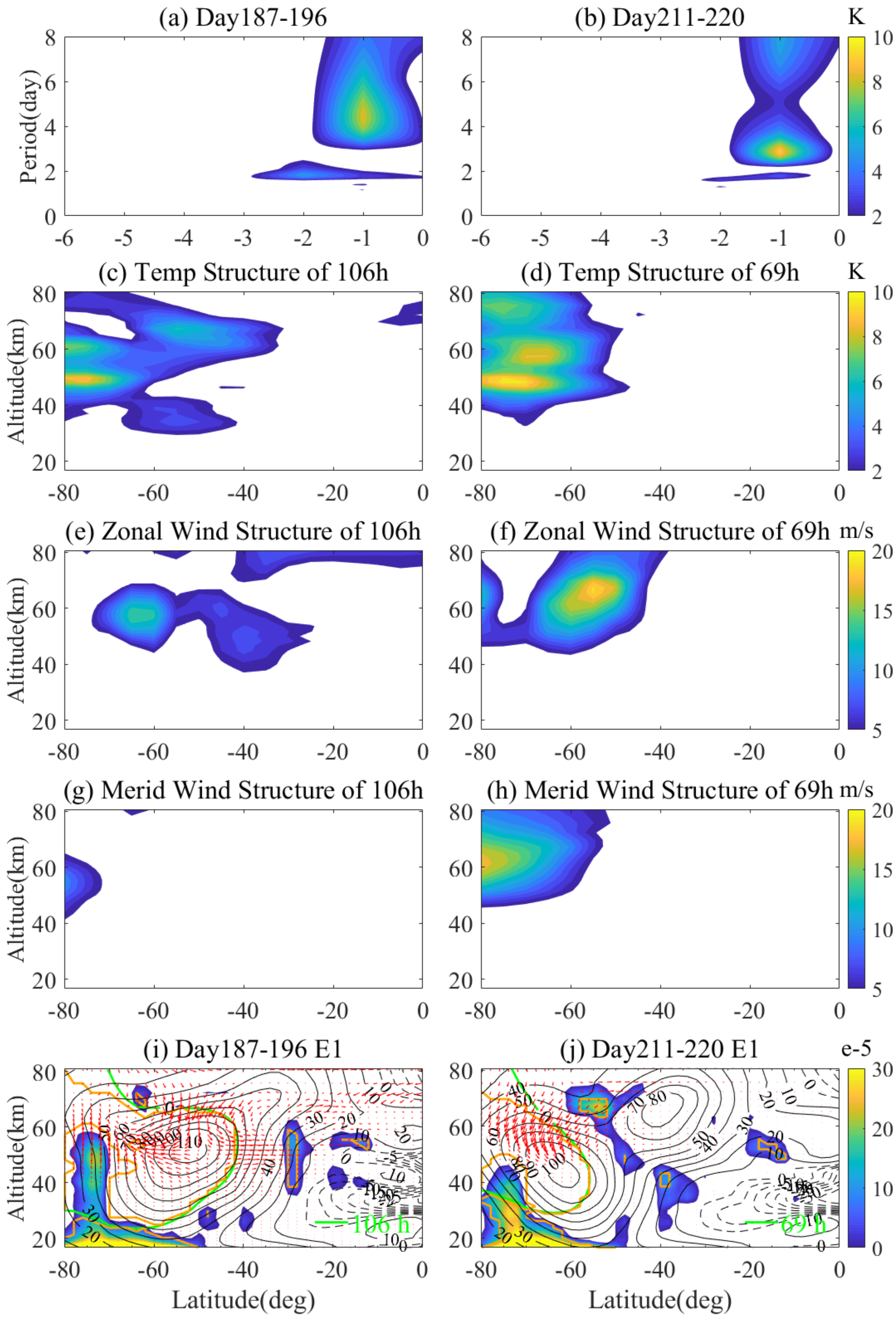
(a) Day187-196
(b) Day211-220
K
Period(day)
(c) Temp Structure of 106h
(d) Temp Structure of 69h
K
Altitude(km)
(e) Zonal Wind Structure of 106h
(f) Zonal Wind Structure of 69h
m/s
(g) Merid Wind Structure of 106h
(h) Merid Wind Structure of 69h
m/s
(i) Day187-196 E1
(j) Day211-220 E1
e-5
106 h
69 h
Latitude(deg)
Latitude(deg)

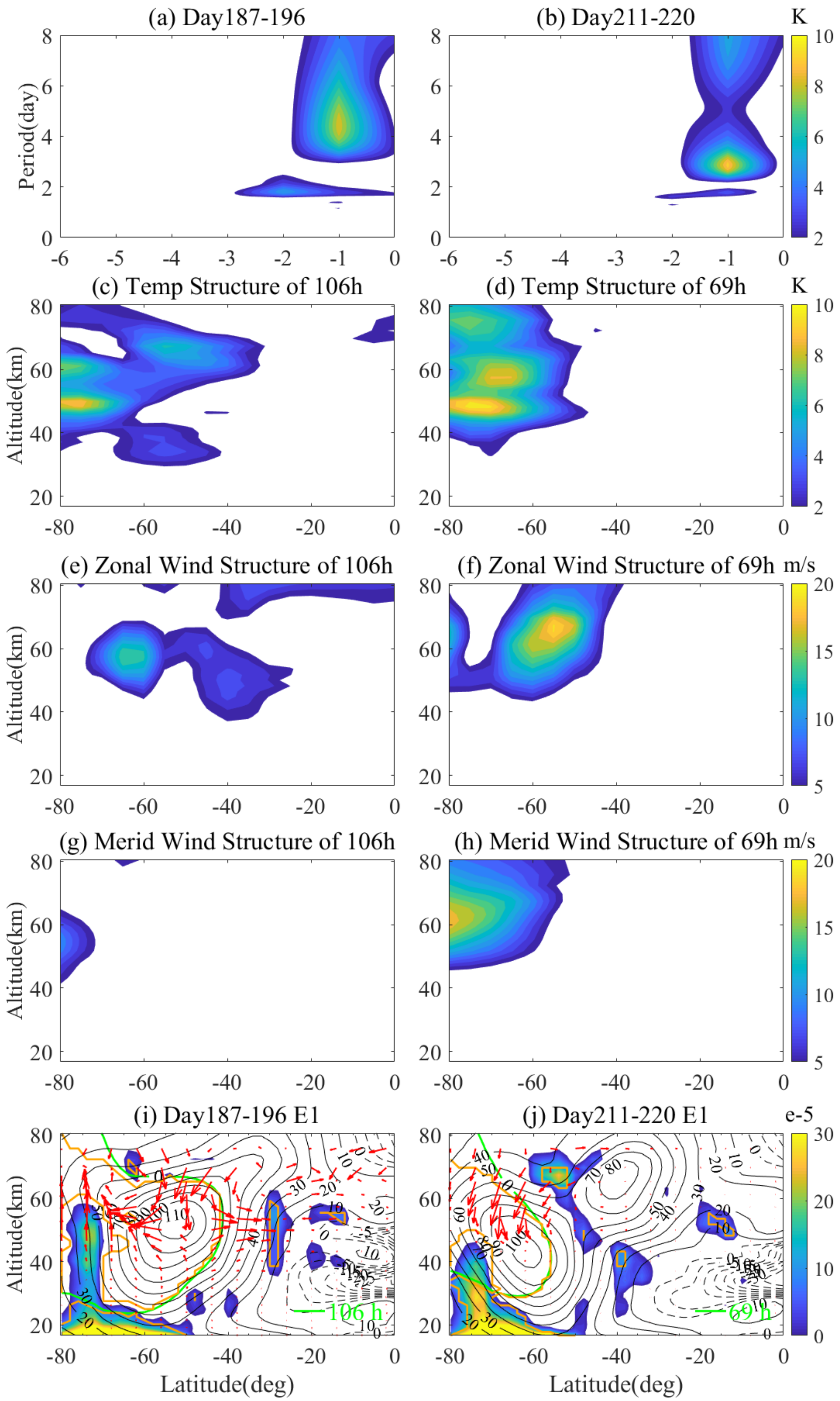

(a) Day187-196
(b) Day211-220
K
Period(day)
(c) Temp Structure of 106h
(d) Temp Structure of 69h
K
Altitude(km)
(e) Zonal Wind Structure of 106h
(f) Zonal Wind Structure of 69h
m/s
(g) Merid Wind Structure of 106h
(h) Merid Wind Structure of 69h
m/s
(i) Day187-196 E1
(j) Day211-220 E1
e-5
106 h
69 h
Latitude(deg)

Figure 4. The (a, b) spectra, (c, d) temperature spatial structures, (e, f) zonal wind spatial structures, (g, h) meridional wind spatial structures, and (i, j) diagnostic analysis of the E1 typical events during 2019 austral winter period. The MERRA-2 temperature data observations at 48.2km and 70-80°S during days 187–196 (Figure 4a), 211–220 (Figure 4d) are utilized, respectively. The instability (blue shaded region), EP fluxes (red arrow), and critical layers (green line) for E1 typical event. The green line represents critical layers of the E1 with the natural period. Regions enclosed by orange solid lines are characterized by the positive refractive index for the E1.

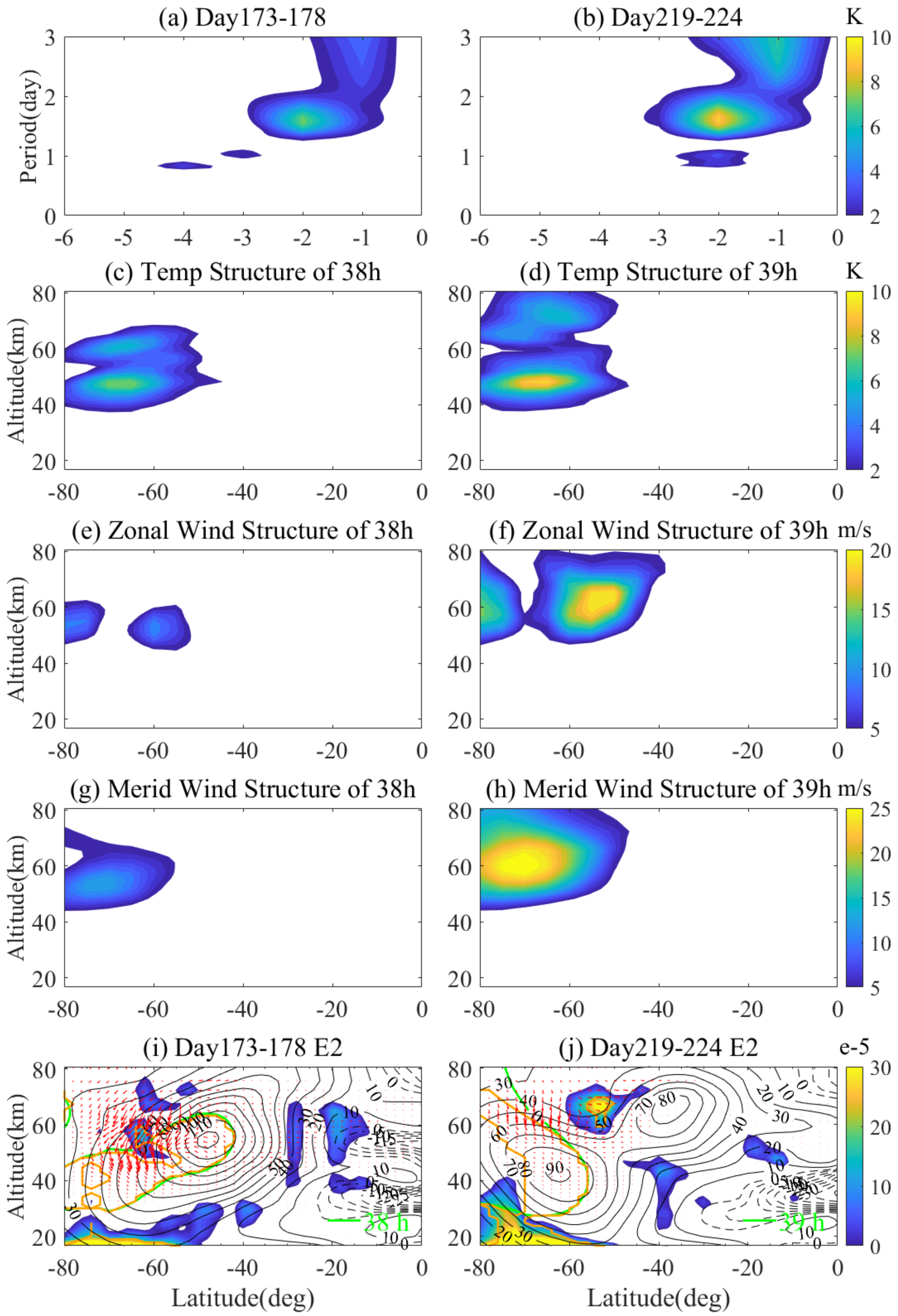

(a) Day173-178
(b) Day219-224
K
Period(day)
(c) Temp Structure of 38h
(d) Temp Structure of 39h
K
Altitude(km)
(e) Zonal Wind Structure of 38h
(f) Zonal Wind Structure of 39h
m/s
(g) Merid Wind Structure of 38h
(h) Merid Wind Structure of 39h
m/s
(i) Day173-178 E2
(j) Day219-224 E2
e-5
38 h
39 h
Latitude(deg)

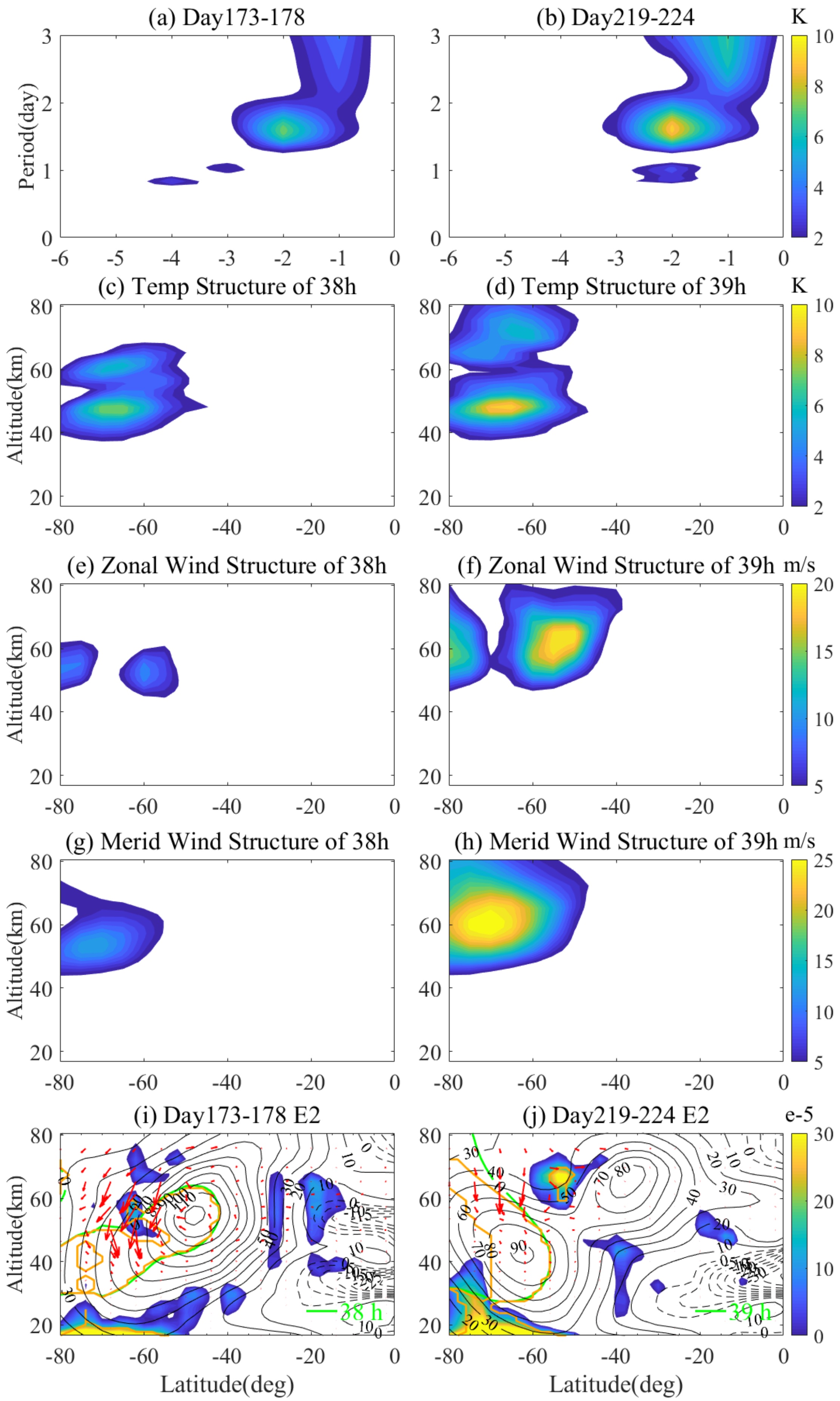
(a) Day173-178
(b) Day219-224
Period(day)
K
(c) Temp Structure of 38h
(d) Temp Structure of 39h
Altitude(km)
(e) Zonal Wind Structure of 38h
(f) Zonal Wind Structure of 39h
m/s
(g) Merid Wind Structure of 38h
(h) Merid Wind Structure of 39h
(i) Day173-178 E2
(j) Day219-224 E2
e-5
38 h
39 h
Latitude(deg)

Figure 5. The same as Figure 4 but for the E2 during the 2019 austral winter period.

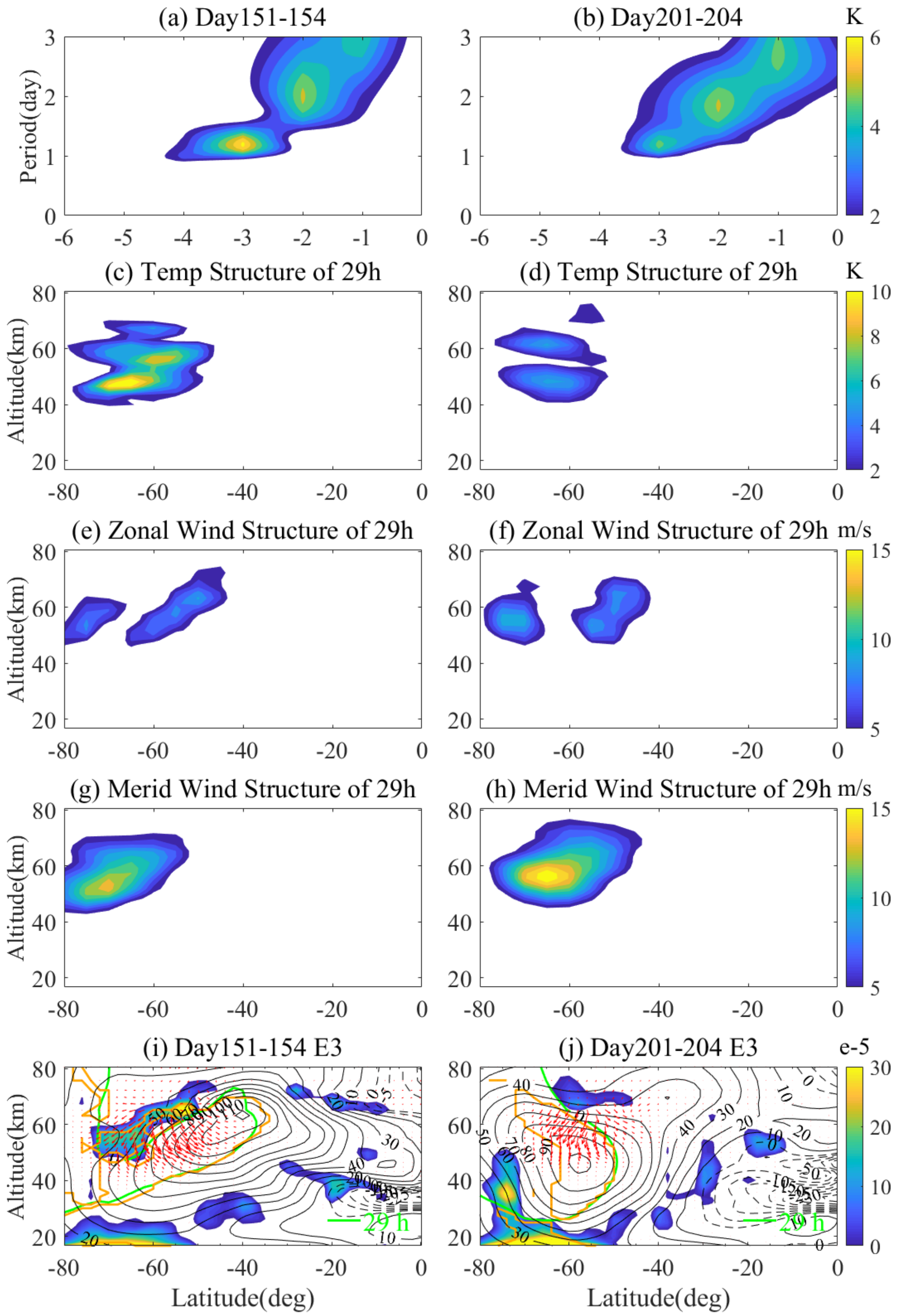

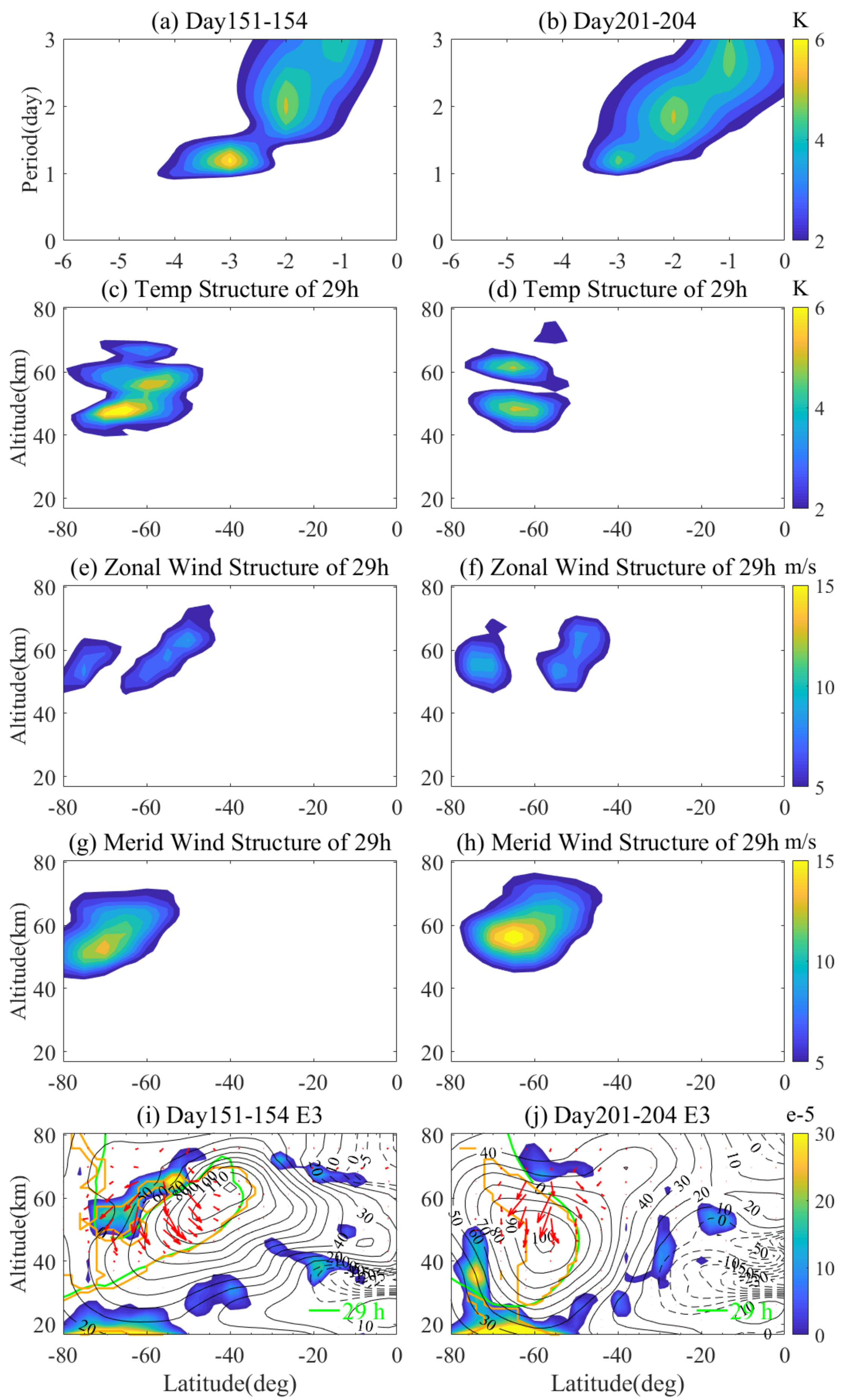
(a) Day151-154
(b) Day201-204
K
Period(day)
(c) Temp Structure of 29h
(d) Temp Structure of 29h
(e) Zonal Wind Structure of 29h
(f) Zonal Wind Structure of 29h
m/s
(g) Merid Wind Structure of 29h
(h) Merid Wind Structure of 29h
(i) Day151-154 E3
(j) Day201-204 E3
e-5
29 h
Altitude(km)
Latitude(deg)

Figure 6. The same as Figure 4 but for the E3 during the 2019 austral winter period.

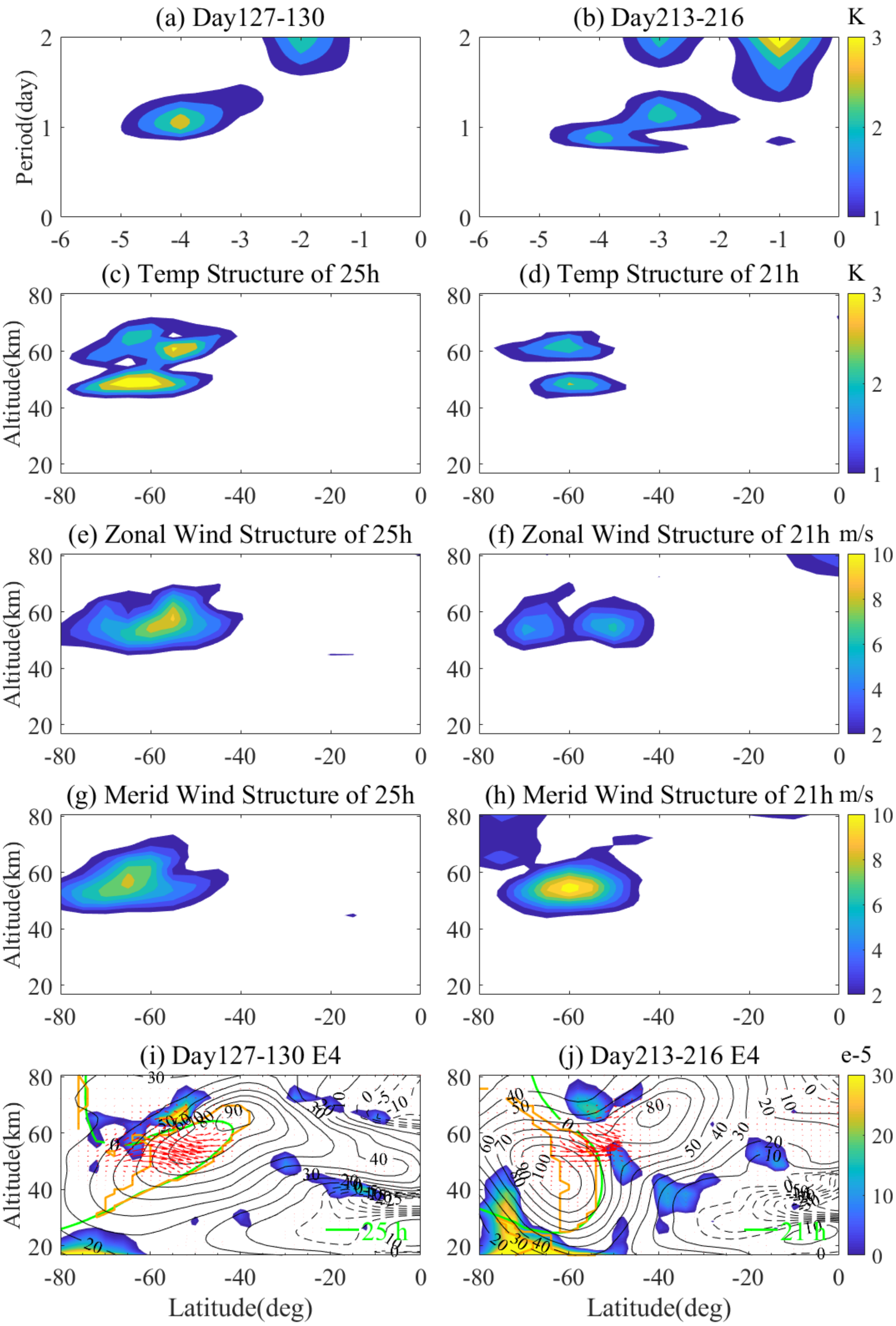

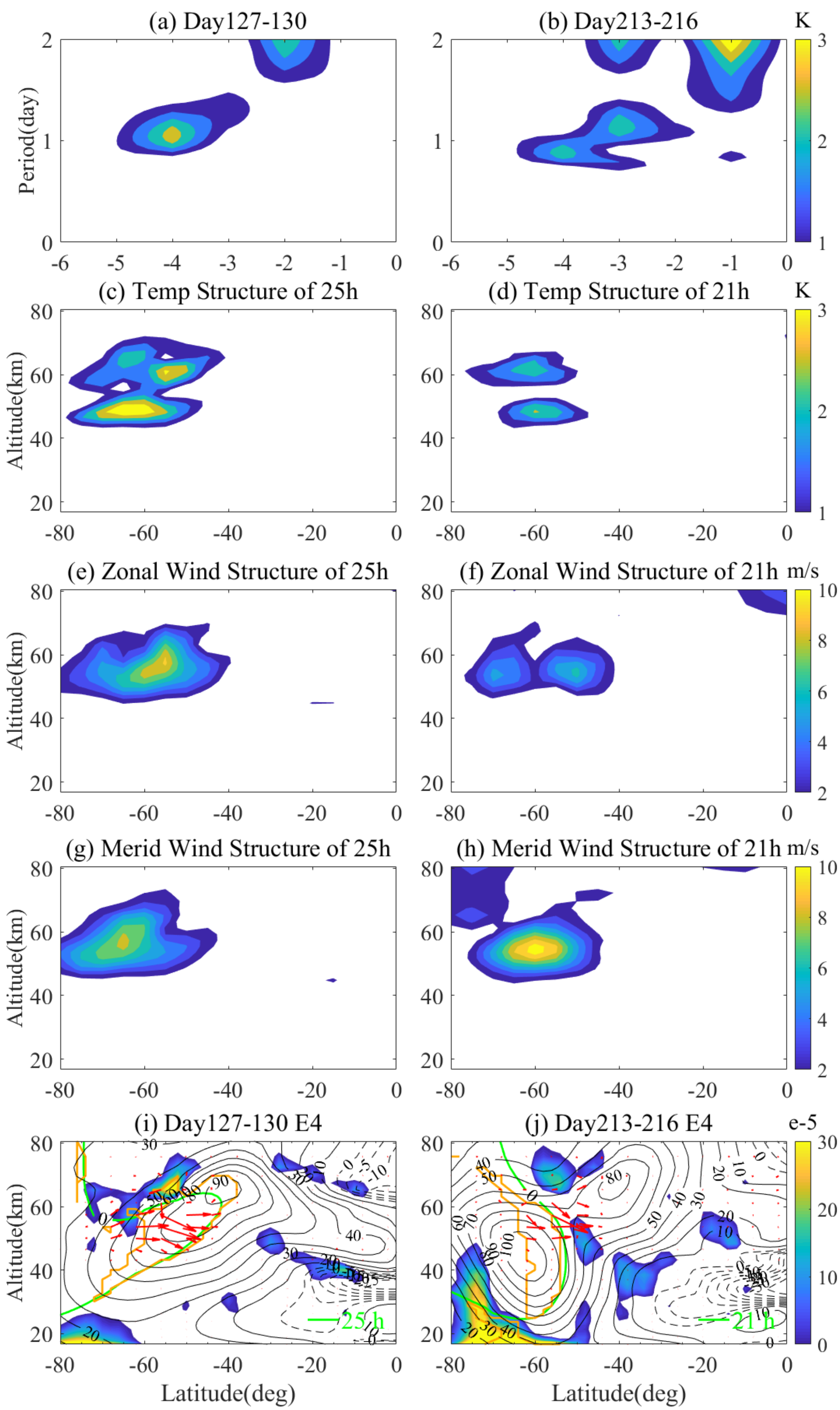
(a) Day127-130
(b) Day213-216
K
Period(day)
(c) Temp Structure of 25h
(d) Temp Structure of 21h
K
(e) Zonal Wind Structure of 25h
(f) Zonal Wind Structure of 21h
m/s
(g) Merid Wind Structure of 25h
(h) Merid Wind Structure of 21h
m/s
(i) Day127-130 E4
(j) Day213-216 E4
e-5
Altitude(km)
Latitude(deg)
25 h
21 h

Figure 7. The same as Figure 4 but for the E4 during the 2019 austral winter period.

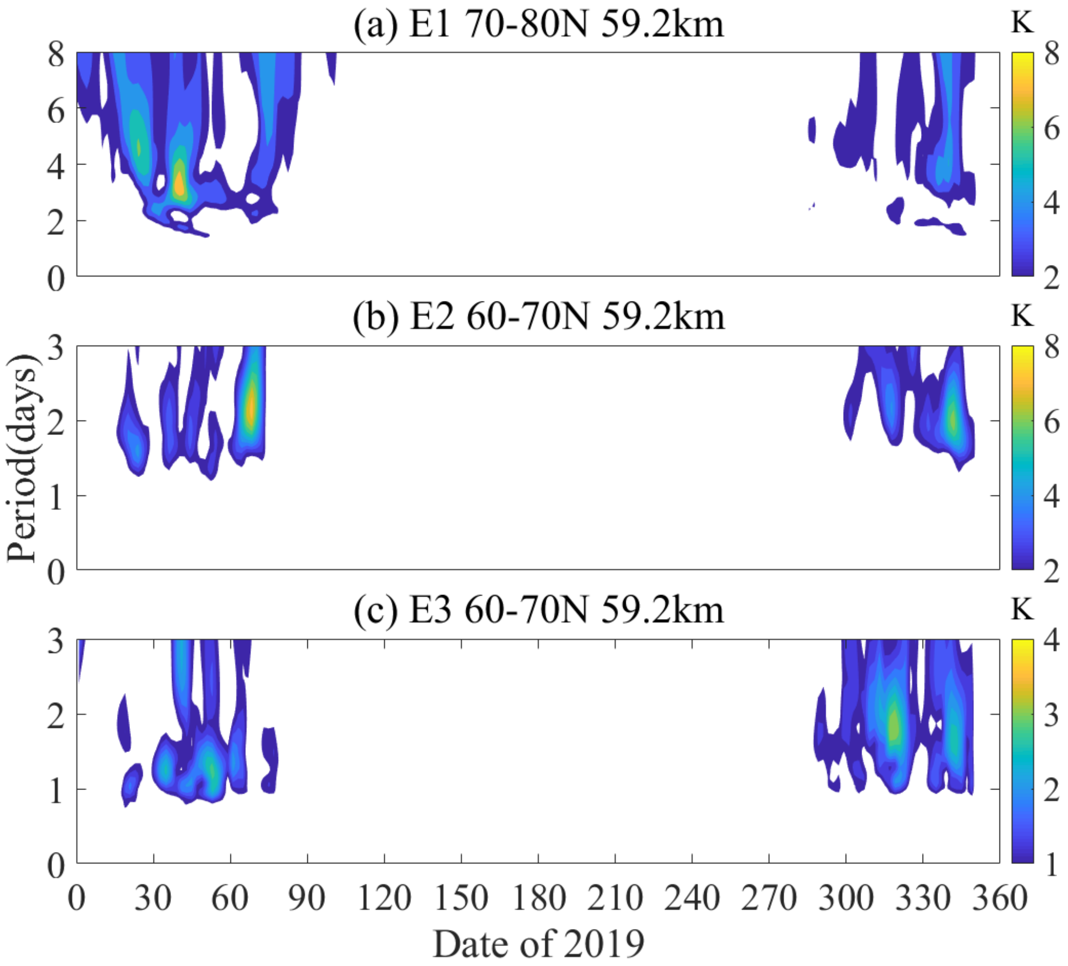

Figure 8. The temporal variations of the (a) E1, (b) E2, and (c) E3 QTDWs during the 2019 boreal winter period.

1043

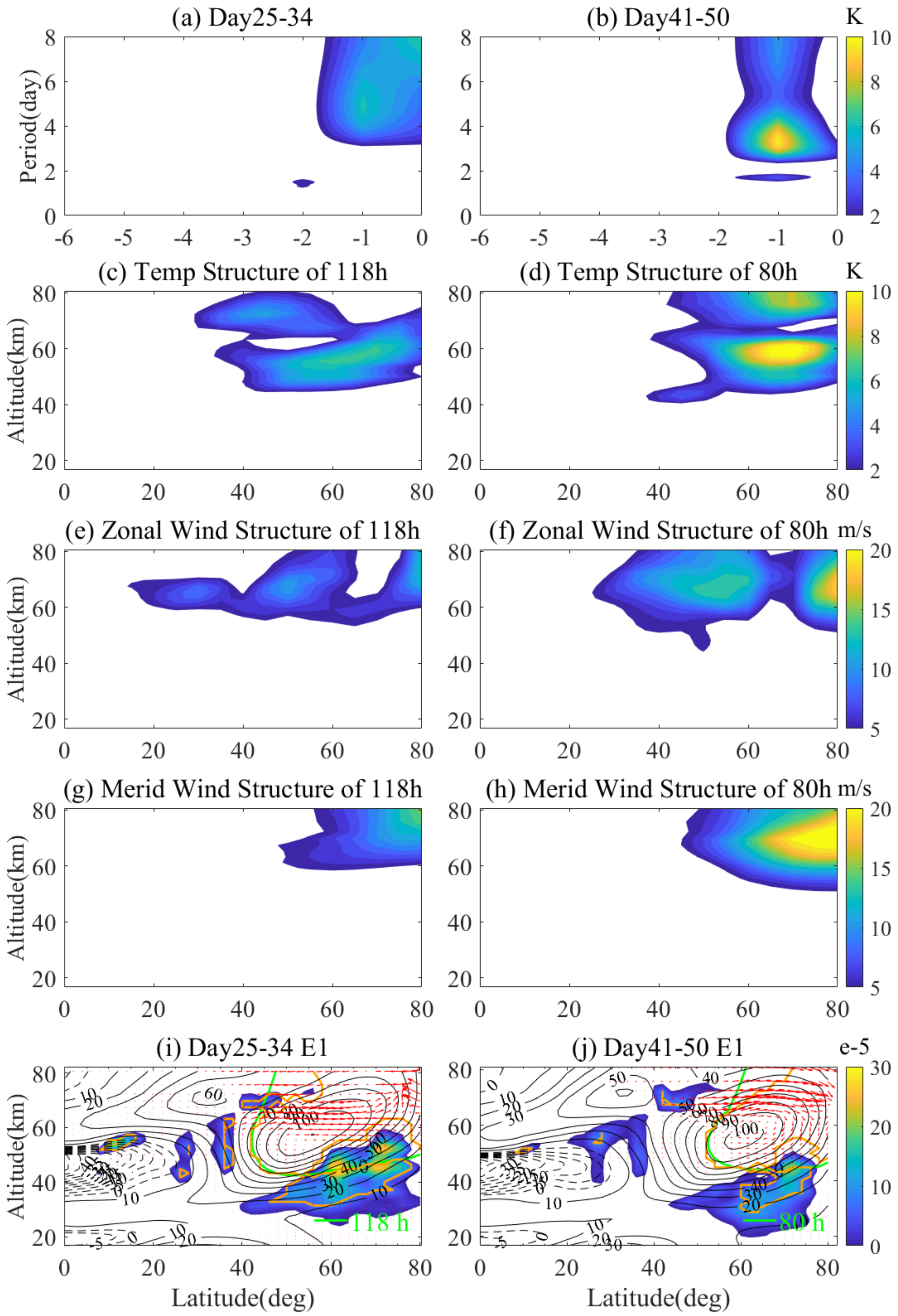

(a) Day25-34
(b) Day41-50
K
Period(day)
(c) Temp Structure of 118h
(d) Temp Structure of 80h
K
Altitude(km)
(e) Zonal Wind Structure of 118h
(f) Zonal Wind Structure of 80h
m/s
(g) Merid Wind Structure of 118h
(h) Merid Wind Structure of 80h
m/s
(i) Day25-34 E1
(j) Day41-50 E1
e-5
118 h
80 h
Latitude(deg)

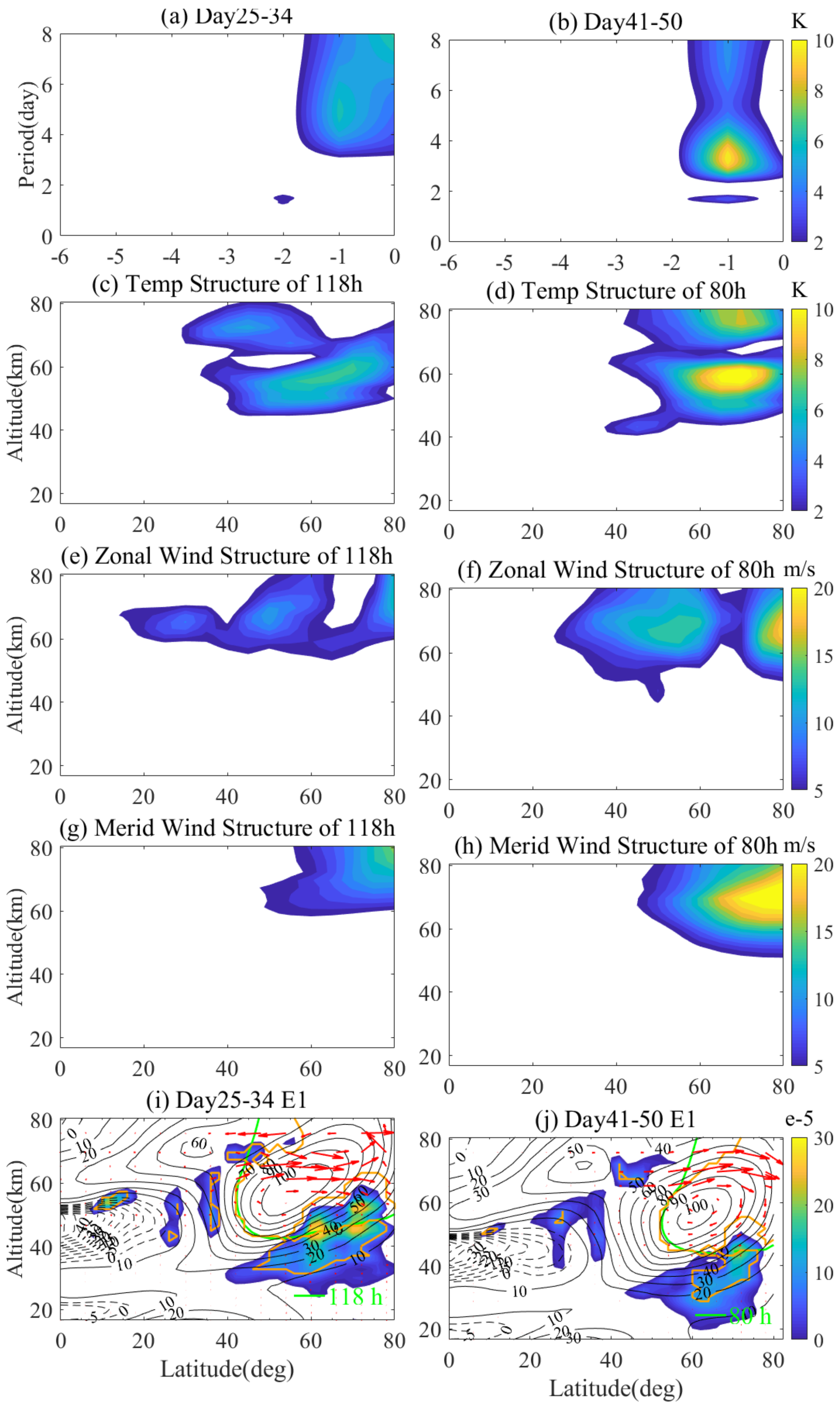
(a) Day25-34
Period(day)
(b) Day41-50
K
(c) Temp Structure of 118h
Altitude(km)
(d) Temp Structure of 80h
K
(e) Zonal Wind Structure of 118h
Altitude(km)
(f) Zonal Wind Structure of 80h
m/s
(g) Merid Wind Structure of 118h
Altitude(km)
(h) Merid Wind Structure of 80h
m/s
(i) Day25-34 E1
Altitude(km)
118 h
Latitude(deg)
(j) Day41-50 E1
e-5
80 h
Latitude(deg)

Figure 9. he (a, b) spectra, (c, d) temperature spatial structures, (e, f) zonal wind spatial structures, (g, h) meridional wind spatial structures, and (i, j) diagnostic analysis of the E1 typical events during 2019 boreal winter period. The E1 events at 48.2km and 70-80˚N were obtained from the MERRA-2 reanalysis.

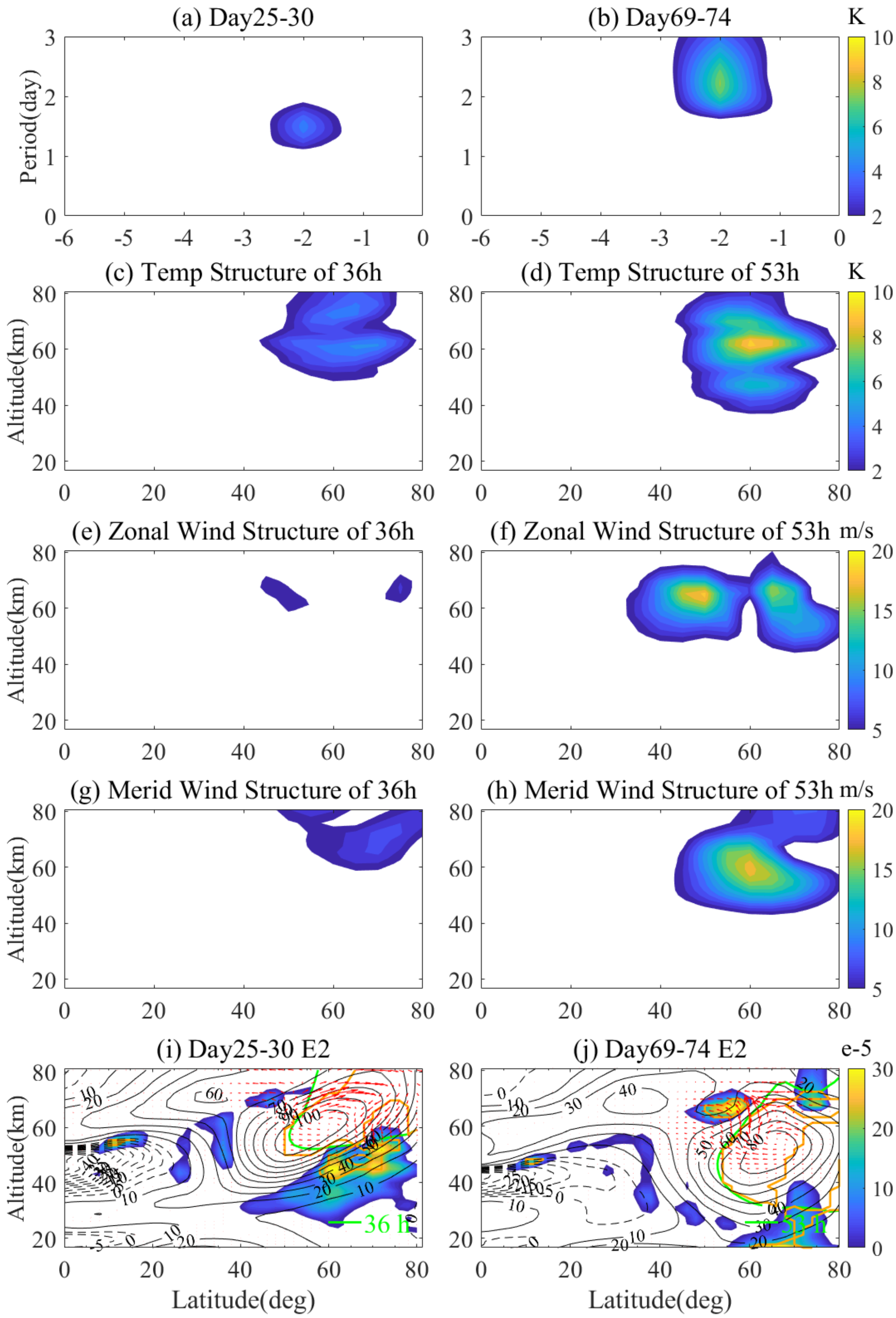
(a) Day25-30
(b) Day69-74
K
Period(day)
(c) Temp Structure of 36h
(d) Temp Structure of 53h
K
Altitude(km)
(e) Zonal Wind Structure of 36h
(f) Zonal Wind Structure of 53h
m/s
(g) Merid Wind Structure of 36h
(h) Merid Wind Structure of 53h
m/s
(i) Day25-30 E2
(j) Day69-74 E2
e-5
36 h
Latitude(deg)

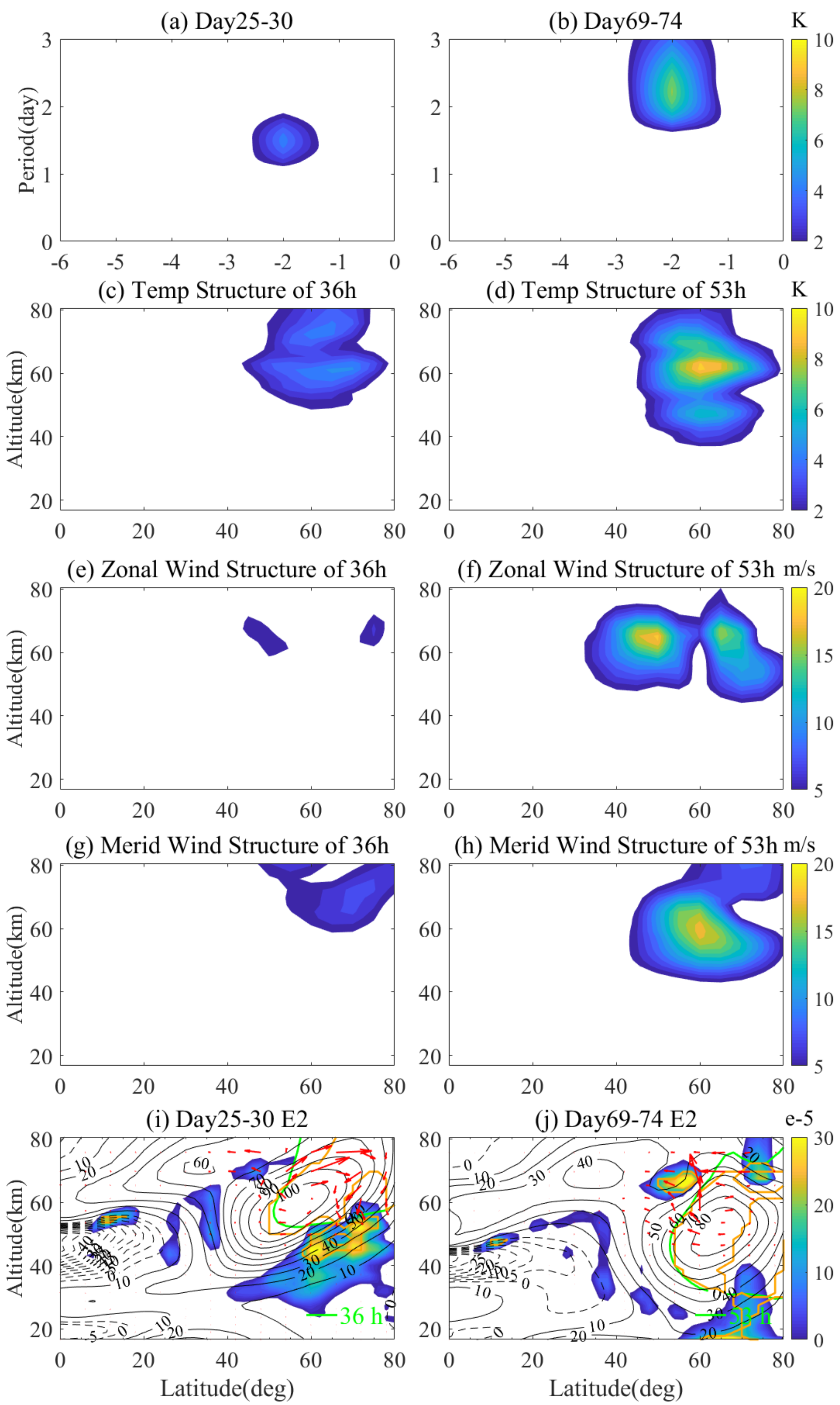

(a) Day25-30
(b) Day69-74
K
Period(day)
(c) Temp Structure of 36h
(d) Temp Structure of 53h
K
(e) Zonal Wind Structure of 36h
(f) Zonal Wind Structure of 53h
m/s
(g) Merid Wind Structure of 36h
(h) Merid Wind Structure of 53h
m/s
(i) Day25-30 E2
(j) Day69-74 E2
e-5
36 h
Altitude(km)
Latitude(deg)

Figure 10. The same as Figure 9 but for the E2 during the 2019 boreal winter period.

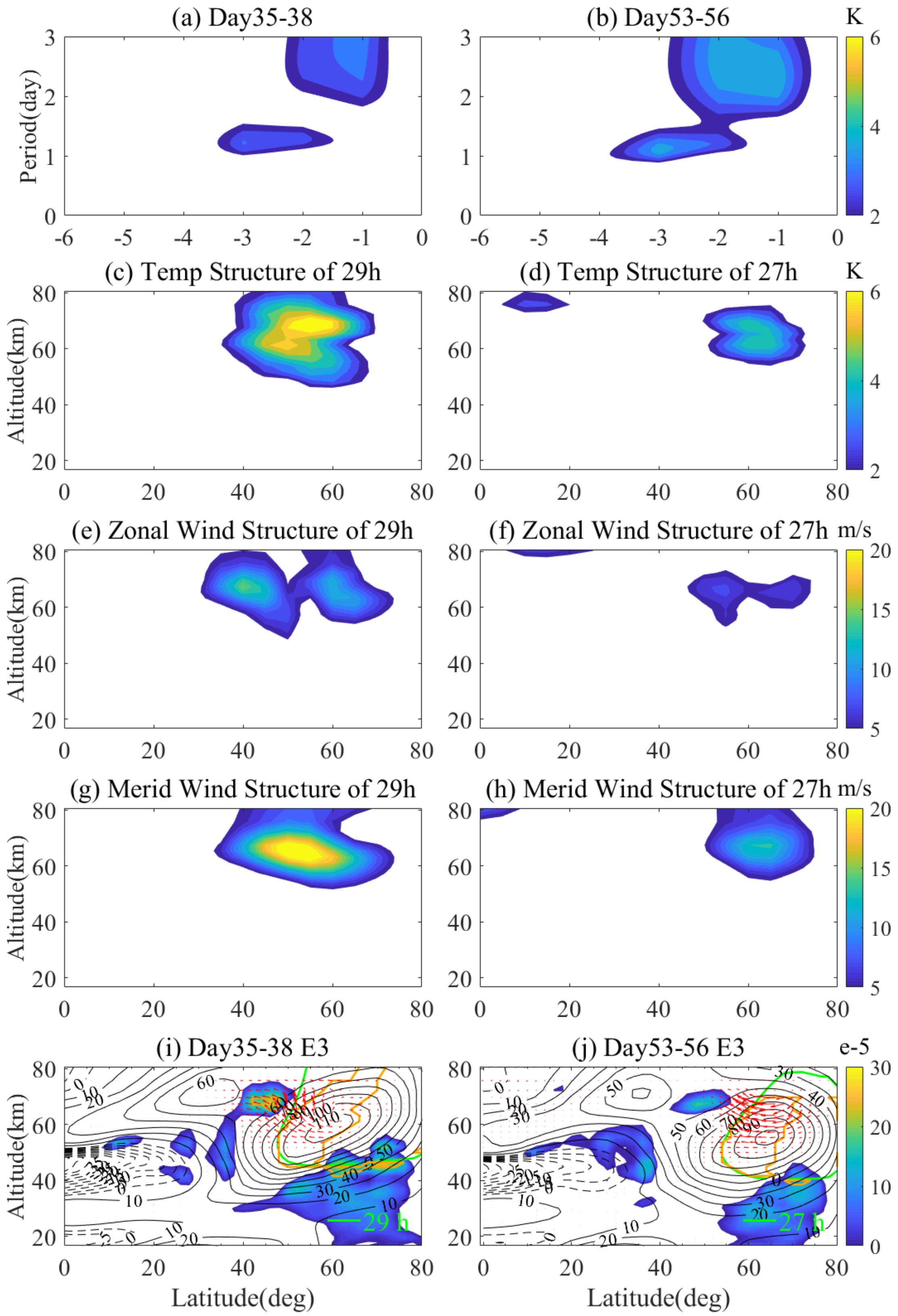

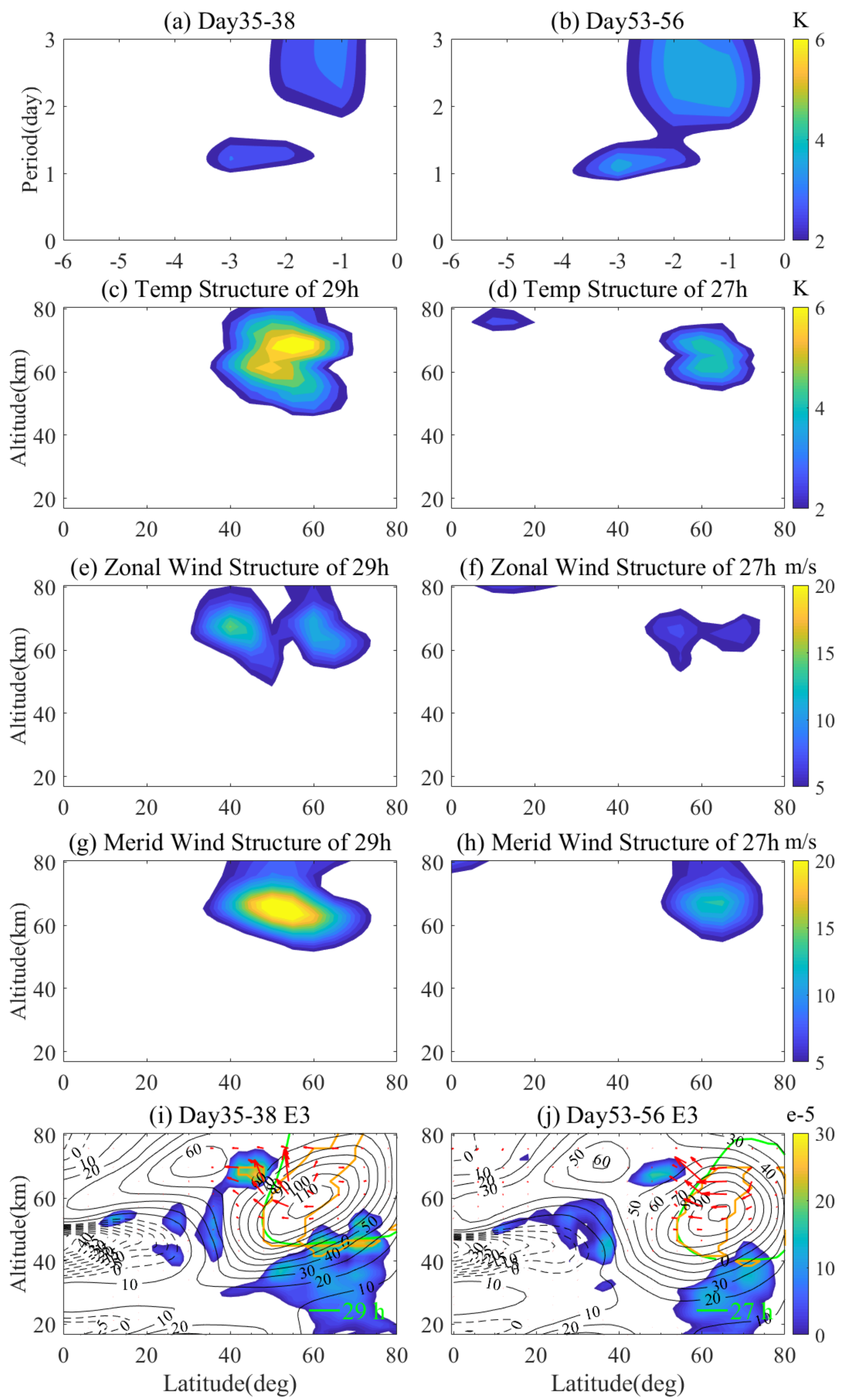
(a) Day35-38
(b) Day53-56
K
Period(day)
(c) Temp Structure of 29h
(d) Temp Structure of 27h
K
(e) Zonal Wind Structure of 29h
(f) Zonal Wind Structure of 27h
m/s
(g) Merid Wind Structure of 29h
(h) Merid Wind Structure of 27h
m/s
(i) Day35-38 E3
(j) Day53-56 E3
e-5
29 h
27 h
Altitude(km)
Latitude(deg)

Figure 11. The same as Figure 9 but for the E3 during the 2019 boreal winter period.

Eastward-propagating planetary wave in the polar middle atmosphere

Abstract. According to MERRA-2 temperature and wind datasets in 2019, this study~~We~~ presented the global variations of the eastward propagating wavenumber 1 (E1), 2 (E2), 3 (E3)~~,~~ and 4 (E4) planetary waves (PWs) and their diagnostic results in the polar middle atmosphere~~, using MERRA-2 temperature and wind datasets in 2019. It is clearly shown that~~. We clearly demonstrated the eastward wave modes exist during winter periods with westward background wind in both hemispheres. The maximum wave amplitudes in the southern hemisphere (SH) are slightly larger and lie lower than those in the northern hemisphere (NH). Moreover,~~It is also found that~~ the wave perturbations peak at lower latitudes with smaller amplitude as the wavenumber increases. The period of the E1 mode varies ~~from 3 to~~ 3-5 days in both hemispheres, while the period of E2 mode is slightly longer in the NH (~48 h) than in the SH (~40 h). The periods of the E3 are ~30 h in both SH and NH, and the period of E4 is ~24 h. Despite the shortening of~~Though the~~ wave periods with the increase of~~become shorter as the~~ wavenumber~~ increases~~, their mean phase speeds are relatively stable, which are ~53 m/s, ~58 m/s, ~55 m/s~~,~~ and ~52 m/s at 70° latitudes for W1,

W2, W3~~,~~ and W4, respectively. The eastward PWs occur earlier with increasing zonal wavenumber, which agrees well with the seasonal variations of the critical layers generated by the background wind. Our diagnostic~~Diagnostic~~ analysis also indicated~~shows~~ that the mean flow instability in the upper stratosphere and upper mesosphere might~~may both~~ contribute to the amplification of the eastward PWs.

1 Introduction

The dominance of large~~Large~~ amplitude planetary waves ~~are dominant~~ in the stratosphere, mesosphere~~,~~ and lower thermosphere regions~~region~~ and their interactions~~interaction~~ with zonal mean winds ~~is~~are the primary driving force of atmospheric dynamics. In addition, sudden stratospheric warmings (SSWs) and quasi-biennial oscillation (QBO) events can dynamically couple the entire atmosphere from the lower atmosphere to the ionosphere (Li et al., 2020; Yamazaki et al., 2020; Yadav et al., 2019; Matthias and Ern, 2018; Stray et al., 2015). Westward propagating planetary wave is one of the prominent features during austral and boreal summer. Westward quasi-2-day waves (Q2DWs) are the most obvious representative waves and one of the most investigated phenomena using~~by~~ planetary wave observations. Most of the previous studies focused on the westward propagating Q2DWs, i.e.,~~including~~ zonal wavenumbers of 2 (W2), 3 (W3)~~,~~ and 4 (W4) modes (Lainer et al., 2018; Gu et al., 2018b; Wang et al., 2017; Pancheva et al., 2016; Gu et al., 2016a; Gu et al., 2016b; Lilienthal and Jacobi, 2015; Gu et al., 2013; Limpasuvan and Wu, 2009; Salby, 1981). However, limited studies were conducted to understand the seasonal~~Seasonal~~ variations of the occurrence date, peak amplitude~~,~~ and wave period for the eastward Q2DWs ~~are rarely studied~~ (Gu et al., 2017; Lu et al., 2013; Alexander and Shepherd, 2010; Sandford et al., 2008; Palo et al., 2007; Merzlyakov and

Pancheva, 2007; Manney and Randel, 1993; Venne and Stanford, 1979).

Typically, Q2DWs ~~usually~~ maximize after the summer solstice in the middle latitudes. The largest wave amplitudes ~~are~~ generally appear~~observed~~ near the mesopause in January–February in the Southern Hemisphere (SH), while in the Northern Hemisphere (NH) in July–August (Tunbridge et al., 2011). W3 and W4 Q2DWs reach amplitudes during austral and boreal summer in the mesosphere and lower thermosphere, respectively. The seasonal variation of westward Q2DWs activity ~~has an~~is obvious~~ seasonal variation~~ (Liu et al., 2019; Gu et al., 2018b; Rao et al., 2017). By observing the long-term Q2DW in the NH and SH, Tunbridge et al. (2011) ~~have observed long-term Q2DW in the NH and SH, and found~~reported that W3 is generally stronger than the other two modes in the SH, reaching the amplitude of ~12K;~~,~~ while W4 is stronger than W3 in the NH, reaching ~4K. Moreover~~In addition~~, W4 ~~is~~ generally lives longer ~~lived~~ than W3, and W4 can~~is~~ still be observed after the ending of W3~~ has ended~~. A previous study has demonstrated~~The results of Liu et al. (2004) show~~ that wave source, instability, critical layer~~,~~ and mean zonal wind are the primary reasons for the seasonal variation of Q2DWs (Liu et al., 2004). By studying the long-term satellite datasets in the SH, Gu et al. (2019) ~~have the long-term observation of satellite datasets in the SH and found~~suggested that the strongest events of W2, W3~~,~~ and W4 could be~~are~~ delayed with increasing the zonal wavenumber, and these events would be indistinguishable during SSWs. ~~Then~~The wave periods of W4, W3 and W2 vary ~~between~~around ~41-56 h, ~45-52 h, and ~45-48 h, respectively. Furthermore~~In addition~~, W2 can be observed using~~in~~ global satellite datasets, but it has an~~showing weaker~~ amplitude weaker than W3 and W4 in the NH and SH (Meek et al., 1996). The propagation and amplification of Q2DWs are primarily modulated by instability, refractive index~~,~~ and critical layer, while the variation of background wind may cause different zonal wavenumber events (Gu et al., 2016a; Gu et al., 2016b). By analyzing the variation of Q2DWs activity during SSWs, Xiong et al. (2018) ~~studied variations in Q2DWs activity during SSWs and found~~noticed that W1 is generated by the nonlinear interaction between SPW2 and W3. During SSWs, ~~Gu et al. (2018b) found that~~ the coupling between the NH and SH can enhance~~enhanced~~ the summer easterly ~~during SSWs~~ and promote~~promoted~~ the nonlinear interaction between W3 and SPW1 ~~during SSWs~~(Gu et al., 2018b).

Some recent~~Recent~~ studies have discovered~~found~~ significant eastward planetary waves in the polar stratosphere and mesosphere regions, with periods of nearly ~~2~~two and ~~4~~four days (Gu et al., 2017; Sandford et al., 2008; Merzlyakov and Pancheva, 2007; Coy et al., 2003; Manney and Randel, 1993). Planetary waves with zonal wavenumbers -1 (E1) and -2 (E2) correspond to 4- and 2-day waves, respectively. ~~In~~

~~addition~~Furthermore, planetary waves of 1.2-day with wavenumber -3 (E3) and 0.8-day with wavenumber -4 (E4) have been reported to contain~~found to have~~ the same phase speeds as E1 and E2 (Manney and Randel, 1993). This series of eastward planetary wave can significantly affect~~has a significant effect on~~ the thermal and dynamic structure of the polar stratosphere, resulting in profound~~significant~~ changes in the wind and temperature of the polar stratosphere (Coy et al., 2003; Venne and Stanford, 1979). Beyond the knowledge about ~~Palo et al. (1999) demonstrated a series of~~ nonlinear interactions between migrating tides and Q2DWs (Palo et al., 1999), further investigation has confirmed~~.~~ ~~Further research, Palo et al. (2007) presented evidence~~ that E2 Q2DW is coupled by nonlinear planetary wave and tides in the mesosphere and lower thermosphere (Palo et al., 2007).

By studying and analyzing satellite datasets, Merzlyakov and Pancheva. (2007) indicated~~analyzed and studied satellite datasets and found~~ that the wave periods of E1 and E2 events range~~is within~~ 1.5-5 days. They reported~~found~~ that EP flux travels~~is~~ from the upper ~~layer~~ to the lower atmosphere, meaning~~suggesting~~ that the upper atmosphere has a dynamic influence on the lower atmosphere. Sandford et al. (2008) reported about significant fluctuations of E2 Q2DW in the polar mesosphere. They ~~found~~indicated the influence of~~that~~ changes in mean zonal winds during a major SSW on~~influenced~~ the propagation of polar

E2. In addition, they proposed~~believe that~~ the significance of E2 fluctuation ~~is representative~~ in the mesosphere ~~and caused~~driven by the instabilities in the polar night jet. ~~Gu et al. (2017) found that the~~For E2, amplitude of ~~E2~~ temperature, zonal wind and meridional wind during the austral winter can reach ~10 K, ~20 m/s~~,~~ and ~30 m/s, respectively;~~ in temperature, zonal wind, and meridional wind in the austral winter,~~ while those during the boreal winter can drop by almost~~the amplitude of E2 decreases by near~~ two-thirds~~ in the boreal winter~~. Lu et al. (2013) found that eastward planetary wave propagation is~~was~~ limited to the winter high latitudes~~, which may be~~ probably because the negative refractive indices equatorward of ~45°S result in evanescent wave characteristics~~, thus preventing the propagation of planetary wave to low latitudes~~. That study suggested that~~They believe that~~ the instability region at ~50-60°S might~~may~~ be induced by the stratospheric polar night jet and/or the "double-jet" structure.

In this study, we use the~~The~~ second modern retrospective research and application analysis (MERRA-2) datasets ~~are used~~ to investigate the eastward propagating wave characteristics in the polar stratospheric and mesospheric region ~~during~~in 2019, including E1, E2, E3 and E4. Specifically~~Particularly~~, we investigate the variation of the occurrence date, peak amplitude~~,~~ and wave period of eastward waves;~~,~~ as well as the role of instability, background wind structure~~,~~ and critical layer in the propagation and amplification of eastward waves. The remaining parts of this paper are organized as follows. ~~In~~ Section 2 describes~~,~~ the data and methods used in this~~our~~ study~~ are described~~. ~~In~~ Section 3 analyzes the global latitude-temporal variation structure of eastward waves ~~in~~during winter~~the~~ in 2019~~ winter~~. The amplification and propagation features of the eastward planetary waves in the NH and SH with different wavenumber events are examined~~investigated~~ in Sections~~Section~~ 3.1 and 3.2, respectively. ~~In~~ Section 3.3 compares and analyzes the eastward waves in the NH and SH. ~~In Section 4 summarizes our~~All research results are summarized in Section 4.

2 Data and Analysis

The least-square method is applied to each time window to extract the E1-, E2-, E3-~~,~~ and E4-wave, with 10-day, 6-day, 4-day, and 4-day, and is used by us to determine the amplitude (Gu et al., 2013). This method has been shown to~~previously been used~~ successfully ~~to~~ identify planetary waves from satellite measurements (Gu et al., 2019; Gu et al., 2018a; Gu et al., 2018b; Gu et al., 2018c; Gu et al., 2013).

$$y = A\cos[2\pi(\sigma\cdot t + s\cdot\lambda)] + B\sin[2\pi(\sigma\cdot t + s\cdot\lambda)] + C \qquad (1)$$

The least-squares method is used to fit the a set of parameters ~~of~~ (~~A, B,~~ A, B and C)~~,~~. ~~Where~~ where ~~(σ, t, s,~~ σ, t, s and λ~~)~~ are the frequency, UT time, zonal wavenumber~~,~~ and longitudes. The amplitude of wave R can~~could~~ be expressed as $R=\sqrt{A^2+B^2}$.

The second modern retrospective research and application analysis (MERRA-2) covers the ~~data is a set of~~ long-term atmospheric reanalysis datasets ~~started~~initiated by NASA in 1980~~, and now using an~~. It has been upgraded recently using~~version of~~ the Goddard Earth Observing System Model, Version 5 (GEOS-5) data assimilation system. Briefly, MERRA-2 includes some updates to the model (Molod et al., 2014; Molod et al., 2012) and the Global Statistical Interpolation (GSI) analysis scheme of Wu et al. (2002). The MERRA-2 data consist of~~includes~~ various meteorological variables, ~~such as~~e.g., net radiation, temperature, relative humidity~~,~~ and wind speed~~, etc~~. The spatial coverage of MERRA-2 data is the globe~~covers the world, with a~~ (spatial resolution: ~~of~~ 0.5°~~*~~×0.625°; ~~and a~~ temporal resolution: ~~of~~ 1 h~~hour~~). This ~~kind of~~ meteorological data ~~is~~are widely used to detect the middle atmosphere such as the planetary wave in the polar atmosphere, global thermal tides, climate variability~~,~~ and aerosol (Ukhov et al., 2020; Sun et al., 2020; Bali et al., 2019; Lu et al., 2013). ~~These~~Many recent studies indicated~~indicate that~~ the feasibility of using MERRA-2 data for the kind of research in present study~~can be used in our research with high authenticity~~. Therefore, we apply the~~The~~ MERRA-2 datasets ~~are used~~ to obtain the variation in background wind, instability, refractive index~~,~~ and critical layer;~~,~~ and explore the rules of eastward planetary waves propagation and amplification through diagnostic analysis.

The critical layer will absorb or reflect planetary waves ~~during upward propagation~~ from the lower atmosphere during upward propagation. Planetary waves that gain sufficient energy in the instability region will be amplified during reflection. In a sense,~~This shows that~~ the critical layer plays an important role in regulating the amplification and propagation of planetary waves (Gu et al., 2016a; Gu et al., 2016b; Liu et al., 2004).

$$\overline{q_\varphi} = 2\Omega\cos\varphi - \left(\frac{\left(\bar{u}\cos\varphi\right)_\varphi}{a\cos\varphi}\right)_\varphi - \frac{a}{\rho}\left(\frac{f^2}{N^2}\rho\bar{u}_z\right)_z \qquad (2)$$

The baroclinic/barotropic instability in the atmospheric space structure is caused by the simultaneous equalization of the negative latitude gradient and the quasi-geostrophic potential vorticity ($\overline{q_\varphi}$). In Equation (2), ~~where (~~ Ω ~~)~~ ~~denote~~is the angular speed of the Earth's rotation;~~,~~ φ is the latitude; $\bar{u}$ is the~~and the latitude and~~ zonal mean zonal wind;~~ are represented by (~~φ ~~and~~ $\bar{u}$~~), in the second part, the (~~ a ~~)~~ is the~~represents~~ the Earth radius;~~, in the last part, (~~ρ, f, ~~and~~ N~~) denote the background~~ ρ is the air density;~~,~~ f is the Coriolis parameter;~~,~~ N~~and~~ is the buoyancy frequency;~~, respectively.~~ subscripts z and φ~~The~~ are the vertical and latitudinal gradients.~~ are represented by subscripts (~~z ~~and~~ φ~~).~~

According to Andrews et al. (1987), the properties of planetary wave propagation can be calculated using ~~define~~ the Eliassen-Palm (EP) flux vectors (F), i.e.,~~ to show the properties of planetary wave propagation,~~

~~calculated as follows:~~

$$F = \rho a\cos\varphi \begin{bmatrix} \dfrac{\overline{u}_z \overline{v'\theta'}}{\overline{\theta}_z} - \overline{v'u'} \\ \left[f - \dfrac{\left(\overline{u}\cos\varphi\right)_\varphi}{a\cos\varphi}\right] \dfrac{\overline{v'\theta'}}{\overline{\theta}_z} - \overline{w'u'} \end{bmatrix} \tag{3}$$

where u' and v' are the planetary wave perturbations in the zonal and meridional wind, respectively;~~,~~ θ' and w' are~~represent~~ the potential temperature and vertical wind, respectively. The planetary wave propagation is only favorable where the square of refractive index m^2 is~~was~~ positive:

$$m^2 = \frac{\overline{q}_\varphi}{a\left(\overline{u}-c\right)} - \frac{s^2}{\left(a\cos\varphi\right)^2} - \frac{f^2}{4N^2H^2} \tag{4}$$

where ~~(~~ s ~~)~~ ~~denote~~is the zonal wavenumber, c is the phase speed~~ is represented by (c)~~, and ~~the (~~ H ~~)~~ ~~represents~~is the scale height. The square of the refractive index is taken as the waveguide of planetary waves, i.e.,~~:~~

$$c = -\upsilon_0 \cos\left(\frac{\varphi\pi}{180}\right) \Big/ sT \tag{5}$$

where ~~(c) denote the phase speed,~~ υ_0 is the equatorial linear velocity~~ is represented by (υ_0), and the (φ) represents the latitude~~, s is the zonal wavenumber and T ~~represent zonal wavenumber and~~is the wave period.~~, respectively.~~

3 Results and Discussion

Figure 1 shows the~~The~~ global temporal-latitude variation structures of E1, E2, E3~~,~~ and E4 extracted from the 2019 MERRA-2 temperature datasets using time windows ~~of~~ 10-, 6-, 4- and 4-days, respectively ~~are shown in Figure 1~~. The mean temperature amplitude~~amplitudes~~ of E1, E2, E3~~,~~ and E4 at 55.4 km during the periods ~~of~~ 3~5-, 1.5~2.5-, 1~1.5-~~,~~ and 0.9~1.1-day~~s~~ are displayed~~shown~~ in Figure 1a, 1b, 1c~~,~~ and 1d, respectively. Eastward waves are characterized by obvious seasonal variations in the SH and NH. In addition, E1, E2 (E3)~~,~~ and E4 reach their maximum amplitude~~amplitudes~~ at 50-80°(S/N). In the SH, the strongest E1 and E2 events occur on days 209-218 and 167-172;~~,~~ while E3 and E4 events occur on days 151-154 and 139-142. This means~~shows~~ that their occurrence date of maximum amplitude gets~~occurs~~ earlier with increasing zonal wavenumber. In addition, the maximum amplitude~~amplitudes~~ of E1, E2, E3~~,~~ and E4 are ~6.0 K, ~4.2 K, ~3.6 K~~,~~ and ~2.4 K, respectively, indicating that their peak amplitude~~amplitudes~~ drop with rising~~decrease with increasing~~ zonal wavenumber. In the NH, the strongest E1, E2, E3 and E4 events occur on days 41-50, 69-74, 35-38 and 63-66, respectively; ~~and~~ the corresponding peak amplitude~~amplitudes~~ are ~5.5 K, ~3.8 K, ~2.8 K and ~1.2 K, respectively. Whilst the~~The~~ results demonstrate~~show~~ the decline of~~that~~ the peak amplitude ~~decreases~~ with increasing zonal wavenumber in the NH, ~~but~~ the occurrence date is irregular. Moreover~~In addition~~, E4 is relatively weak in the NH and difficult~~almost impossible~~ to find, so W4 is insignificant~~out of the discussion~~ in the NH. Figure 2 presents~~shows~~ the changes in zonal mean zonal wind at 70°S and 70°N in

2019. It can be seen~~is found~~ that the background wind on days 90-240 (70˚S) is dominated by westward wind, and reaches~~reached~~ ~80 m/s at ~50 km on days 210;~~, while~~ it is dominated by eastward wind in late and early 2019, and reaches ~-40 m/s at ~60 km. Meanwhile, the background wind is primarily westerly wind in late and early 2019 (70˚N), and reaches ~90 m/s at ~60 km on days 50;~~,~~ while on days 120-240, the background wind is primarily easterly wind, and the amplitude reaches -40 m/s on days 200. Compared with Figure 1, the results show that the eastward wave modes exist during winter periods with westward background wind in both hemispheres.

3.1 In the Southern Hemisphere

Figure 3 shows that observed maximum amplitude is at ~~observed to be~~ ~48.2 km and ~70-80°S for E1;~~, and E2 and E3 at~~ ~48.2km and ~60-70°S for E2 and E3;~~, while E4 at~~ ~48.2km and ~50-60°S for E4. ~~The~~For E1, the observed maximum perturbation ~~observed for E1 occur~~ occurs on days 211-220 (with an amplitude of ~8.5 K), and the remaining fluctuations occur on days 161-170, 187-196 and 231-240~~, while the~~. For E2, the observed maximum perturbation happens~~ maximizes~~ at days 219-224 (with an amplitude of ~7.8 K), and ~~also shows~~ three peaks appear on~~at~~ days 139-144, 173-178~~,~~ and 187-192. Regarding E3~~Besides~~, the strongest perturbation~~E3~~ occurs on days 151-154 (with an amplitude of ~5.2 K), while~~and~~ the rest are distributed on days 141-144, 201-204~~,~~

and 209-202. E4 perturbations are distributed on days 127-130, 145-148, 161-164, 213-216, with weak amplitude of ~3 K. Since~~According to~~ earlier~~previous~~ studies mentioned that~~,~~ the wave period of the eastward wave can vary,~~varies. Therefore,~~ we also investigate the periodic variabilities~~variability~~ of E1, E2, E3~~,~~ and E4~~ has also been investigated~~. The results show that the period corresponding to the maximum perturbation of E1 falls between ~106 (days 187-196) and ~69 h (days 211-220), and their wave periods vary significantly~~greatly~~. Nonetheless~~However~~, the wave period of E2 gradually changes from ~42 h (days 139-144) to ~38 h (days 219-224), and its stability is stronger than that of E1. ~~In addition, the~~The wave periods of E3 and E4 are about ~39 h and ~24 h, respectively. These results reflect that~~Thus,~~ E2, E3~~,~~ and E4 wave periods are more stable compared to~~than~~ E1.

The spectra, spatial (vertical and latitudinal) structures of temperature, zonal and meridional wind, and diagnostic analysis of E1 are extracted from the two corresponding ~~two representative~~ events~~,~~ (refer to~~as shown in~~ Figure 4). Figures~~Figure~~ 4a, 4b show~~shows~~ the least-squares fitting spectra for MERRA-2 temperature on days 187–196, 211-220 at ~48.2 km and ~70-80°S, when and where the E1 maximizes. An eastward wavenumber -1 signal with the periods~~period~~ of ~106 h and ~69 h clearly dominates the whole spectrum. The temperature spatial structures~~structure~~ corresponding to these E1 (i.e., ~106 h and ~69 h) are displayed~~is shown~~ in Figures~~Figure~~ 4c, 4d. The temperature spatial structure of E1 exhibits~~presents an~~ obvious amplitude bimodal structure at ~70-80˚S and ~50 km, and ~70-80˚S and ~60 km, with the maximum at ~70-80˚S and ~50 km. The strongest temperature amplitude of E1 occurs at ~50 km and ~70-80˚S with an amplitude of ~10 K on the days 211-220, and the other peak is ~9K (~70-80˚S and ~60 km). The temperature amplitude of ~9K occurs at ~50 km and ~70-80˚S during days 187-196, and the rest is ~7K (~70-80˚S and ~60 km). The corresponding spatial structures of zonal wind and meridional wind of these E1 are~~is~~ shown in Figures 4e, 4f, 4g~~,~~ and 4h. The maximum zonal wind amplitude of E1 occurs at ~60-70˚S and ~60 km with an amplitude of ~14 m/s on days 187-196, and ~20 m/s at ~50-60˚S and ~60 km on days 211-220. The amplitude of E1 meridional wind hits~~reaches~~ ~10 m/s at ~70-80˚S and ~55 km (days 187-196) and ~17 m/s at ~70-80˚S and ~60 km (days 211-220), respectively.

Figures~~Figure~~ 4i, 4j show~~shows~~ the diagnostic analysis results for the E1 events during days 187–196~~,~~ and 211–220, respectively. Apparently,~~It is clear that~~ the EP flux vectors is more favorable to propagate in the SH winter and is dramatically amplified by the mean flow instabilities and appropriate background winds at polar and between ~40 km and ~80 km, with EP flux propagating into the upper atmosphere (Figure 4i). Meanwhile, there is an EP flux at the mid-latitudes and

~60-80 km, which propagates into the lower atmosphere. The wave-mean flow interactions near its critical layer (106 h) of the green curve amplifies E1, and the positive refractive index region surrounded by the yellow curve also enhances E1 propagation. In addition, the strong instability and weak background wind at ~70-80˚S and ~40-60 km provide sufficient energy for the upward EP flux to propagate and amplify. Nevertheless~~However~~, the downward propagating EP flux is amplified by weak instability and strong background wind at ~50-60˚S and ~60-70 km. Besides, both upward and downward EP fluxes~~flux~~ eventually propagate toward the equator at ~50 km. Figure 4j shows that EP flux on days 211-220 propagates downward and amplifies after the interaction of the critical layer (~69 h).~~, f~~ Facilitated by the positive refractive index region, which strong instability and weak background wind at ~50-60˚S and ~60-70 km provide sufficient energy, and ultimately point towards the equator at ~50 km. The results show that the weak background wind and strong instability in the polar region can promote the upward propagation and amplification of ~~the~~ EP flux. Meanwhile, the appropriate background wind and instability in the mid-latitudes~~mid-latitude~~ are also conducive to the downward propagation and amplification of EP flux. In other words, instability and appropriate background wind dominate~~play a dominant role in~~ the propagation and amplification of ~~the~~ E1.

For E2, ~~The~~the spectra are observed at ~48.2 km and ~60-70°S on days 173-178~~,~~ and 219-224~~ for E2,~~ when the eastward wavenumber -2 becomes the primary wave mode with the wave periods~~period of~~ ~38 h and ~39 h, respectively (as shown in Figures~~Figure~~ 5a, 5b). The temperature spatial structures~~structure~~ corresponding to these E2 (~38 h and ~39 h) are~~is~~ presented~~shown~~ in Figures~~Figure~~ 5c, 5d. The temperature spatial structure of E2 shows an obvious amplitude bimodal structure at ~60-70°S and ~50 km, and ~60-70°S and ~60 km, with the maximum at ~60-70°S and ~50 km. The maximum temperature amplitude of E1 occurs at ~50 km and ~60-70°S with an amplitude of ~7.5 K on the days 173-178, and the other peak is ~6 K (~70°S and ~60 km). The temperature amplitude of ~10 K happens~~occurs~~ at ~50 km and ~60-70°S during days 219-224, and the rest is ~6 K (~70°S and ~60 km). The corresponding spatial structures of zonal wind and meridional wind of these E2 are~~is~~ illustrated~~shown~~ in Figures 5e, 5f, 5g~~,~~ and 5h. The zonal wind spatial structure of E2 shows an obvious amplitude bimodal structure at ~50-60°S and ~60 km, and ~70-80°S and ~60 km, with the maximum at ~50-60°S and ~60 km. The maximum zonal wind amplitude~~amplitudes~~ of E2 appear~~occur~~ at ~50-60°S and ~60 km with an amplitude of ~10 m/s on days 173-178, and the other peak is ~9 m/s (~70-80°S and ~60 km). The zonal wind amplitude of ~20 m/s occurs at ~50-60°S and ~60 km on days 219-224, and the rest is ~15 m/s (~70-80°S and ~60 km). The amplitude of E2 meridional wind reaches ~13 m/s at

~70-80˚S and ~60 km (days 173-178) and ~27 m/s at ~70-80˚S and ~60 km (days 219-224), respectively.

~~The results in~~ Figures 5i and 5j illustrate~~show~~ the diagnostic analysis during days 173-178~~,~~ and 219-224 for E2, respectively. Obviously,~~It is clear that~~ E2 is more likely~~favorable~~ to propagate in the SH winter and is dramatically amplified by the mean flow instabilities at the middle-high latitudes between ~40 km and ~80 km.~~, with~~ With EP flux propagating into the lower atmosphere, ~~and EP flux~~it eventually propagates~~propagate~~ toward the equator at ~50 km. Besides, E2 is amplified and propagated by the wave-mean flow interactions near its critical layer (~38 h) of the green curve, and the promoting effect of the positive refractive index region surrounded by the yellow curve. Meanwhile, the weak instability and strong background wind at ~50-60˚S and ~50-70 km provide the energy for the propagation and amplification of EP flux into the lower atmosphere during days 173-178 (Figure 5i). According to~~In~~ the diagnostic analysis of days 219-224, ~~it is found that~~ E2 obtains sufficient energy from strong instability and strong background wind at ~50-60˚S and ~60-70 km~~, and~~. It is amplified and propagated into the lower atmosphere through the critical layer and positive refractive index action~~,~~ (as shown in Figure 5j). The results show that the background wind at ~50-60˚S and ~50-70 km is weaker on days 173-178 than on days 219-224;~~,~~ and the instability at ~50-60˚S and ~60-70 km is stronger on days 219-224 than on days 173-178. ~~According to Figure 5a, 5b~~Our results show~~shows~~ that E2 has absorbed sufficient energy to be amplified under the background conditions during days 219-224 (Figures 5a, 5b).

Figures 6a and 6b show the observed spectra of E3 at ~48.2 km and ~60-70°S on days 151-154 and 201-204, and the wave periods~~period~~ of locked wavenumber -3 are~~is~~ ~29 h and ~29 h, respectively. The corresponding temperature spatial structures of these E3 (i.e., ~29 h and ~29 h) are displayed~~ is shown~~ in Figures~~Figure~~ 6c, 6d. The temperature spatial structure of E3 shows an obvious amplitude bimodal structure at ~60-70˚S and ~50 km, and ~60-70˚S and ~60 km, with the maximum at ~60-70˚S and ~50 km. Besides, E3 also has a weak peak at ~60-70˚S and ~70 km. The strongest temperature amplitude of E3 occurs at ~50 km and ~60-70˚S with an amplitude of ~6K on the days 151-154, and the other peak is ~5 K (~60-70˚S and ~60 km). The temperature amplitude of ~5 K happens~~occurs~~ at ~50 km (~60 km) and ~60-70˚S during days 201-204. The corresponding spatial structures of zonal wind and meridional wind of these E3 ~~is~~are shown in Figures 6e, 6f, 6g~~,~~ and 6h. The zonal wind spatial structure of E3 shows an obvious amplitude bimodal structure at ~70-80˚S and ~60 km, and ~50-60˚S and ~60 km. The zonal wind amplitudes of E3 occur at ~70-80˚S and ~60 km (~50-60˚S and ~60 km) with an amplitude of ~9 m/s on days 151-154, and ~9 m/s at ~70-80˚S and ~60 km (~50-60˚S and ~60 km) on days 201-204. The amplitude of

E3 meridional wind hits~~reaches~~ ~13 m/s at ~60-70˚S and ~55 km (days 151-154) and ~16 m/s at ~60-70˚S and ~55 km (days 201-204), respectively.

EP flux of E3 is similar to that of E2. The instability and appropriate background wind at the mid-high latitudes between ~50 km and ~70 km dramatically amplify the propagation of E3, which is enhanced by the interaction near the critical layer (~29 h) and the positive refractive index region~~.~~ (Figures 6i and 6j). Notably, ~~It is worth noting that~~ the strong instability and weak background wind at ~50-60˚S and ~60-70 km on days 151-154 provide sufficient energy for the propagation and amplification of EP flux into the lower atmosphere, and ultimately point toward~~towards~~ the equator at 50 km. During days 201-204, the~~The~~ EP flux propagates~~propagate~~ ~~to~~into the lower atmosphere~~ during days 201-204,~~ and ~~is~~gets amplified by interaction at the critical layer (~29 h). Besides~~In addition~~, weak instability and weak background wind at ~50-60˚S and ~60-70 km provide the energy to amplify the E3 propagation. ~~Combine with Figure~~Figures 6c~~,~~ 6d indicate that~~,~~ the stronger the instability at ~50-60˚S and ~60-70 km, the stronger the temperature amplitude of E3. We believe that the background wind and instability at ~50-60˚S and ~60-70 km are the main~~primary~~ reasons for the propagation and amplification of EP flux into the lower atmosphere.

~~The~~For E4, the spectra appear~~are observed to be~~ at ~48.2 km and

~50-60°S on days 127-130~~,~~ and 213-216~~ for E4,~~ when the eastward wavenumber -4 signal with the wave period of ~25 h and ~21 h~~, as shown in Figure~~ (see Figures 7a, 7b). The corresponding temperature spatial structures of these E4 (i.e., ~25 h and ~21 h) are~~ is~~ shown in Figures~~Figure~~ 7c, 7d. The temperature spatial structure of E4 shows an obvious amplitude bimodal structure at ~50-60˚S and ~50 km, and ~50-60˚S and ~60 km, with the maximum at ~50-60˚S and ~50 km. The maximum temperature amplitude of E4 occurs at ~50 km and ~50-60˚S with an amplitude of ~4 K on the days 127-130, and the other peak is ~3 K (~60-70˚S and ~60 km). The temperature amplitude of ~3 K occurs at ~50 km (~60 km) during days 213-216. The corresponding spatial structures of zonal wind and meridional wind of these E4 are presented~~is shown~~ in Figures 7e, 7f, 7g~~,~~ and 7h. The zonal wind spatial structure of E4 shows an obvious amplitude bimodal structure at ~50-60˚S and ~55 km, and ~60-70˚S and ~55 km, with the maximum at ~50-60˚S and ~55 km. The maximum zonal wind amplitude of E4 happens~~occurs~~ at ~50-60˚S and ~55 km with an amplitude of ~9 m/s on days 127-130, and the other peak is ~5K (~60-70˚S and ~55 km). The zonal wind amplitude of ~5 m/s occurs at ~50-60˚S (~60-70˚S) and ~55 km on days 213-216. The amplitude of E4 meridional wind reaches ~8 m/s at ~60-70˚S and ~55 km (days 127-130) and ~10 m/s at ~60-70˚S and ~55 km (days 213-216), respectively.

~~Figures 7i and 7j show d~~Diagnostic analysis for E4 on days 127-130~~,~~ and 213-216 ~~for E4~~are shown in Figures 7i and 7j, respectively. The results demonstrate~~show~~ that E4 is dramatically amplified by the mean flow instabilities at the middle-high latitudes between ~50 km and ~70 km~~, with~~. With EP flux propagating into the lower atmosphere, ~~and EP flux~~it finally propagates ~~eventually propagate~~ toward the equator at ~50 km. E4 is amplified and propagated by the wave-mean flow interaction near the critical layer (~25 h, ~21 h), and the positive refractive index region generates~~provides~~ the promoting effect. The strong instability and weak background wind at ~50-60˚S and ~60-70 km provide sufficient energy for the propagation and amplification of EP flux into the lower atmosphere during days 127-130. Besides, E4 obtains energy from weak instability and weak background wind at ~50-60˚S and ~60-70 km on days 213-216, and it is amplified and propagated into the lower atmosphere. The background wind at ~50-60˚S and ~60-70 km on days 127-130 is similar to on days 213-216, and the instability at ~50-60˚S and ~60-70 km is stronger on days 127-30 than on days 213-216. According to Figures~~Figure~~ 7a~~,~~ and 7b, ~~results shows that~~ E4 absorbs~~has absorbed~~ sufficient energy to be amplified under the background conditions on days 127-130, and~~. The~~ the temperature amplitude on 127-130 days is stronger.

3.2 In the Northern Hemisphere

Figure 8 shows that the observed maximum amplitude appears at ~~is observed to be~~ ~59.2 km and ~70-80°N for E1, and the E2 and E3 peaks at ~59.2 km and ~60-70°N. The maximum perturbation of E1 occurs~~is observed to be at~~ on days 41-50 (with an amplitude of ~8K), while~~and~~ the remaining fluctuations occur~~fluctuation occur~~ on days 25-34~~,~~ and 339-348. Besides, the strongest E2 occurs on days 69-74 (with an amplitude of ~7 K), and the rest are distributed on days 25-30, 317-322~~,~~ and 341-346~~, while~~. By contrast, the E3 maximizes on~~at~~ days 35-38 (with an amplitude of ~3K), and also shows a peak~~one peaks at~~ on days 53-56. Based on the study of the wave period in the SH for eastward wave, the periodic variabilities of E1, E2 and E3~~variability~~ in the NH ~~for E1, E2, and E3 is~~ are also examined~~investigated~~. The wave period~~periods~~ of E1 decreases~~decreased~~ from a maximum of ~118 h (days 25-34) to ~80 h (days 41-50), indicating the instability of ~~that~~ the wave period of E1 ~~is unstable~~ in the NH. The E2 events occur on days 25-30, 69-74, 317-322~~,~~ and 341-346, of which the corresponding wave periods are ~36, ~53, ~52~~,~~ and ~48 h, which are stronger and more stable than E1. Besides, the wave period of E3 is relatively stable at ~29 h and ~27 h. Thus, E2 and E3 wave periods are more stable than E1.

The spectra, spatial (vertical and latitudinal) structures of temperature, zonal and meridional wind, and diagnostic analysis of E1 are extracted from the corresponding representative events (~~,~~ as shown in

Figure 9). Figures 9a and 9b show the observed spectra of E1 at ~59.2 km and ~70-80°N on days 25-34 and 41-50, and the wave periods~~period~~ of locked wavenumber -1 ~~is~~are ~118 h and ~80 h, respectively. The corresponding temperature spatial structures of these E1 (~118 h and ~80 h) are~~is~~ shown in Figures~~Figure~~ 9c, 9d. The temperature spatial structure of E1 shows an obvious amplitude bimodal structure during days 25-34 at ~60-70°N and ~60 km, and ~40-50°N and ~70 km, with the maximum at ~60-70°N and ~60 km. On top of that~~Besides~~, E1 also has bimodal structure on days 41-50 at ~60-70°N and ~60 km, and ~60-70°N and ~70 km. The strongest temperature amplitude of E1 occurs at ~60-70°N and ~60 km with an amplitude of ~7 K on the days 25-34, and the other peak is ~4 K (~40-50°N and ~70 km). The temperature amplitude of ~10 K occurs at ~60 km and ~60-70°N during days 41-50, and the rest is ~8 K (~60-70°N and ~70 km). The corresponding spatial structures of zonal wind and meridional wind of these E1 are illustrated~~is shown~~ in Figures 9e, 9f, 9g~~,~~ and 9h. The zonal wind spatial structure of E1 presents~~shows~~ an obvious amplitude bimodal structure at ~70-80°N and ~70 km, and ~50-60°N and ~70 km. The zonal wind amplitude of ~13 m/s occurs at ~70-80°N and ~70 km on days 25-34, and the rest is ~10 m/s (~50-60°N and ~70 km). In addition, there is a weak peak of 9K during days 25-34 (~30-40°N and ~70 km). The maximum zonal wind amplitude of E1 occurs at ~70-80°N and ~70 km with an amplitude of ~19 m/s on days

41-50, and the other peak is ~13K (~50-60°N and ~70 km). The amplitude of E1 meridional wind hits~~reaches~~ ~14 m/s at ~70-80°N and ~70 km (days 25-34) and ~22 m/s at ~70-80°N and ~70 km (days 41-50), respectively.

The diagnostic analysis results for E1 (in Figures 9i and 9j) suggest~~show~~ the dramatic amplification of~~that~~ E1 ~~is dramatically amplified~~ by the mean flow instabilities at the middle-high latitudes between ~50 km and ~70 km~~, with~~. With the propagation of EP flux ~~propagating~~ into the polar lower atmosphere, ~~and EP flux~~it eventually propagates~~propagate~~ toward the equator at ~50 km. The wave-mean flow interaction near the critical layers (~118 h, ~80 h) amplifies and propagates E1, and the promoting effect of the positive refractive index region amplifies E1. Furthermore~~Besides~~, the weak instability and strong background wind at ~40-50°N and ~60-70 km generate the~~provide~~ energy for the propagation and amplification of EP flux into the polar lower atmosphere during days 25-34. The E1 obtains sufficient energy from weak instability and suitable background wind on days 41-50 at ~40-50°N and ~60-70 km, and is amplified and propagated into the polar lower atmosphere through the critical layer and positive refractive index action. The background wind at ~40-50°N and ~60-70 km is stronger on days 25-34 than on days 41-50, but their instability is similar, indicating that stronger background winds might weaken~~may be unfavorable to~~ E1 propagation and amplification at the mid-northern latitudes. ~~According to Figure 9a, 9b~~Our results show~~shows~~ that E1 absorbs~~has absorbed sufficient~~ adequate energy to be amplified under the background conditions during days 41-50, reflecting~~showing a~~ stronger temperature amplitude (see Figures 9a, 9b).

For E2, the~~The~~ spectra are ~~observed to be~~ at ~59.2 km and ~60-70°N on days 25-30~~,~~ and 69-74~~ for E2,~~ when the eastward wavenumber -2 signal with the period ~~of~~ ~36 h and ~53 h~~,~~ (as shown in Figures~~Figure~~ 10a, 10b). The corresponding temperature spatial structures of these E2 (i.e., ~36 h and ~53 h) are presented~~is shown~~ in Figures~~Figure~~ 10c, 10d. The temperature spatial structure of E2 demonstrates~~shows~~ an obvious amplitude bimodal structure at ~60-70˚N and ~60 km, and ~60-70˚N and ~70 km, with the maximum at ~60-70˚N and ~60 km. The maximum temperature amplitude of E2 occurs at ~60-70˚N and ~60 km with an amplitude of ~5 K on days 25-30, and the other peak is ~4 K (~60-70˚N and ~70 km). The temperature amplitude of ~9 K occurs on days 69-74 at ~60˚S and ~60 km, and the other peaks are ~7 K (~60-70˚N and ~70 km), ~5 K (~60-70˚N and ~50 km). The corresponding spatial structures of zonal wind and meridional wind of these E2 ~~is~~are shown in Figures 10e, 10f, 10g~~,~~ and 10h. The zonal wind spatial structure of E2 shows an obvious amplitude bimodal structure at ~60-70˚N and ~60 km, and ~40-50˚N and ~60 km, with the maximum at ~40-50˚N and ~60 km. The maximum zonal wind amplitude of E2 appears~~occurs~~ at ~60-70˚N and ~60 km (~40-50˚N and ~60 km) with an amplitude of ~6 m/s on days 25-30. Zonal wind amplitude occurs at ~40-50˚N and ~60 km with an amplitude of ~18 m/s on days 41-50, and the other peak is ~16 K (~60-70˚N and ~60km). The amplitude of E2 meridional wind reaches ~7 m/s at ~60-70˚N and ~70 km (days 25-30) and ~18 m/s at ~60-70˚N and ~60 km (days 41-50), respectively.

~~Figures 10i and 10j show~~ The diagnostic analysis of E2 on days 25-30~~,~~ and 69-74 are shown in Figures 10i and 10j, respectively~~for E2~~. ~~It is clear that~~Apparently, E2 is significantly~~dramatically~~ amplified by the mean flow instabilities at the middle-high latitudes between ~40 km and ~70 km, with EP flux propagating into the polar lower atmosphere, and EP flux eventually propagate toward the equator at ~50 km. E2 is amplified and propagated by the wave-mean flow interaction near the critical layers (~36 h, ~53 h), and the positive refractive index region provides the promoting effect. The weak instability and strong background wind at ~50-60˚N and ~60-70 km provide the energy for the propagation and amplification of EP flux into the polar lower atmosphere during days 25-30. Moreover~~Besides~~, E2 obtains sufficient energy from strong instability and suitable background wind at ~50-60˚N and ~60-70 km on days 69-74, and it is amplified and propagated into the polar lower atmosphere. The background wind at ~50-60˚N and ~60-70 km on days

127-130 is similar to on days 213-216, and the instability at ~50-60˚S and ~60-70 km is stronger on days 127-30 than on days 213-216. Although~~The~~ the background wind at ~50-60˚N and ~60-70 km is stronger on days 25-30 than on days 69-74, ~~but~~ the instability at ~50-60˚N and ~60-70 km is stronger on days 69-74 than on days 25-30. ~~According to Figure 10a, 10b~~The temperature amplitude results indicate~~shows~~ that E2 absorbs~~has absorbed~~ sufficient energy to be amplified under the background conditions on days 69-74, with stronger~~the~~ temperature amplitude on days 69-74 ~~is stronger~~(Figures 10a, 10b).

Figures 11a and 11b show the observed spectra of E3 at ~59.2km and ~60-70°N on days 35-38 and 53-56, and the wave periods~~period~~ of locked wavenumber -3 ~~is~~are ~29 h and ~27 h, respectively. The corresponding temperature spatial structures of these E3 (i.e., ~29 h and ~27 h) are~~is~~ shown in Figures~~Figure~~ 11c, 11d. The temperature spatial structure of E3 shows an obvious amplitude bimodal structure at ~50-60˚N and ~60 km, and ~50-60˚N and ~70 km, with the maximum at ~50-60˚N and ~60 km. The strongest temperature amplitude of E3 occurs at ~60 km and ~50-60˚N with an amplitude of ~6 K on the days 35-38, and the other peak is ~5 K (~50-60˚N and ~70 km). The temperature amplitude of ~4 K occurs at ~60 km (~70 km) and ~50-60˚N during days 53-56. The corresponding spatial structures of zonal wind and meridional wind of these E3 are illustrated~~is shown~~ in Figures 6e, 6f, 6g~~,~~ and 6h. The zonal wind spatial structure of E3 shows an obvious amplitude bimodal structure at ~40-50°N and ~70 km, and ~60-70°N and ~70 km. The zonal wind amplitudes of E3 occur at ~40-50°N and ~70 km with an amplitude of ~15 m/s on days 35-38, and ~12 m/s at ~60-70°N and ~70 km. The maximum zonal wind amplitude of E3 appears~~occurs~~ at ~40-50°N and ~70 km (~60-70°N and ~70 km) with an amplitude of ~7 m/s (~6 m/s) on days 53-56. The amplitude of E3 meridional wind reaches ~22 m/s at ~50-60°N and ~70 km (days 35-38) and ~12 m/s at ~60-70°N and ~70 km (days 53-56), respectively.

Obviously, the instability and appropriate background wind at the mid-latitudes~~mid-latitude~~ between ~50 km and ~70 km and the interaction near the critical layers (~29 h, ~27 h) dramatically amplify the propagation of E3~~, as shown in~~ (see Figures 11i and 11j). The background wind is similar on days 35-38 and 53-56, and the former is relatively~~more~~ unstable. This finding indicates that the E3 in propagation is more likely to gather~~get~~ sufficient energy to be amplified on days 35-38. The instability and appropriate background wind at the mid-high latitudes between ~50 km and ~70 km drastically~~dramatically~~ amplify the propagation of E3, which is enhanced by the interaction near the critical layers (~29 h, ~27 h) and the positive refractive index region~~.~~ (Figures~~Figure~~ 11i, 11j). In particular,~~It is worth noting that~~ the strong instability and weak background wind at ~50-60°N and ~60-70 km on days 35-38 generate~~provide~~ sufficient energy for the propagation and amplification of EP flux into the lower atmosphere, and ultimately point toward~~towards~~ the equator at 50 km. The EP flux propagates~~propagate~~ to the lower atmosphere during days 35-38, and it is amplified by interactions at the critical layer (~29 h). In addition, weak instability and weak background winds on days 53-56 at ~50-60°N and ~60-70 km provide the energy to amplify E3 propagation. Combine with Figures~~Figure~~ 11c, 11d, the stronger the instability at ~50-60°N and ~60-70 km, the stronger the temperature amplitude of E3. The results show that the instability on days 35-38 at ~50-60°N and ~60-70 km are the primary reasons for the propagation and amplification of EP flux into the lower atmosphere.

3.3 Comparison between SH and NH

The observed latitude and maximum amplitude for eastward planetary waves (i.e., E1, E2, E3, E4) decrease and weaken with increasing zonal wavenumber in the SH, reaching ~70-80°S, ~60-70°S, ~60-70°S~~,~~ and ~50-60°S, and ~10 K, ~9 K, ~6 K, and ~3 K, respectively. In addition, the occurrence date gets~~is~~ earlier with increasing zonal wavenumber. The temperature spatial structure demonstrates~~shows~~ a bimodal-peak structure (~50 and ~60 km), mainly~~primarily~~ located at ~50 km. The maximum zonal wind amplitudes of E1 and E2, E3 and E4 are almost the same~~equivalents~~, which are ~20 m/s and ~10 m/s, respectively. The maximum meridional wind amplitudes of E1, E2, E3 and E4 are ~17 m/s, ~27 m/s, ~16 m/s~~,~~ and ~11 m/s, respectively. The wave period of E1 tends to get shorter from 5 to 3 days;~~,~~ while E2 and E3 are close to ~40 h and ~30 h;~~,~~ and~~while~~ E4 remains at ~24 h. E1, E2, E3~~,~~ and E4 are more favorable to propagation in the SH winter and are abruptly~~dramatically~~ amplified by the mean flow instabilities at the middle latitudes between ~40 km and ~70 km~~, with~~. With the propagation of EP flux ~~propagating~~ into the lower atmosphere, and it finally propagates~~EP flux eventually propagate~~ toward the equator at ~50 km. In addition, the propagation of EP flux for E1 to the upper atmosphere might~~may~~ be influenced by the instability and background wind at the Antarctic ~50km.

The observed latitudes of E1, E2 (E3) decrease with increasing wavenumber in the NH, which are ~70-80°N, ~60-70°N~~,~~ and ~60-70°N. With bimodal-peak structure located at ~70 km, the~~The~~ temperature spatial structures~~structure~~ of E1, E2~~,~~ and E3 ~~presents a bimodal-peak structure, primarily located at ~70km, reaches~~reach ~10 K, ~9 K~~,~~ and ~6 K, respectively. The maximum zonal wind amplitude for E1, E2 and E3 occur~~occurs~~ at ~50-80°N and ~70 km, and their amplitude are~~is~~ almost equal to ~18 m/s. The maximum meridional winds~~wind~~ of E1, E2 and E3 occur at ~50-80°N and ~70 km~~,~~ with amplitudes of ~22 m/s, ~18 m/s and ~22 m/s, respectively. The wave period of E1 tends to be shorter from 5-3 days;~~,~~ and E2 and E3 are close to ~48 h and ~30 h. In addition, E1, E2~~,~~ and E3 are more favorable to propagation in the NH winter and are dramatically amplified by the mean flow instabilities at the middle latitudes between ~40 km and ~70 km, with the propagation of EP flux ~~propagating~~ into the lower atmosphere and then~~, and EP flux eventually propagate~~ toward the equator at ~50 km.

4 Summary and Conclusions

Based on the MERRA-2 temperature and wind observations in 2019, we~~We~~ present for the first time an extensive study of the global variation for eastward planetary wave activity, including zonal wave numbers of -1 (E1), -2 (E2), -3 (E3), -4 (E4)~~,~~ in the stratosphere and mesosphere.~~, using the MERRA-2 temperature and wind observations in 2019.~~ The temperature and wind amplitude~~amplitudes~~ and wave periods of each event were determined using~~by~~ 2-D least-squares fitting. Our study covered~~includes~~ the spatial and temporal patterns~~behaviors~~ of the eastward planetary waves in both hemispheres with a comprehensive diagnostic analysis on their propagation and amplification. The key findings of this~~the~~ study are summarized below~~as follows~~:

1. The latitudes for the maximum (temperature, zonal and meridional wind) amplitudes of E1, E2, E3~~,~~ and E4 decrease with increasing wavenumber in the SH and NH. The E1, E2, E3~~,~~ and E4 events occur earlier with increasing zonal wavenumber in the SH. In addition,

eastward wave modes exist during summer periods with westward background wind in both hemispheres.

2. The temperature spatial structures of E1, E2, E3~~,~~ and E4 present a double-peak structure, which is located at ~50 km and ~60 km in SH, ~60 km~~,~~ and ~70 km in SH. Furthermore~~In addition~~, the lower peak is usually larger than the higher one.

3. The maximum (temperature, zonal and meridional wind) amplitude~~amplitudes~~ of E1, E2~~,~~ and E3 decline~~decrease~~ with rising~~increasing~~ zonal wavenumber in the SH and NH. The maximum temperature amplitude~~amplitudes~~ in the SH are slightly larger and lie lower than those in the NH. In addition, the meridional wind amplitude~~amplitudes~~ are slightly larger than the zonal wind in the SH and NH.

4. The wave period of the E1 mode ranges ~~varies from 3 to~~ 3-5 days in both hemispheres, while the period of E2 mode is slightly longer in the NH (~48 h) than in the SH (~40 h). The periods of E3 ~~are ~30 h~~ in both SH and NH are ~30 h, while~~and~~ the period of E4 is ~24 h.

5. The eastward planetary wave is more favorable to propagate in the winter hemisphere and is drastically~~dramatically~~ amplified by the mean flow instabilities and appropriate background winds at polar region and the middle latitudes between ~40 km and ~80 km. Furthermore, the amplification of planetary waves through wave-mean flow interaction

occurs~~most~~ easily ~~occurs near~~close to its critical layer. In addition, the direction of EP flux ultimately points towards the equator.

6. The strong instability and appropriate background wind in the lower layer of the Antarctic region might generate adequate~~may provide sufficient~~ energy to promote the E1 propagation and amplification to the upper atmosphere.

Overall, this study demonstrated~~This study demonstrates~~ how the background zonal wind in the polar middle atmosphere affects the dynamics of eastward planetary waves in the polar middle atmosphere.

717

Data availability. MERRA-2 data are available at http://disc.gsfc.nasa.gov.

Code availability. Code is available at http://hdl.pid21.cn/21.86116.7/04.99.01293.

Author contributions. LT carried out the data processing and analysis and wrote the manuscript. SYG and XKD contributed to reviewing the article.

Competing interests. The authors declare that they have no conflict of interest.

Acknowledgements. This work was performed in the framework of the Space Physics Research (SPR). The authors thank NASA for free online access to the MERRA-2 temperature reanalysis.

Financial support. This research work was supported by the National Natural Science Foundation of China (41704153, 41874181, and 41831071).

References

Alexander, S. P. and Shepherd, M. G.: Planetary wave activity in the polar lower stratosphere, Atmos. Chem. Phys., 10, 707-718, 10.5194/acp-10-707-2010, 2010.

Andrews, D., Holton, J., and Leovy, C.: Middle Atmosphere Dynamics, 489 pp.1987.

Bali, K., Dey, S., Ganguly, D., and Smith, K. R.: Space-time variability of ambient PM2.5 diurnal pattern over India from 18-years (2000–2017) of MERRA-2 reanalysis data, Atmos. Chem. Phys. Discuss., 2019, 1-23, 10.5194/acp-2019-731, 2019.

Coy, L., Štajner, I., DaSilva, A. M., Joiner, J., Rood, R. B., Pawson, S., and Lin, S. J.: High-Frequency Planetary Waves in the Polar Middle Atmosphere as Seen in a Data Assimilation System, Journal of the Atmospheric Sciences, 60, 2975-2992, 10.1175/1520-0469(2003)060<2975:Hpwitp>2.0.Co;2, 2003.

Gu, S.-Y., Liu, H.-L., Dou, X., and Jia, M.: Ionospheric Variability Due to Tides and Quasi-Two Day Wave Interactions, Journal of Geophysical Research: Space Physics, 123, 1554-1565, https://doi.org/10.1002/2017JA025105, 2018a.

Gu, S.-Y., Dou, X., Pancheva, D., Yi, W., and Chen, T.: Investigation of the Abnormal Quasi 2-Day Wave Activities During the Sudden Stratospheric Warming Period of January 2006, Journal of Geophysical Research: Space Physics, 123, 6031-6041, https://doi.org/10.1029/2018JA025596, 2018b.

Gu, S.-Y., Liu, H.-L., Pedatella, N. M., Dou, X., and Liu, Y.: On the wave number 2 eastward propagating quasi 2 day wave at middle and high latitudes, Journal of Geophysical Research: Space Physics, 122, 4489-4499, https://doi.org/10.1002/2016JA023353, 2017.

Gu, S.-Y., Liu, H.-L., Pedatella, N. M., Dou, X., and Shu, Z.: The quasi-2 day wave activities during

2007 boreal summer period as revealed by Whole Atmosphere Community Climate Model, Journal of Geophysical Research: Space Physics, 121, 7256-7268, https://doi.org/10.1002/2016JA022867, 2016a.

Gu, S.-Y., Li, T., Dou, X., Wu, Q., Mlynczak, M. G., and Russell Iii, J. M.: Observations of Quasi-Two-Day wave by TIMED/SABER and TIMED/TIDI, Journal of Geophysical Research: Atmospheres, 118, 1624-1639, https://doi.org/10.1002/jgrd.50191, 2013.

Gu, S.-Y., Liu, H.-L., Pedatella, N. M., Dou, X., Li, T., and Chen, T.: The quasi 2 day wave activities during 2007 austral summer period as revealed by Whole Atmosphere Community Climate Model, Journal of Geophysical Research: Space Physics, 121, 2743-2754, https://doi.org/10.1002/2015JA022225, 2016b.

Gu, S.-Y., Ruan, H., Yang, C.-Y., Gan, Q., Dou, X., and Wang, N.: The Morphology of the 6-Day Wave in Both the Neutral Atmosphere and F Region Ionosphere Under Solar Minimum Conditions, Journal of Geophysical Research: Space Physics, 123, 4232-4240, https://doi.org/10.1029/2018JA025302, 2018c.

Gu, S.-Y., Dou, X.-K., Yang, C.-Y., Jia, M., Huang, K.-M., Huang, C.-M., and Zhang, S.-D.: Climatology and Anomaly of the Quasi-Two-Day Wave Behaviors During 2003–2018 Austral Summer Periods, Journal of Geophysical Research: Space Physics, 124, 544-556, https://doi.org/10.1029/2018JA026047, 2019.

Lainer, M., Hocke, K., and Kämpfer, N.: Long-term observation of midlatitude quasi 2-day waves by a water vapor radiometer, Atmos. Chem. Phys., 18, 12061-12074, 10.5194/acp-18-12061-2018, 2018.

Li, H., Pilch Kedzierski, R., and Matthes, K.: On the forcings of the unusual Quasi-Biennial

Oscillation structure in February 2016, Atmos. Chem. Phys., 20, 6541-6561, 10.5194/acp-20-6541-2020, 2020.

Lilienthal, F. and Jacobi, C.: Meteor radar quasi 2-day wave observations over 10 years at Collm (51.3° N, 13.0° E), Atmos. Chem. Phys., 15, 9917-9927, 10.5194/acp-15-9917-2015, 2015.

Limpasuvan, V. and Wu, D. L.: Anomalous two-day wave behavior during the 2006 austral summer, Geophysical Research Letters, 36, https://doi.org/10.1029/2008GL036387, 2009.

Liu, G., England, S. L., and Janches, D.: Quasi Two-, Three-, and Six-Day Planetary-Scale Wave Oscillations in the Upper Atmosphere Observed by TIMED/SABER Over ~17 Years During 2002–2018, Journal of Geophysical Research: Space Physics, 124, 9462-9474, https://doi.org/10.1029/2019JA026918, 2019.

Liu, H. L., Talaat, E. R., Roble, R. G., Lieberman, R. S., Riggin, D. M., and Yee, J. H.: The 6.5-day wave and its seasonal variability in the middle and upper atmosphere, Journal of Geophysical Research: Atmospheres, 109, https://doi.org/10.1029/2004JD004795, 2004.

Lu, X., Chu, X., Fuller-Rowell, T., Chang, L., Fong, W., and Yu, Z.: Eastward propagating planetary waves with periods of 1–5 days in the winter Antarctic stratosphere as revealed by MERRA and lidar, Journal of Geophysical Research: Atmospheres, 118, 9565-9578, https://doi.org/10.1002/jgrd.50717, 2013.

Manney, G. L. and Randel, W. J.: Instability at the Winter Stratopause: A Mechanism for the 4-Day Wave, Journal of Atmospheric Sciences, 50, 3928-3938, 10.1175/1520-0469(1993)050<3928:IATWSA>2.0.CO;2, 1993.

Matthias, V. and Ern, M.: On the origin of the mesospheric quasi-stationary planetary waves in the unusual Arctic winter 2015/2016, Atmospheric Chemistry and Physics, 18, 4803-4815,

10.5194/acp-18-4803-2018, 2018.

Meek, C. E., Manson, A. H., Franke, S. J., Singer, W., Hoffmann, P., Clark, R. R., Tsuda, T., Nakamura, T., Tsutsumi, M., Hagan, M., Fritts, D. C., Isler, J., and I. Portnyagin, Y.: Global study of northern hemisphere quasi-2-day wave events in recent summers near 90 km altitude, Journal of Atmospheric and Terrestrial Physics, 58, 1401-1411, https://doi.org/10.1016/0021-9169(95)00120-4, 1996.

Merzlyakov, E. G. and Pancheva, D. V.: The 1.5–5-day eastward waves in the upper stratosphere–mesosphere as observed by the Esrange meteor radar and the SABER instrument, Journal of Atmospheric and Solar-Terrestrial Physics, 69, 2102-2117, https://doi.org/10.1016/j.jastp.2007.07.002, 2007.

Molod, A., Takacs, L., Suarez, M., and Bacmeister, J.: Development of the GEOS-5 atmospheric general circulation model: evolution from MERRA to MERRA2, Geoscientific Model Development Discussions, 7, 10.5194/gmdd-7-7575-2014, 2014.

Molod, A., Takacs, L., Suarez, M., Bacmeister, J., Song, I. S., and Eichmann, A.: The GEOS-5 Atmospheric General Circulation Model: Mean Climate and Development from MERRA to Fortuna, 2012.

Palo, S. E., Roble, R. G., and Hagan, M. E.: Middle atmosphere effects of the quasi-two-day wave determined from a General Circulation Model, Earth, Planets and Space, 51, 629-647, 10.1186/BF03353221, 1999.

Palo, S. E., Forbes, J. M., Zhang, X., Russell Iii, J. M., and Mlynczak, M. G.: An eastward propagating two-day wave: Evidence for nonlinear planetary wave and tidal coupling in the mesosphere and lower thermosphere, Geophysical Research Letters, 34,

https://doi.org/10.1029/2006GL027728, 2007.

Pancheva, D., Mukhtarov, P., Siskind, D. E., and Smith, A. K.: Global distribution and variability of quasi 2 day waves based on the NOGAPS-ALPHA reanalysis model, Journal of Geophysical Research: Space Physics, 121, 11,422-411,449, https://doi.org/10.1002/2016JA023381, 2016.

Rao, N. V., Ratnam, M. V., Vedavathi, C., Tsuda, T., Murthy, B. V. K., Sathishkumar, S., Gurubaran, S., Kumar, K. K., Subrahmanyam, K. V., and Rao, S. V. B.: Seasonal, inter-annual and solar cycle variability of the quasi two day wave in the low-latitude mesosphere and lower thermosphere, Journal of Atmospheric and Solar-Terrestrial Physics, 152-153, 20-29, https://doi.org/10.1016/j.jastp.2016.11.005, 2017.

Salby, M. L.: The 2-day wave in the middle atmosphere: Observations and theory, Journal of Geophysical Research: Oceans, 86, 9654-9660, https://doi.org/10.1029/JC086iC10p09654, 1981.

Sandford, D. J., Schwartz, M. J., and Mitchell, N. J.: The wintertime two-day wave in the polar stratosphere, mesosphere and lower thermosphere, Atmos. Chem. Phys., 8, 749-755, 10.5194/acp-8-749-2008, 2008.

Stray, N. H., Orsolini, Y. J., Espy, P. J., Limpasuvan, V., and Hibbins, R. E.: Observations of planetary waves in the mesosphere-lower thermosphere during stratospheric warming events, Atmos. Chem. Phys., 15, 4997-5005, 10.5194/acp-15-4997-2015, 2015.

Sun, J., Veefkind, J. P., van Velthoven, P., Tilstra, L. G., Chimot, J., Nanda, S., and Levelt, P. F.: Defining aerosol layer height for UVAI interpretation using aerosol vertical distributions characterized by MERRA-2, Atmos. Chem. Phys. Discuss., 2020, 1-36, 10.5194/acp-2020-39, 2020.

Tunbridge, V. M., Sandford, D. J., and Mitchell, N. J.: Zonal wave numbers of the summertime 2 day planetary wave observed in the mesosphere by EOS Aura Microwave Limb Sounder, Journal of Geophysical Research: Atmospheres, 116, https://doi.org/10.1029/2010JD014567, 2011.

Ukhov, A., Mostamandi, S., da Silva, A., Flemming, J., Alshehri, Y., Shevchenko, I., and Stenchikov, G.: Assessment of natural and anthropogenic aerosol air pollution in the Middle East using MERRA-2, CAMS data assimilation products, and high-resolution WRF-Chem model simulations, Atmospheric Chemistry and Physics, 20, 9281-9310, 10.5194/acp-20-9281-2020, 2020.

Venne, D. E. and Stanford, J. L.: Observation of a 4–Day Temperature Wave in the Polar Winter Stratosphere, Journal of the Atmospheric Sciences, 36, 2016-2019, 10.1175/1520-0469(1979)036<2016:Ooatwi>2.0.Co;2, 1979.

Wang, J. C., Chang, L. C., Yue, J., Wang, W., and Siskind, D. E.: The quasi 2 day wave response in TIME-GCM nudged with NOGAPS-ALPHA, Journal of Geophysical Research: Space Physics, 122, 5709-5732, https://doi.org/10.1002/2016JA023745, 2017.

Wu, W.-S., Purser, R. J., and Parrish, D. F.: Three-Dimensional Variational Analysis with Spatially Inhomogeneous Covariances, Monthly Weather Review, 130, 2905-2916, 10.1175/1520-0493(2002)130<2905:TDVAWS>2.0.CO;2, 2002.

Xiong, J., Wan, W., Ding, F., Liu, L., Hu, L., and Yan, C.: Two Day Wave Traveling Westward With Wave Number 1 During the Sudden Stratospheric Warming in January 2017, Journal of Geophysical Research: Space Physics, 123, 3005-3013, https://doi.org/10.1002/2017JA025171, 2018.

Yadav, S., Vineeth, C., Kumar, K. K., Choudhary, R. K., Pant, T. K., and Sunda, S.: Role of the phase of Quasi-Biennial Oscillation in modulating the influence of SSW on Equatorial Ionosphere, 2019 URSI Asia-Pacific Radio Science Conference (AP-RASC), 9-15 March 2019, 1-4, 10.23919/URSIAP-RASC.2019.8738274,

Yamazaki, K., Nakamura, T., Ukita, J., and Hoshi, K.: A tropospheric pathway of the stratospheric quasi-biennial oscillation (QBO) impact on the boreal winter polar vortex, Atmos. Chem. Phys., 20, 5111-5127, 10.5194/acp-20-5111-2020, 2020.

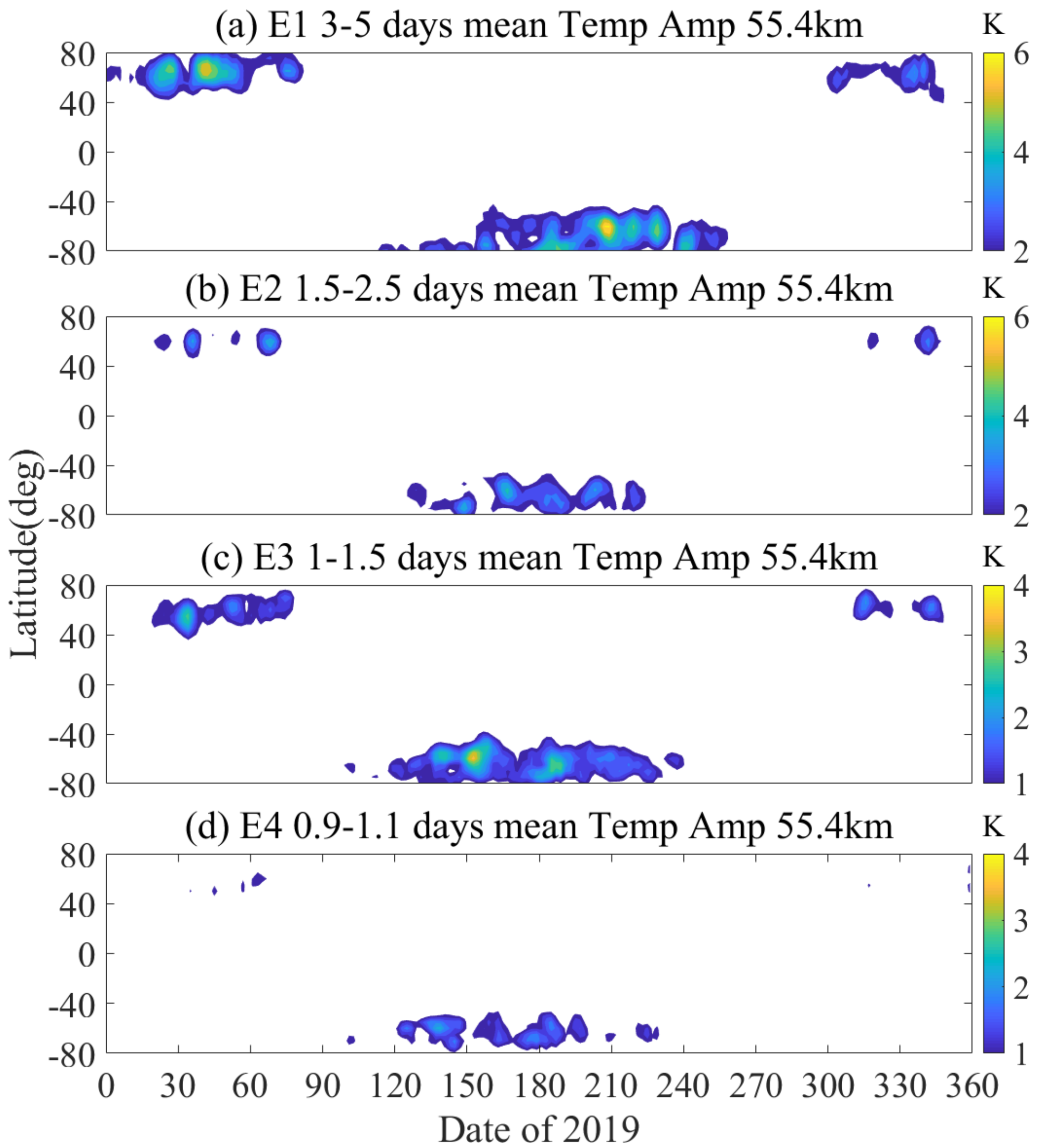

Figure 1. The global latitude-temporal variation structures of the (a) E1, (b) E2, (c) E3~~,~~ and (d) E4 planetary waves during 2019. White areas represent small amplitude data (corresponds to the right color bar). The confidence interval is 0.95.

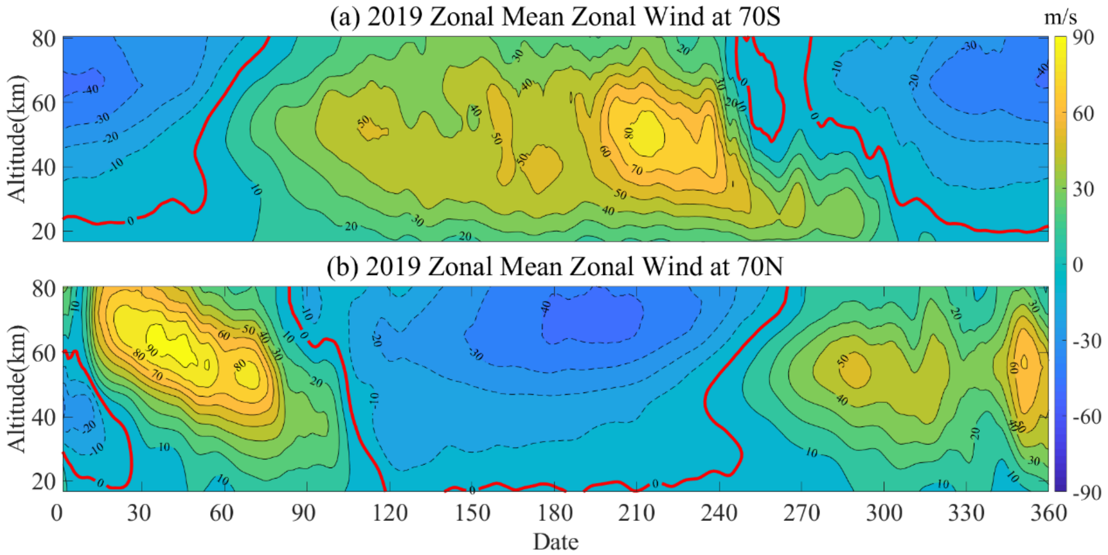

Figure 2. The zonal mean zonal wind variations of ~~the~~ (a) ~~the~~ 70°S and (b) 70°N during 2019. The dotted line represents east wind, the solid line represents west wind, and the red solid line is 0 m/s.

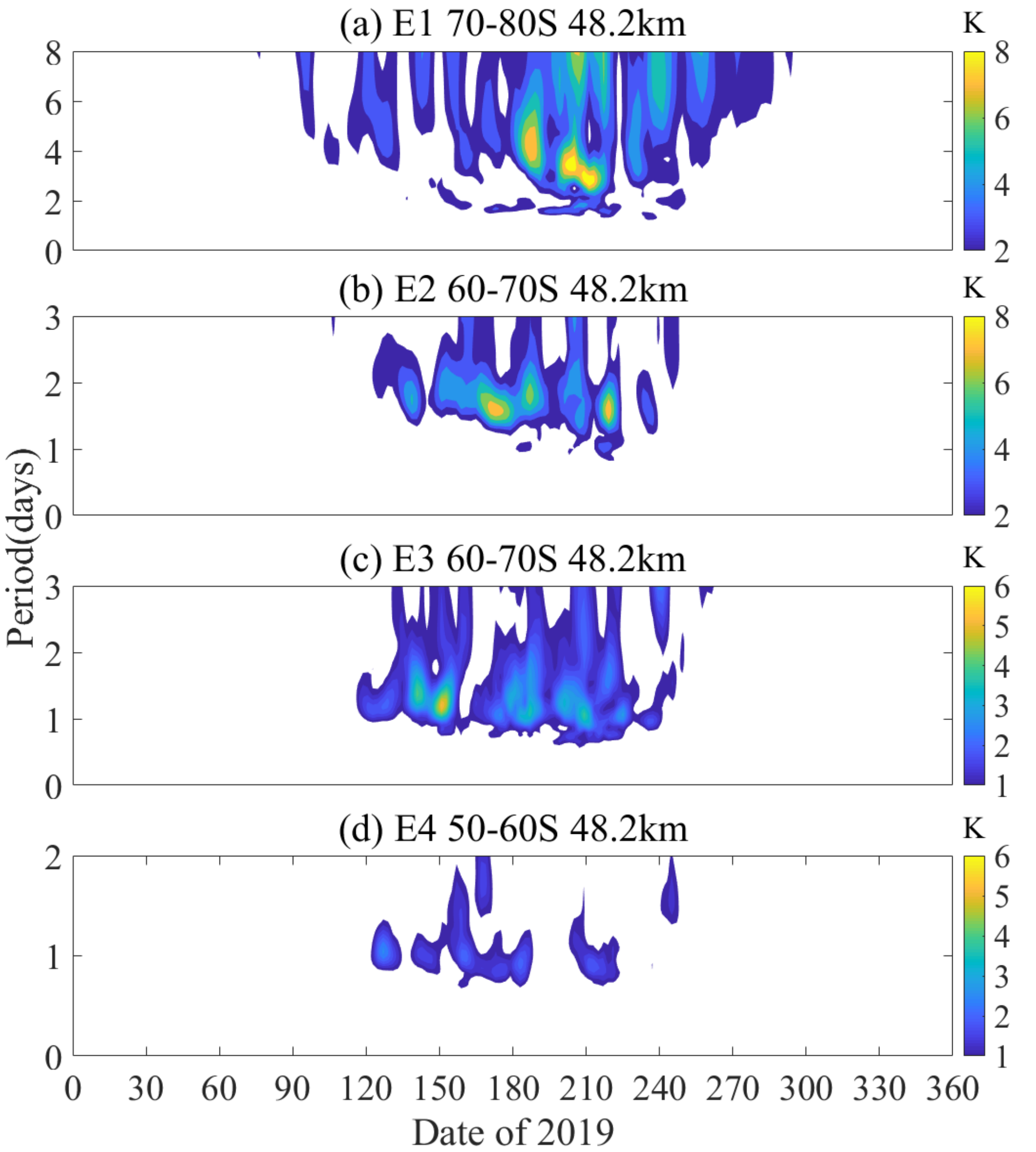

Figure 3. The temporal variations of ~~the~~ (a) E1, (b) E2, (c) E3~~,~~ and (d) E4 QTDWs during 2019 austral winter period.

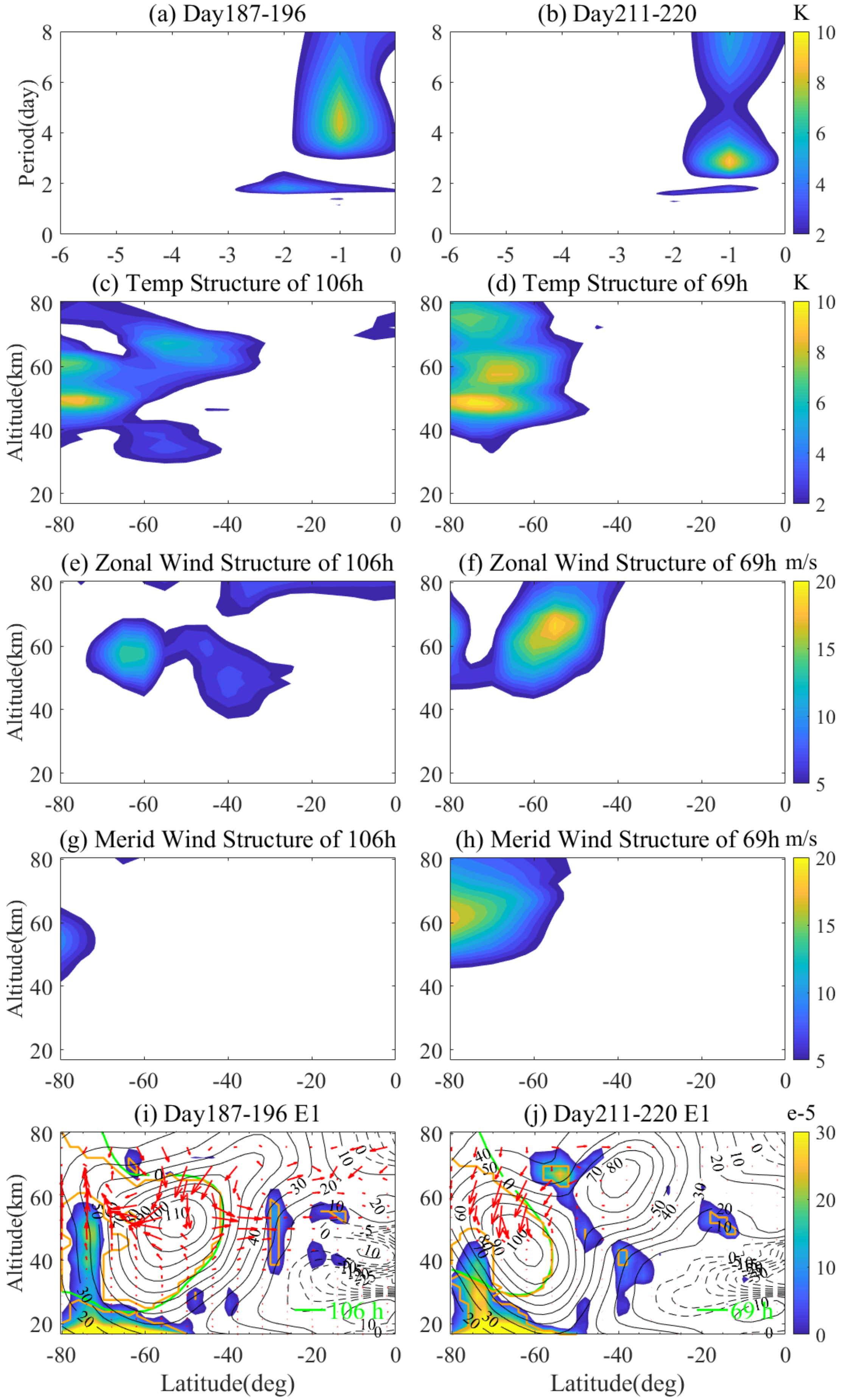

(a) Day187-196
(b) Day211-220
Period(day)
(c) Temp Structure of 106h
(d) Temp Structure of 69h
(e) Zonal Wind Structure of 106h
(f) Zonal Wind Structure of 69h
(g) Merid Wind Structure of 106h
(h) Merid Wind Structure of 69h
(i) Day187-196 E1
(j) Day211-220 E1
Altitude(km)
Latitude(deg)
K
m/s
e-5
106 h
69 h

890

Figure 4. The (a, b) spectra, (c, d) temperature spatial structures, (e, f) zonal wind spatial structures, (g, h) meridional wind spatial structures, and (i, j) diagnostic analysis of the E1 typical events during 2019 austral winter period. The MERRA-2 temperature data observations at 48.2 km and 70-80°S during days 187–196 (Figure 4a), 211–220 (Figure 4d) are utilized, respectively. The instability (blue shaded region), EP fluxes (red arrow), and critical layers (green line) for E1 typical event. The green line represents critical layers of ~~the~~ E1 with the natural period. Regions enclosed by orange solid lines are characterized by the positive refractive index for the E1.

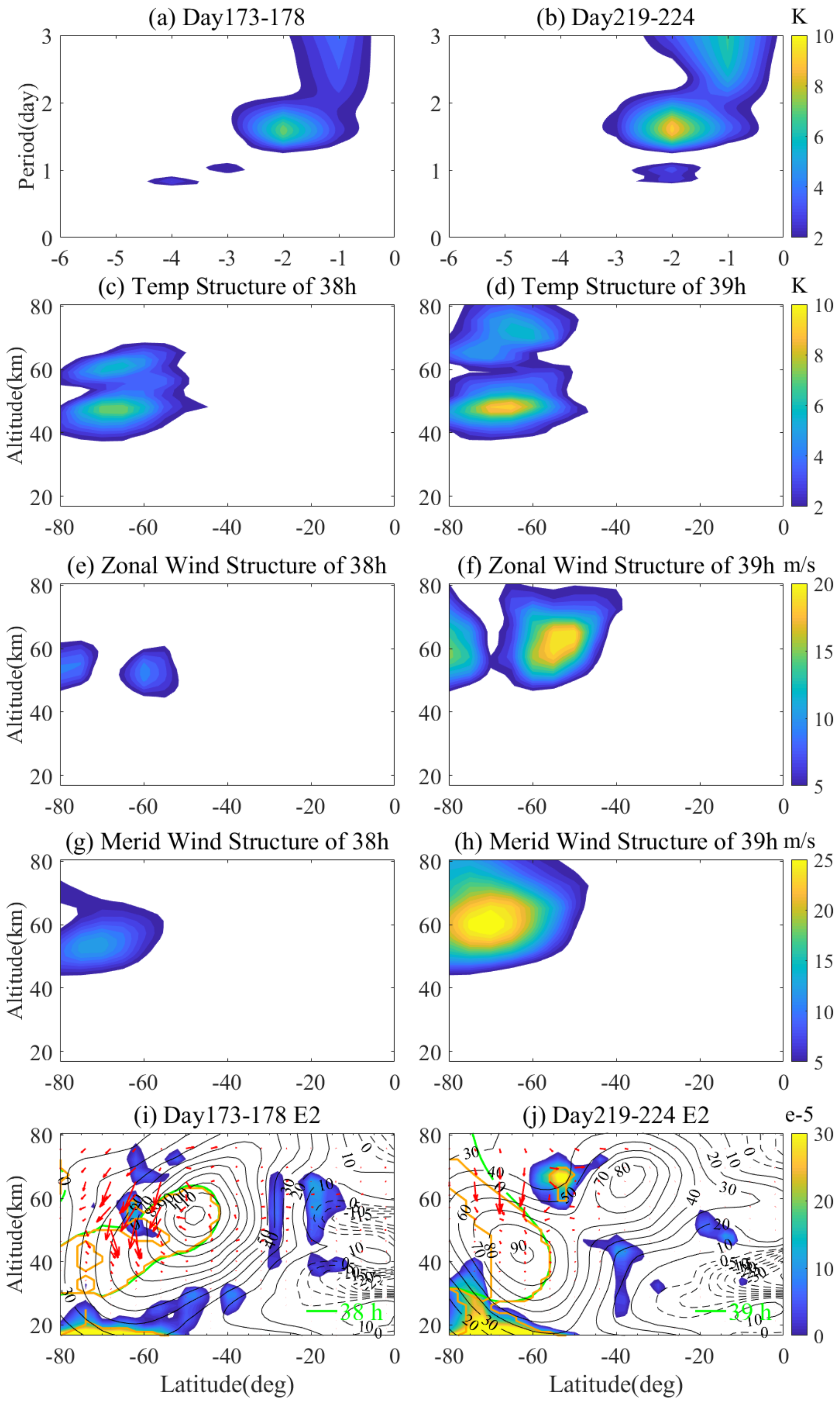
(a) Day173-178
(b) Day219-224
K
Period(day)
(c) Temp Structure of 38h
(d) Temp Structure of 39h
K
Altitude(km)
(e) Zonal Wind Structure of 38h
(f) Zonal Wind Structure of 39h
m/s
(g) Merid Wind Structure of 38h
(h) Merid Wind Structure of 39h
m/s
(i) Day173-178 E2
(j) Day219-224 E2
e-5
38 h
39 h
Latitude(deg)

Figure 5. ~~The same~~Same as Figure 4 but for ~~the~~ E2 during the 2019 austral winter period.

903

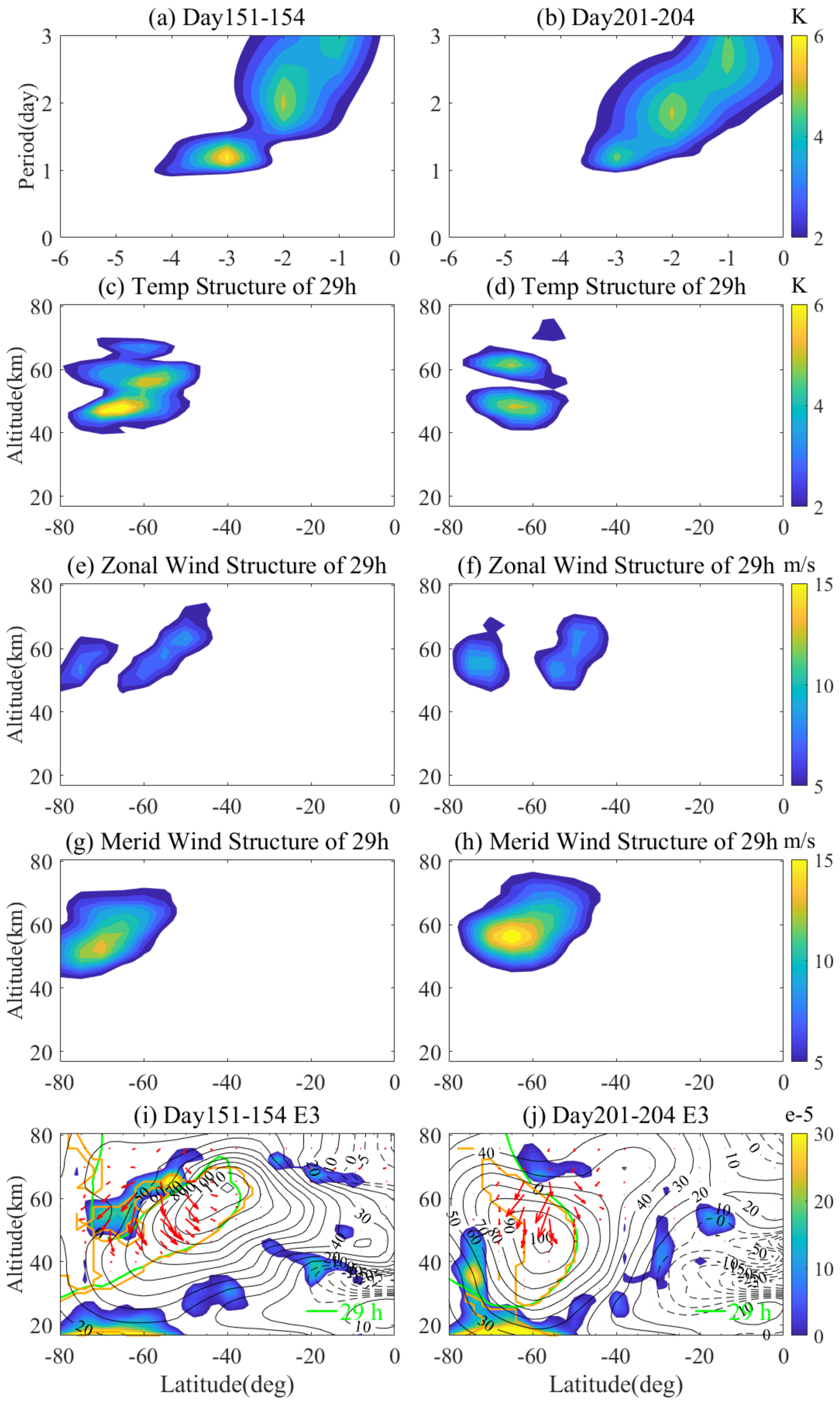

(a) Day151-154
(b) Day201-204
K
Period(day)
(c) Temp Structure of 29h
(d) Temp Structure of 29h
K
Altitude(km)
(e) Zonal Wind Structure of 29h
(f) Zonal Wind Structure of 29h
m/s
(g) Merid Wind Structure of 29h
(h) Merid Wind Structure of 29h
m/s
(i) Day151-154 E3
(j) Day201-204 E3
e-5
29 h
Latitude(deg)

Figure 6. ~~The same~~Same as Figure 4 but for ~~the~~ E3 during the 2019 austral winter period.

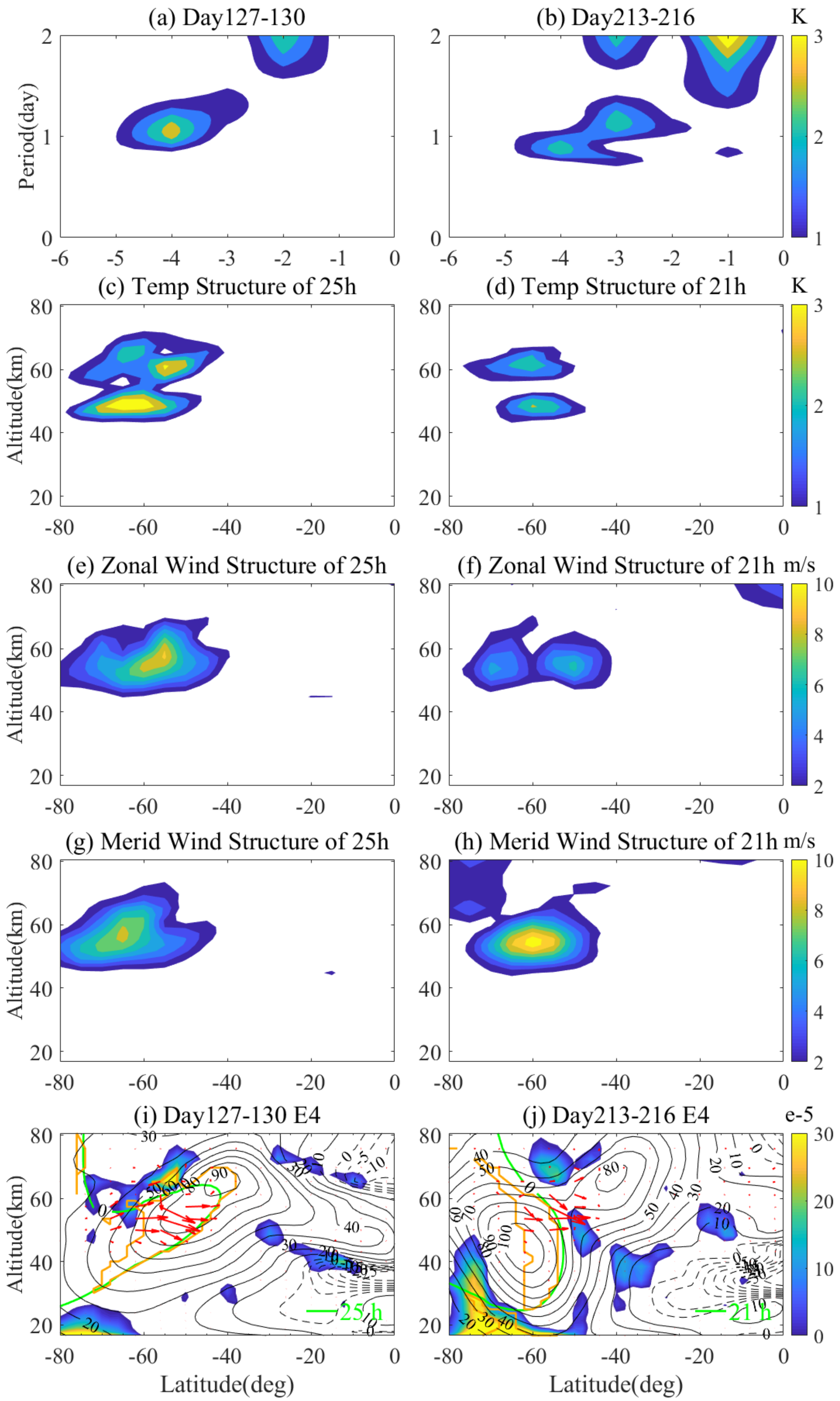

(a) Day127-130
(b) Day213-216
(c) Temp Structure of 25h
(d) Temp Structure of 21h
(e) Zonal Wind Structure of 25h
(f) Zonal Wind Structure of 21h
(g) Merid Wind Structure of 25h
(h) Merid Wind Structure of 21h
(i) Day127-130 E4
(j) Day213-216 E4
Period(day)
Altitude(km)
Latitude(deg)
K
m/s
e-5
25h
21h

906

Figure 7. ~~The same~~Same as Figure 4 but for ~~the~~ E4 during the 2019 austral winter period.

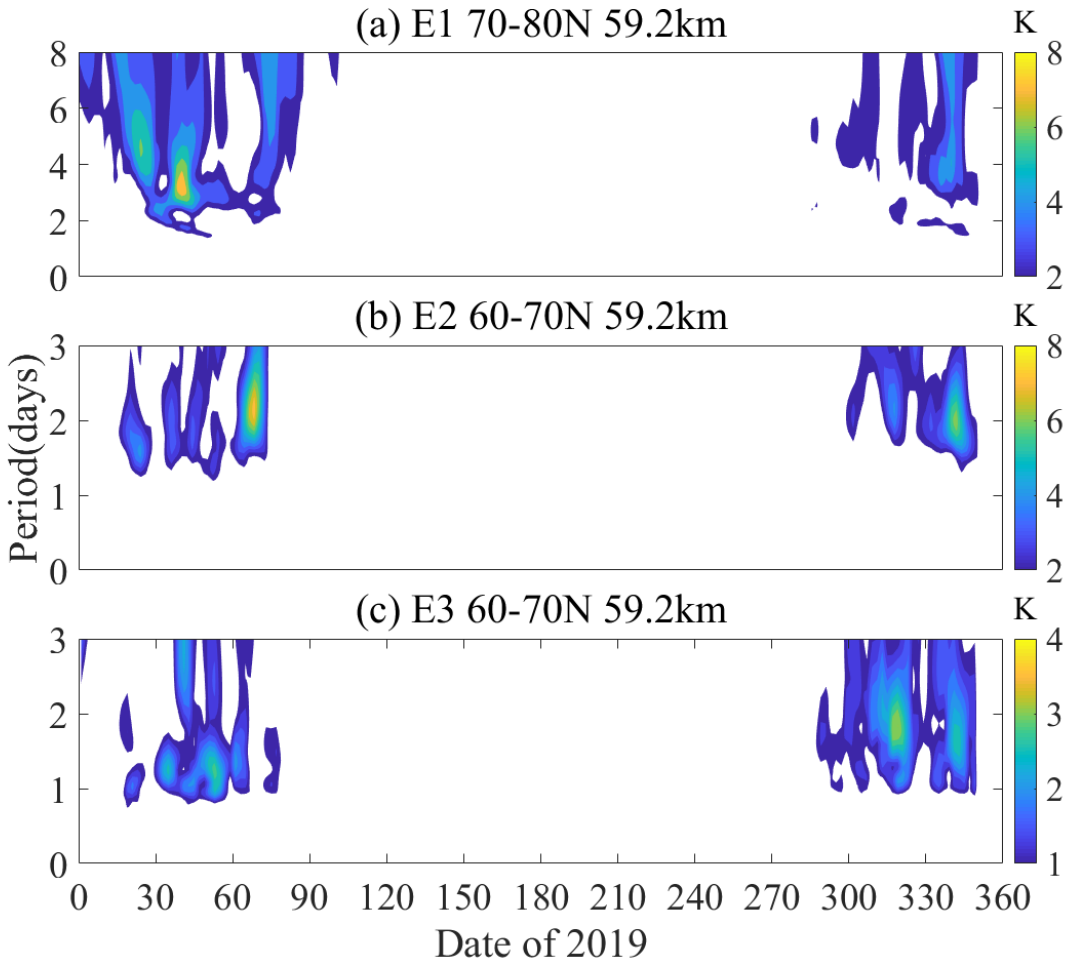

Figure 8. The temporal variations of ~~the~~ (a) E1, (b) E2~~,~~ and (c) E3 QTDWs during the 2019 boreal winter period.

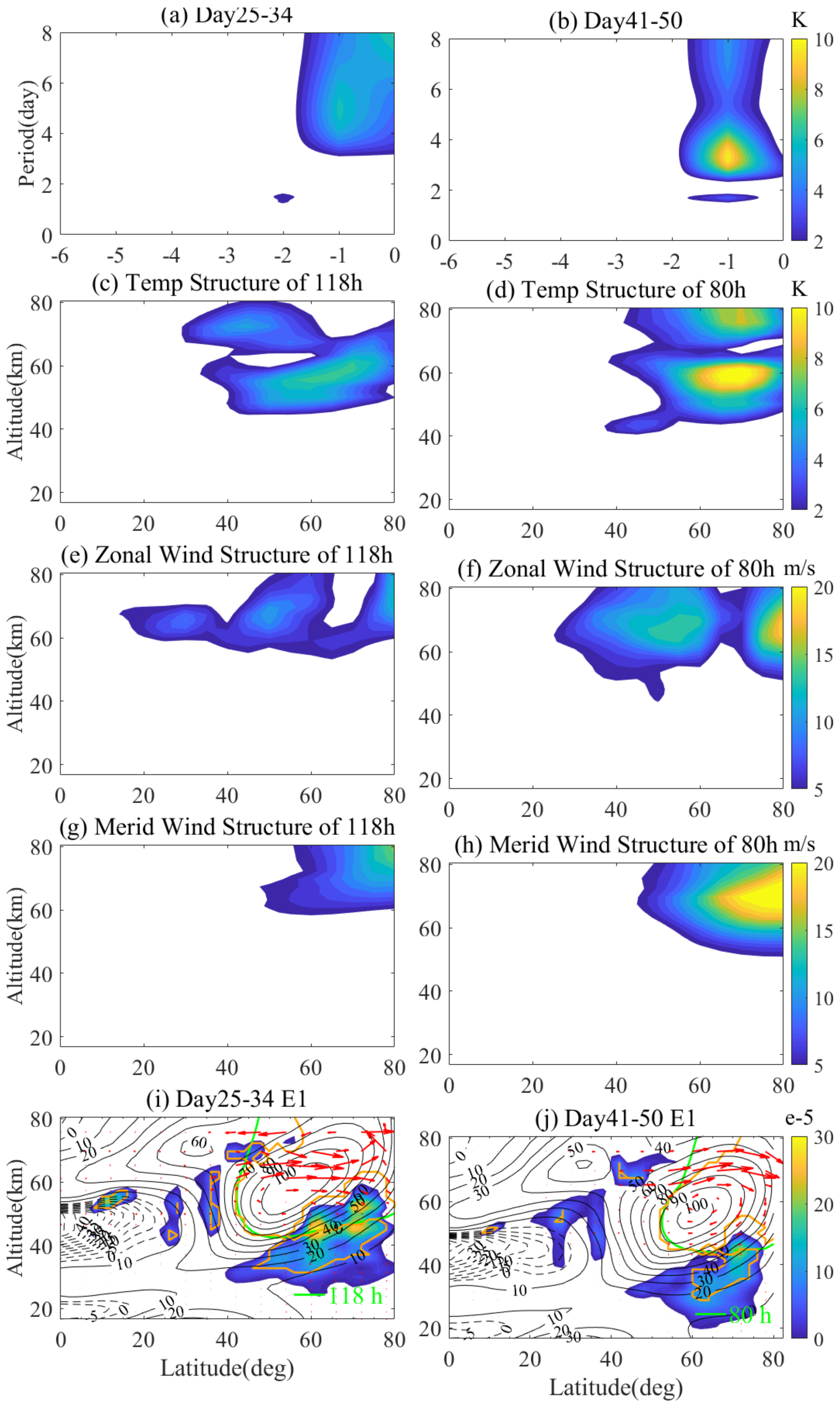
(a) Day25-34
(b) Day41-50
K
Period(day)
(c) Temp Structure of 118h
(d) Temp Structure of 80h
(e) Zonal Wind Structure of 118h
(f) Zonal Wind Structure of 80h
m/s
(g) Merid Wind Structure of 118h
(h) Merid Wind Structure of 80h
Altitude(km)
(i) Day25-34 E1
(j) Day41-50 E1
e-5
118 h
80 h
Latitude(deg)

912

Figure 9. ~~he~~The (a, b) spectra, (c, d) temperature spatial structures, (e, f) zonal wind spatial structures, (g, h) meridional wind spatial structures~~,~~ and (i, j) diagnostic analysis of the E1 typical events during 2019 boreal winter period. The E1 events at 48.2 km and 70-80°N were obtained from the MERRA-2 reanalysis.

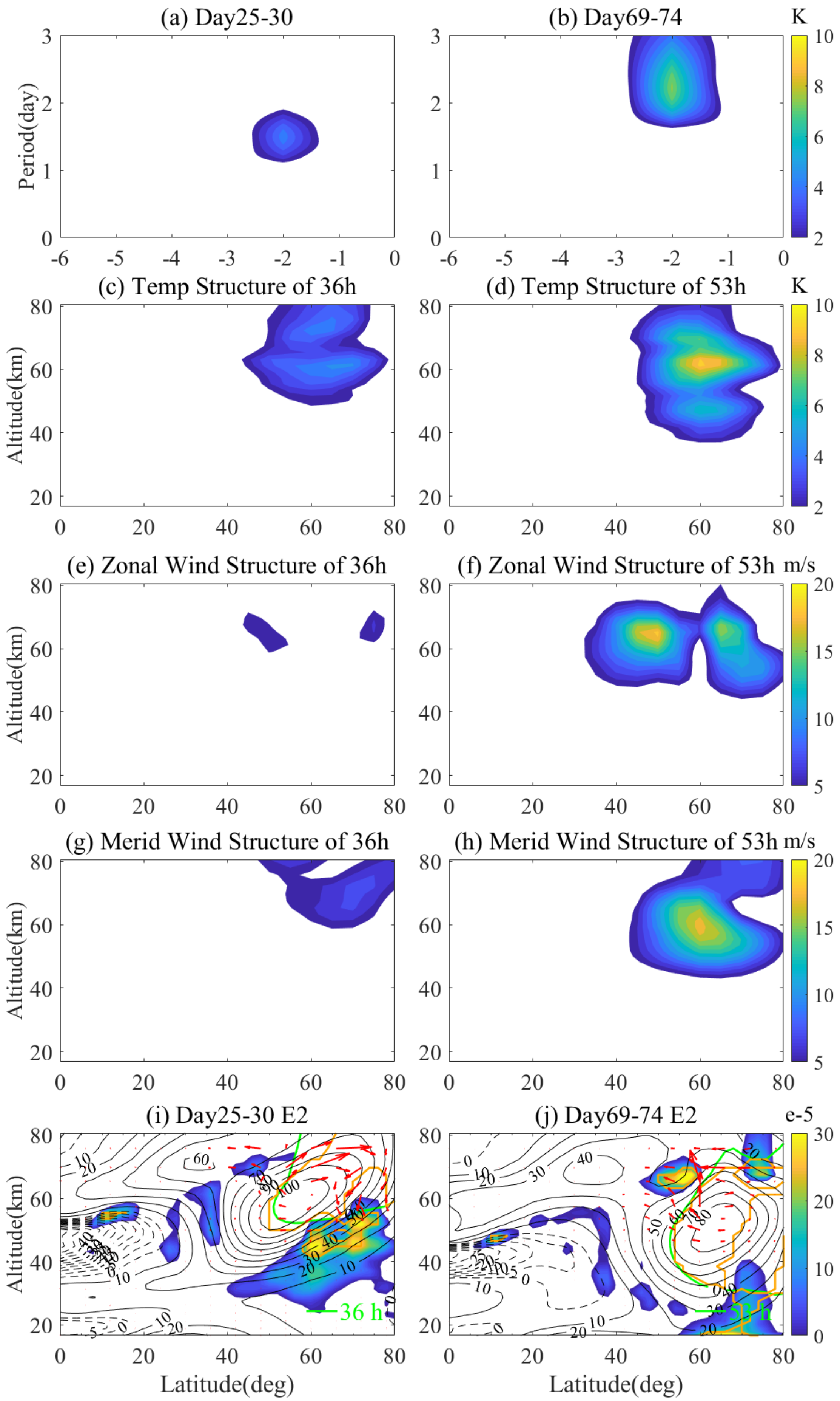

(a) Day25-30
(b) Day69-74
Period(day)
K
(c) Temp Structure of 36h
(d) Temp Structure of 53h
(e) Zonal Wind Structure of 36h
(f) Zonal Wind Structure of 53h
m/s
(g) Merid Wind Structure of 36h
(h) Merid Wind Structure of 53h
(i) Day25-30 E2
(j) Day69-74 E2
e-5
Altitude(km)
36 h
53 h
Latitude(deg)

917

Figure 10. ~~The same~~Same as Figure 9 but for ~~the~~ E2 during the 2019 boreal winter period.

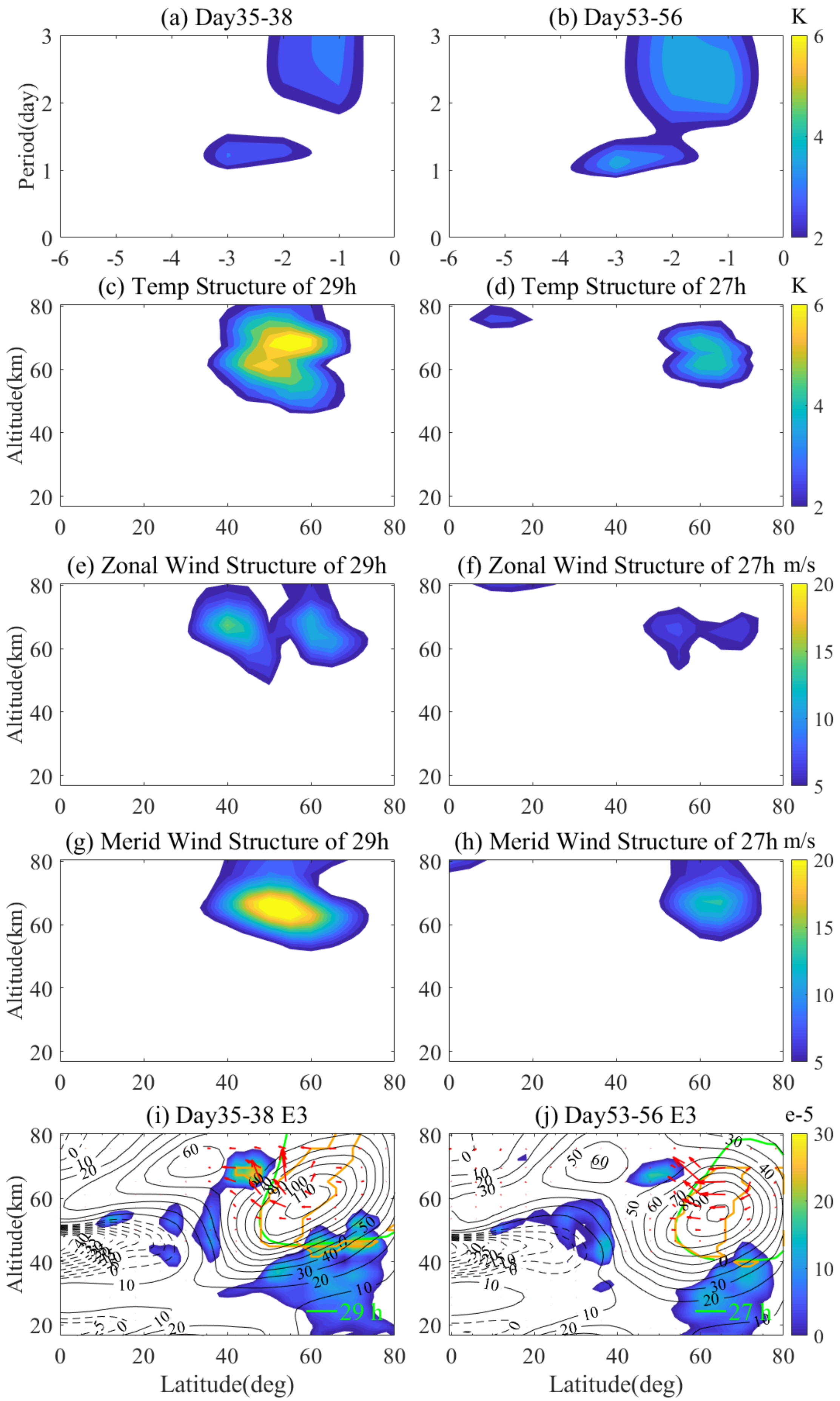

(a) Day35-38
(b) Day53-56
K
Period(day)
(c) Temp Structure of 29h
(d) Temp Structure of 27h
K
(e) Zonal Wind Structure of 29h
(f) Zonal Wind Structure of 27h
m/s
(g) Merid Wind Structure of 29h
(h) Merid Wind Structure of 27h
m/s
(i) Day35-38 E3
(j) Day53-56 E3
e-5
29 h
27 h
Altitude(km)
Latitude(deg)

Figure 11. ~~The same~~Same as Figure 9 but for ~~the~~ E3 during the 2019 boreal winter period.

Eastward-propagating planetary wave in the polar middle atmosphere

Liang Tang[1], Sheng-Yang Gu[1*], Xian-Kang Dou[1]

[1] Electronic Information School, Wuhan University, Wuhan, China.

*Corresponding author: Sheng-Yang Gu, (gushengyang@whu.edu.cn)

Abstract. According to MERRA-2 temperature and wind datasets in 2019, this study presented the global variations of the eastward propagating wavenumber 1 (E1), 2 (E2), 3 (E3) and 4 (E4) planetary waves (PWs) and their diagnostic results in the polar middle atmosphere. We clearly demonstrated the eastward wave modes exist during winter periods with westward background wind in both hemispheres. The maximum wave amplitudes in the southern hemisphere (SH) are slightly larger and lie lower than those in the northern hemisphere (NH). Moreover, the wave perturbations peak at lower latitudes with smaller amplitude as the wavenumber increases. The period of the E1 mode varies 3-5 days in both hemispheres, while the period of E2 mode is slightly longer in the NH (~48 h) than in the SH (~40 h). The periods of the E3 are ~30 h in both SH and NH, and the period of E4 is ~24 h. Despite the shortening of wave periods with the increase of wavenumber, their mean phase speeds are relatively stable, which are ~53 m/s, ~58 m/s, ~55 m/s and ~52 m/s at 70° latitudes for W1, W2, W3 and W4, respectively. The eastward PWs occur earlier with increasing zonal wavenumber, which agrees well with the seasonal variations of the critical layers generated by the background wind. Our diagnostic analysis also indicated that the mean flow instability in the upper stratosphere and upper mesosphere might contribute to the amplification of the eastward PWs.

1 Introduction

The dominance of large amplitude planetary waves in the stratosphere, mesosphere and lower thermosphere regions and their interactions with zonal mean winds are the primary driving force of atmospheric dynamics. In addition, sudden stratospheric warmings (SSWs) and quasi-biennial oscillation (QBO) events can dynamically couple the entire atmosphere from the lower atmosphere to the ionosphere (Li et al., 2020; Yamazaki et al., 2020; Yadav et al., 2019; Matthias and Ern, 2018; Stray et al., 2015). Westward propagating planetary wave is one of the prominent features during austral and boreal summer. Westward quasi-2-day waves (Q2DWs) are the most obvious representative waves and one of the most investigated phenomena using planetary wave observations. Most of the previous studies focused on the westward propagating Q2DWs, i.e., zonal wavenumbers of 2 (W2), 3 (W3) and 4 (W4) modes (Lainer et al., 2018; Gu et al., 2018b; Wang et al., 2017; Pancheva et al., 2016; Gu et al., 2016a; Gu et al., 2016b; Lilienthal and Jacobi, 2015; Gu et al., 2013; Limpasuvan and Wu, 2009; Salby, 1981). However, limited studies were conducted to understand the seasonal variations of the occurrence date, peak amplitude and wave period for the eastward Q2DWs (Gu et al., 2017; Lu et al., 2013; Alexander and Shepherd, 2010; Sandford et al., 2008; Palo et al., 2007; Merzlyakov and Pancheva, 2007; Manney and Randel, 1993; Venne and

Stanford, 1979).

Typically, Q2DWs maximize after the summer solstice in the middle latitudes. The largest wave amplitudes generally appear near the mesopause in January–February in the Southern Hemisphere (SH), while in the Northern Hemisphere (NH) in July–August (Tunbridge et al., 2011). W3 and W4 Q2DWs reach amplitudes during austral and boreal summer in the mesosphere and lower thermosphere, respectively. The seasonal variation of westward Q2DWs activity is obvious (Liu et al., 2019; Gu et al., 2018b; Rao et al., 2017). By observing the long-term Q2DW in the NH and SH, Tunbridge et al. (2011) reported that W3 is generally stronger than the other two modes in the SH, reaching the amplitude of ~12K; while W4 is stronger than W3 in the NH, reaching ~4K. Moreover, W4 generally lives longer than W3, and W4 can still be observed after the ending of W3. A previous study has demonstrated that wave source, instability, critical layer and mean zonal wind are the primary reasons for the seasonal variation of Q2DWs (Liu et al., 2004). By studying the long-term satellite datasets in the SH, Gu et al. (2019) suggested that the strongest events of W2, W3 and W4 could be delayed with increasing the zonal wavenumber, and these events would be indistinguishable during SSWs. The wave periods of W4, W3 and W2 vary around ~41-56 h, ~45-52 h, and ~45-48 h, respectively. Furthermore, W2 can be observed using global satellite datasets, but it has an amplitude weaker than W3 and W4 in the NH and SH (Meek et al., 1996). The propagation and amplification of Q2DWs are primarily modulated by instability, refractive index and critical layer, while the variation of background wind may cause different zonal wavenumber events (Gu et al., 2016a; Gu et al., 2016b). By analyzing the variation of Q2DWs activity during SSWs, Xiong et al. (2018) noticed that W1 is generated by the nonlinear interaction between SPW2 and W3. During SSWs, the coupling between the NH and SH can enhance the summer easterly and promote the nonlinear interaction between W3 and SPW1 (Gu et al., 2018b).

Some recent studies have discovered significant eastward planetary waves in the polar stratosphere and mesosphere regions, with periods of nearly two and four days (Gu et al., 2017; Sandford et al., 2008; Merzlyakov and Pancheva, 2007; Coy et al., 2003; Manney and Randel, 1993). Planetary waves with zonal wavenumbers -1 (E1) and -2 (E2) correspond to 4- and 2-day waves, respectively. Furthermore, planetary waves of 1.2-day with wavenumber -3 (E3) and 0.8-day with wavenumber -4 (E4) have been reported to contain the same phase speeds as E1 and E2 (Manney and Randel, 1993). This series of eastward planetary wave can significantly affect the thermal and dynamic structure of the polar stratosphere, resulting in profound changes in the wind and temperature of the polar stratosphere (Coy et al., 2003; Venne and Stanford, 1979). Beyond the knowledge about nonlinear interactions between migrating tides and Q2DWs (Palo et al., 1999), further investigation has confirmed that E2 Q2DW ~~is c~~could~~oupled~~ be generated by the nonlinear interaction between planetary wave and tides in the mesosphere and lower thermosphere (MLT) (Palo et al., 2007). We should note that the E2 Q2DW generated in the MLT region is different from that in the polar stratosphere, which is discussed in this paper.

By studying and analyzing satellite datasets, Merzlyakov and Pancheva. (2007) indicated that the wave periods of E1 and E2 events range 1.5-5 days. They reported that EP flux travels from the upper to the lower atmosphere, meaning that the upper atmosphere has a dynamic influence on the lower atmosphere. Sandford et al. (2008) reported about significant fluctuations of E2 Q2DW in the polar mesosphere. They indicated the influence of changes in mean zonal winds during a major SSW on the propagation of polar E2. In addition, they proposed the significance of E2 fluctuation in the mesosphere driven by the instabilities in the polar night jet. For E2, amplitude of temperature, zonal wind and meridional wind during the austral winter can reach ~10 K, ~20 m/s and ~30 m/s, respectively; while those during the boreal winter can drop by almost two-thirds. Lu et al. (2013) found that eastward planetary wave propagation is limited to the winter high latitudes probably because the negative refractive indices equatorward of ~45°S result in evanescent wave characteristics. That study suggested that the instability region at

~50-60°S might be induced by the stratospheric polar night jet and/or the "double-jet" structure.

In this study, we use the second modern retrospective research and application analysis (MERRA-2) datasets to investigate the eastward propagating wave characteristics of the stratosphere and mesosphere in polar region in 2019, including E1, E2, E3 and E4. Specifically, we investigate the variation of the occurrence date, peak amplitude and wave period of eastward waves; as well as the role of instability, background wind structure and critical layer in the propagation and amplification of eastward waves. The remaining parts of this paper are organized as follows. Section 2 describes the data and methods used in this study. Section 3 analyzes the global latitude-temporal variation structure of eastward waves during winter in 2019. The amplification and propagation features of the eastward planetary waves in the NH and SH with different wavenumber events are examined in Sections 3.1 and 3.2, respectively. Section 3.3 compares and analyzes the eastward waves in the NH and SH. All research results are summarized in Section 4.

2 Data and Analysis

To extract the E1-, E2-, E3- and E4-wave, we apply the least-square method to each time window (e.g., 10-day, 6-day, 4-day and 4-day), and then use time window to determine the amplitude. (Gu et al., 2013). This method has been shown to successfully identify planetary waves from satellite measurements (Gu et al., 2019; Gu et al., 2018a; Gu et al., 2018b; Gu et al., 2018c; Gu et al., 2013).

$$y = A\cos[2\pi(\sigma \cdot t + s \cdot \lambda)] + B\sin[2\pi(\sigma \cdot t + s \cdot \lambda)] + C \qquad (1)$$

The least-squares method is used to fit the a set of parameters (*A, B* and C), where *σ, t, s* and λ are the frequency, UT time, zonal wavenumber and longitudes. The amplitude of wave R can be expressed as $R = \sqrt{A^2 + B^2}$.

The second modern retrospective research and application analysis (MERRA-2) covers the long-term atmospheric reanalysis datasets initiated by NASA in 1980. It has been upgraded recently using the Goddard Earth Observing System Model, Version 5 (GEOS-5) data assimilation system. Briefly, MERRA-2 includes some updates to the model (Molod et al., 2014; Molod et al., 2012) and the Global Statistical Interpolation (GSI) analysis scheme of Wu et al. (2002). The MERRA-2 data consist of various meteorological variables, e.g., net radiation, temperature, relative humidity and wind speed. The spatial coverage of MERRA-2 data is the globe (spatial resolution: 0.5°×0.625°; temporal resolution: 1 h). This meteorological data are widely used to detect the middle atmosphere such as the planetary wave in the polar atmosphere, global thermal tides, climate variability and aerosol (Ukhov et al., 2020; Sun et al., 2020; Bali et al., 2019; Lu et al., 2013). Many recent studies indicated the feasibility of using MERRA-2 data for the kind of research in present study. Therefore, we apply the MERRA-2 datasets to obtain the variation in background wind, instability, refractive index and critical layer; and explore the patterns of eastward planetary waves propagation and amplification through diagnostic analysis.

The critical layer will absorb or reflect planetary waves from the lower atmosphere during upward propagation. Planetary waves that gain sufficient energy in the unstable region will be amplified during reflection. In a sense, the critical layer plays an important role in regulating the amplification and propagation of planetary waves (Gu et al., 2016a; Gu et al., 2016b; Liu et al., 2004).

$$\overline{q_\varphi} = 2\Omega\cos\varphi - \left(\frac{\left(\bar{u}\cos\varphi\right)_\varphi}{a\cos\varphi}\right)_\varphi - \frac{a}{\rho}\left(\frac{f^2}{N^2}\rho\bar{u}_z\right)_z \qquad (2)$$

The baroclinic/barotropic instability in the atmospheric space structure is caused by the simultaneous equalization of the negative latitude gradient and the quasi-geostrophic potential vorticity ($\overline{q_\varphi}$). In Equation (2), Ω is the angular speed of the Earth's rotation; φ is the latitude; $\bar{u}$ is the zonal mean zonal wind; a is the Earth radius; ρ is the air density; f is the Coriolis parameter; N is the buoyancy frequency; subscripts z and φ are the vertical and latitudinal gradients.

According to Andrews et al. (1987), the properties of planetary wave propagation can be calculated using the Eliassen-Palm (EP) flux vectors (F), i.e.,

$$F=\rho a\cos\varphi\begin{bmatrix}\dfrac{\overline{u}_z\overline{v'\theta'}}{\overline{\theta}_z}-\overline{v'u'}\\ \left[f-\dfrac{\left(\overline{u}\cos\varphi\right)_\varphi}{a\cos\varphi}\right]\dfrac{\overline{v'\theta'}}{\overline{\theta}_z}-\overline{w'u'}\end{bmatrix} \tag{3}$$

where u' and v' are the planetary wave perturbations in the zonal and meridional wind, respectively; θ' and w' are the potential temperature and vertical wind, respectively. The planetary wave propagation is only favorable where the square of refractive index m^2 is positive:

$$m^2=\frac{\overline{q_\varphi}}{a\left(\overline{u}-c\right)}-\frac{s^2}{\left(a\cos\varphi\right)^2}-\frac{f^2}{4N^2H^2} \tag{4}$$

where s is the zonal wavenumber, c is the phase speed and H is the scale height. The square of the refractive index is taken as the waveguide of planetary waves, i.e.,

$$c=-\upsilon_0\cos\left(\frac{\varphi\pi}{180}\right)\Big/sT \tag{5}$$

where υ_0 is the equatorial linear velocity, s is the zonal wavenumber and T is the wave period.

3 Results and Discussion

Figure 1 shows the global temporal-latitude variation structures of E1, E2, E3 and E4 extracted from the 2019 MERRA-2 temperature datasets using time windows 10-, 6-, 4- and 4-days, respectively. The mean temperature amplitude of E1, E2, E3 and E4 at 55.4 km during the periods 3~5-, 1.5~2.5-, 1~1.5- and 0.9~1.1-day are displayed in Figure 1a, 1b, 1c and 1d, respectively. Eastward waves are characterized by obvious seasonal variations in the SH and NH. In addition, E1, E2 (E3) and E4 reach their maximum amplitude at 50-80˚(S/N). In the SH, the strongest E1 and E2 events occur on days 209-218 and 167-172; while E3 and E4 events occur on days 151-154 and 139-142. This means that their occurrence date of maximum amplitude gets earlier with increasing zonal wavenumber. In addition, the maximum amplitude of E1, E2, E3 and E4 are ~6.0 K, ~4.2 K, ~3.6 K and ~2.4 K, respectively, indicating that their peak amplitude drop with rising zonal wavenumber. In the NH, the strongest E1, E2, E3 and E4 events occur on days 41-50, 69-74, 35-38 and 63-66, respectively; the corresponding peak amplitude are ~5.5 K, ~3.8 K, ~2.8 K and ~1.2 K, respectively. Whilst the results demonstrate the decline of the peak amplitude with increasing zonal wavenumber in the NH, the occurrence date is irregular. Moreover, E4 is relatively weak in the NH and difficult to find, so W4 is insignificant in the NH. Figure 2 presents the changes in zonal mean zonal wind at 70˚S and 70˚N in 2019. It can be seen that the background wind on days 90-240 (70˚S) is dominated by westward wind, and reaches ~80 m/s at ~50 km on days 210; it is dominated by eastward wind in late and early 2019, and reaches ~-40 m/s at ~60 km. Meanwhile, the background wind is primarily westerly wind in late and early 2019 (70˚N), and reaches ~90 m/s at ~60 km on days 50; while on days 120-240, the background wind is primarily easterly wind, and the amplitude reaches -40 m/s on days 200. Compared with Figure 1, the results show that the eastward wave modes exist during winter periods with westward background wind in both hemispheres.

3.1 In the Southern Hemisphere

Figure 3 shows that observed maximum temperature amplitude is at ~48.2 km and ~70-80°S for E1; ~48.2km and ~60-70°S for E2 and E3; ~48.2km and ~50-60°S for E4. For E1, the observed maximum perturbation occurs on days 211-220 (with an amplitude of ~8.5 K), and the remaining fluctuations occur on days 161-170, 187-196 and 231-240. For E2, the observed maximum perturbation happens at days 219-224 (with an amplitude of ~7.8 K), and three peaks appear on days 139-144, 173-178 and 187-192. Regarding E3, the strongest perturbation occurs on days 151-154 (with an amplitude of ~5.2 K), while the rest are distributed on days 141-144, 201-204 and 209-202. E4 perturbations are distributed on days 127-130, 145-148, 161-164, 213-216, with weak amplitude of ~3 K. Since earlier studies mentioned that the wave period of the eastward wave can vary, we also investigate the periodic variabilities of E1, E2, E3 and E4. The results show that the period corresponding to the maximum perturbation of E1 falls between ~106 (days 187-196) and ~69 h (days 211-220), and their wave periods vary significantly. Nonetheless, the wave period of E2 gradually changes from ~42 h (days 139-144) to ~38 h (days 219-224), and its stability is stronger than that of E1. The wave periods of E3 and E4 are about ~39 h and ~24 h, respectively. These results reflect that E2, E3 and E4 wave periods are more stable compared to E1.

The spectra, spatial (vertical and latitudinal) structures of temperature, zonal and meridional wind, and diagnostic analysis of E1 are extracted from the two corresponding events (refer to Figure 4). Figures 4a, 4b show the least-squares fitting spectra for MERRA-2 temperature on days 187–196, 211-220 at ~48.2 km and ~70-80°S, when and where the E1 maximizes. An eastward wavenumber -1 signal with the periods of ~106 h and ~69 h clearly dominates the whole spectrum. The temperature spatial structures corresponding to these E1 (i.e., ~106 h and ~69 h) are displayed in Figures 4c, 4d. The temperature spatial structure of E1 exhibits obvious amplitude bimodal structure at ~70-80˚S and ~50 km, and ~70-80˚S and ~60 km, with the maximum at ~70-80˚S and ~50 km. The strongest temperature amplitude of E1 occurs at ~50 km and ~70-80˚S with an amplitude of ~10 K on the days 211-220, and the other peak is ~9K (~70-80˚S and ~60 km). The temperature amplitude of ~9K occurs at ~50 km and ~70-80˚S during days 187-196, and the rest is ~7K (~70-80˚S and ~60 km). The corresponding spatial structures of zonal wind and meridional wind of these E1 are shown in Figures 4e, 4f, 4g and 4h. The maximum zonal wind amplitude of E1 occurs at ~60-70˚S and ~60 km with an amplitude of ~14 m/s on days 187-196, and ~20 m/s at ~50-60˚S and ~60 km on days 211-220. The amplitude of E1 meridional wind hits ~10 m/s at ~70-80˚S and ~55 km (days 187-196) and ~17 m/s at ~70-80˚S and ~60 km (days 211-220), respectively.

Figures 4i, 4j show the diagnostic analysis results for the E1 events during days 187–196 and 211–220, respectively. Apparently, the EP flux vectors is more favorable to propagate in the SH winter and is dramatically amplified by the mean flow instabilities and appropriate background winds at polar region and between ~40 km and ~80 km, with EP flux propagating into the upper atmosphere (Figure 4i). Meanwhile, there is an EP flux at the mid-latitudes and ~60-80 km, which propagates into the lower atmosphere. The wave-mean flow interaction near its critical layer (106 h) of the green curve amplifies E1, and the positive refractive index region surrounded by the yellow curve also enhances E1 propagation. In addition, the strong instability and weak background wind at ~70-80˚S and ~40-60 km provide sufficient energy for the upward EP flux to propagate and amplify. Nevertheless, the downward propagating EP flux is amplified by weak instability and strong background wind at ~50-60˚S and ~60-70 km. Besides, both upward and downward EP fluxes eventually propagate toward the equator at ~50 km. Figure 4j shows that EP flux on days 211-220 propagates downward and amplifies after the interaction of the critical layer (~69 h). The positive refractive index region, strong instability and weak background wind at ~50-60˚S and ~60-70 km provide sufficient energy for E1 amplification and propagation, and ultimately point towards the equator at ~50 km. The results show that the weak background wind and strong instability in the polar region can promote the upward propagation and amplification of EP flux. Meanwhile, the appropriate background wind and instability in the mid-latitudes are also conducive to the downward propagation and amplification of EP flux. In other words, instability and appropriate background wind dominate the propagation and amplification of E1.

For E2, the spectra are observed at ~48.2 km and ~60-70°S on days 173-178 and 219-224 when the eastward wavenumber -2 becomes the primary wave mode with the wave periods ~38 h and ~39 h, respectively (as shown in Figures 5a, 5b). The temperature spatial structures corresponding to these E2 (~38 h and ~39 h) are presented in Figures 5c, 5d. The temperature spatial structure of E2 shows an obvious amplitude bimodal structure at ~60-70˚S and ~50 km, and ~60-70˚S and ~60 km, with the maximum at ~60-70˚S and ~50 km. The maximum temperature amplitude of E1 occurs at ~50 km and ~60-70˚S with an amplitude of ~7.5 K on the days 173-178, and the other peak is ~6 K (~70˚S and ~60 km). The temperature amplitude of ~10 K happens at ~50 km and ~60-70˚S during days 219-224, and the rest is ~6 K (~70˚S and ~60 km). The corresponding spatial structures of zonal wind and meridional wind of these E2 are illustrated in Figures 5e, 5f, 5g and 5h. The zonal wind spatial structure of E2 shows an obvious amplitude bimodal structure at

~50-60˚S and ~60 km, and ~70-80˚S and ~60 km, with the maximum at ~50-60˚S and ~60 km. The maximum zonal wind amplitude of E2 appear at ~50-60˚S and ~60 km with an amplitude of ~10 m/s on days 173-178, and the other peak is ~9 m/s (~70-80˚S and ~60 km). The zonal wind amplitude of ~20 m/s occurs at ~50-60˚S and ~60 km on days 219-224, and the rest is ~15 m/s (~70-80˚S and ~60 km). The amplitude of E2 meridional wind reaches ~13 m/s at ~70-80˚S and ~60 km (days 173-178) and ~27 m/s at ~70-80˚S and ~60 km (days 219-224), respectively.

Figures 5i and 5j illustrate the diagnostic analysis during days 173-178 and 219-224 for E2, respectively. Obviously, E2 is more likely to propagate in the SH winter and is dramatically amplified by the mean flow instabilities at the middle-high latitudes between ~40 km and ~80 km. With EP flux propagating into the lower atmosphere, it eventually propagates toward the equator at ~50 km. Besides, E2 is amplified and propagated by the wave-mean flow interactions near its critical layer (~38 h) of the green curve, and the promoting effect of the positive refractive index region surrounded by the yellow curve. Meanwhile, the weak instability and strong background wind at ~50-60˚S and ~50-70 km provide the energy for the propagation and amplification of EP flux into the lower atmosphere during days 173-178 (Figure 5i). According to the diagnostic analysis of days 219-224, E2 obtains sufficient energy from strong instability and strong background wind at ~50-60˚S and ~60-70 km. It is amplified and propagated into the lower atmosphere through the critical layer and positive refractive index action (as shown in Figure 5j). The results show that the background wind at ~50-60˚S and ~50-70 km is weaker on days 173-178 than on days 219-224; and the instability at ~50-60˚S and ~60-70 km is stronger on days 219-224 than on days 173-178. Our results show that E2 has absorbed sufficient energy to be amplified under the background conditions during days 219-224 (Figures 5a, 5b).

Figures 6a and 6b show the observed spectra of E3 at ~48.2 km and ~60-70°S on days 151-154 and 201-204, and the wave periods of locked wavenumber -3 are ~29 h and ~29 h, respectively. The corresponding temperature spatial structures of these E3 (i.e., ~29 h and ~29 h) are displayed in Figures 6c, 6d. The temperature spatial structure of E3 shows an obvious amplitude bimodal structure at ~60-70˚S and ~50 km, and ~60-70˚S and ~60 km, with the maximum at ~60-70˚S and ~50 km. Besides, E3 also has a weak peak at ~60-70˚S and ~70 km. The strongest temperature amplitude of E3 occurs at ~50 km and ~60-70˚S with an amplitude of ~6K on the days 151-154, and the other peak is ~5 K (~60-70˚S and ~60 km). The temperature amplitude of ~5 K happens at ~50 km (~60 km) and ~60-70˚S during days 201-204. The corresponding spatial structures of zonal wind and meridional wind of these E3 are shown in Figures 6e, 6f, 6g and 6h. The zonal wind spatial structure of E3 shows an obvious amplitude bimodal structure at ~70-80˚S and ~60 km, and ~50-60˚S and ~60 km. The zonal wind amplitudes of E3 occur at ~70-80˚S and ~60 km (~50-60˚S and ~60 km) with an amplitude of ~9 m/s on days 151-154, and ~9 m/s at ~70-80˚S and ~60 km (~50-60˚S and ~60 km) on days 201-204. The amplitude of E3 meridional wind hits ~13 m/s at ~60-70˚S and ~55 km (days 151-154) and ~16 m/s at ~60-70˚S and ~55 km (days 201-204), respectively.

EP flux of E3 is similar to that of E2. The instability and appropriate background wind at the mid-high latitudes between ~50 km and ~70 km dramatically amplify the propagation of E3, which is enhanced by the interaction near the critical layer (~29 h) and the positive refractive index region (Figures 6i and 6j). Notably, the strong instability and weak background wind at ~50-60˚S and ~60-70 km on days 151-154 provide sufficient energy for the propagation and amplification of EP flux into the lower atmosphere, and ultimately point toward the equator at 50 km. During days 201-204, the EP flux propagates into the lower atmosphere and gets amplified by interaction at the critical layer (~29 h). Besides, weak instability and weak background wind at ~50-60˚S and ~60-70 km provide the energy to amplify the E3 propagation. Figures 6c 6d indicate that the stronger the instability at ~50-60˚S and ~60-70 km, the stronger the temperature amplitude of E3. We believe that the background wind and instability at ~50-60˚S and ~60-70 km are the main reasons for the propagation and amplification of EP flux into the lower atmosphere.

For E4, the spectra appear at ~48.2 km and ~50-60°S on days 127-130 and 213-216 when the eastward wavenumber -4 signal with the wave period of ~25 h and ~21 h (see Figures 7a, 7b). The corresponding temperature spatial structures of these E4 (i.e., ~25 h and ~21 h) are shown in Figures 7c, 7d. The temperature spatial structure of E4 shows an obvious amplitude bimodal structure at ~50-60˚S and ~50 km, and ~50-60˚S and ~60 km, with the maximum at ~50-60˚S and ~50 km. The maximum temperature amplitude of E4 occurs at ~50 km and ~50-60˚S with an amplitude of ~4 K on the days 127-130, and the other peak is ~3 K (~60-70˚S and ~60 km). The temperature amplitude of ~3 K occurs at ~50 km (~60 km) during days 213-216. The corresponding spatial structures of zonal wind and meridional wind of these E4 are presented in Figures 7e, 7f, 7g and 7h. The zonal wind spatial structure of E4 shows an obvious amplitude bimodal structure at ~50-60˚S and ~55 km, and ~60-70˚S and ~55 km, with the maximum at ~50-60˚S and ~55 km. The maximum zonal wind amplitude of E4 happens at ~50-60˚S and ~55 km with an amplitude of ~9 m/s on days 127-130, and the other peak is ~5K (~60-70˚S and ~55 km). The zonal wind amplitude of ~5 m/s occurs at ~50-60˚S (~60-70˚S) and ~55 km on days 213-216. The amplitude of E4 meridional wind reaches ~8 m/s at ~60-70˚S and ~55 km (days 127-130) and ~10 m/s at ~60-70˚S and ~55 km (days 213-216), respectively.

Diagnostic analysis for E4 on days 127-130 and 213-216 are shown in Figures 7i and 7j, respectively. The results demonstrate that E4 is dramatically amplified by the mean flow instabilities at the middle-high latitudes between ~50 km and ~70 km. With EP flux propagating into the lower atmosphere, it finally propagates toward the equator at ~50 km. E4 is amplified and propagated by the wave-mean flow interaction near the critical layer (~25 h, ~21 h), and the positive refractive index region generates the promoting effect. The strong instability and weak background wind at ~50-60˚S and ~60-70 km provide sufficient energy for the propagation and amplification of EP flux into the lower atmosphere during days 127-130. Besides, E4 obtains energy from weak instability and weak background wind at ~50-60˚S and ~60-70 km on days 213-216, and it is amplified and propagated into the lower atmosphere. The background wind at ~50-60˚S and ~60-70 km on days 127-130 is similar to on days 213-216, and the instability at ~50-60˚S and ~60-70 km is stronger on days 127-30 than on days 213-216. According to Figures 7a and 7b, E4 absorbs sufficient energy to be amplified under the background conditions on days 127-130, and the temperature amplitude on 127-130 days is stronger.

3.2 In the Northern Hemisphere

Figure 8 shows that the observed maximum temperature amplitude appears at ~59.2 km and ~70-80°N for E1, and the E2 and E3 peaks at

~59.2 km and ~60-70°N. The maximum perturbation of E1 occurs on days 41-50 (with an amplitude of ~8K), while the remaining fluctuations occur on days 25-34 and 339-348. Besides, the strongest E2 occurs on days 69-74 (with an amplitude of ~7 K), and the rest are distributed on days 25-30, 317-322 and 341-346. By contrast, the E3 maximizes on days 35-38 (with an amplitude of ~3K), and also shows a peak on days 53-56. Based on the study of the wave period in the SH for eastward wave, the periodic variabilities of E1, E2 and E3 in the NH are also examined. The wave period of E1 decreases from a maximum of ~118 h (days 25-34) to ~80 h (days 41-50), indicating the instability of the wave period of E1 in the NH. The E2 events occur on days 25-30, 69-74, 317-322 and 341-346, of which the corresponding wave periods are ~36, ~53, ~52 and ~48 h, which are stronger and more stable than E1. Besides, the wave period of E3 is relatively stable at ~29 h and ~27 h. Thus, E2 and E3 wave periods are more stable than E1.

The spectra, spatial (vertical and latitudinal) structures of temperature, zonal and meridional wind, and diagnostic analysis of E1 are extracted from the corresponding representative events (as shown in Figure 9). Figures 9a and 9b show the observed spectra of E1 at ~59.2 km and ~70-80°N on days 25-34 and 41-50, and the wave periods of locked wavenumber -1 are ~118 h and ~80 h, respectively. The corresponding temperature spatial structures of these E1 (~118 h and ~80 h) are shown in Figures 9c, 9d. The temperature spatial structure of E1 shows an obvious amplitude bimodal structure during days 25-34 at ~60-70˚N and ~60 km, and ~40-50˚N and ~70 km, with the maximum at ~60-70˚N and ~60 km. On top of that, E1 also has bimodal structure on days 41-50 at ~60-70˚N and ~60 km, and ~60-70˚N and ~70 km. The strongest temperature amplitude of E1 occurs at ~60-70˚N and ~60 km with an amplitude of ~7 K on the days 25-34, and the other peak is ~4 K (~40-50˚N and ~70 km). The temperature amplitude of ~10 K occurs at ~60 km and ~60-70˚N during days 41-50, and the rest is ~8 K (~60-70˚N and ~70 km). The corresponding spatial structures of zonal wind and meridional wind of these E1 are illustrated in Figures 9e, 9f, 9g and 9h. The zonal wind spatial structure of E1 presents an obvious amplitude bimodal structure at ~70-80˚N and ~70 km, and ~50-60˚N and ~70 km. The zonal wind amplitude of ~13 m/s occurs at ~70-80˚N and ~70 km on days 25-34, and the rest is ~10 m/s (~50-60˚N and ~70 km). In addition, there is a weak peak of 9K during days 25-34 (~30-40˚N and ~70 km). The maximum zonal wind amplitude of E1 occurs at ~70-80˚N and ~70 km with an amplitude of ~19 m/s on days 41-50, and the other peak is ~13K (~50-60˚N and ~70 km). The amplitude of E1 meridional wind hits ~14 m/s at ~70-80˚N and ~70 km (days 25-34) and ~22 m/s at ~70-80˚N and ~70 km (days 41-50), respectively.

The diagnostic analysis results for E1 (in Figures 9i and 9j) suggest the dramatic amplification of E1 by the mean flow instabilities at the middle-high latitudes between ~50 km and ~70 km. With the propagation of EP flux into the polar lower atmosphere, it eventually propagates toward the equator at ~50 km. The wave-mean flow interaction near the critical layers (~118 h, ~80 h) amplifies and propagates E1, and the promoting effect of the positive refractive index region amplifies E1. Furthermore, the weak instability and strong background wind at ~40-50˚N and ~60-70 km generate the energy for the propagation and amplification of EP flux into the polar lower atmosphere during days 25-34. The E1 obtains sufficient energy from weak instability and suitable background wind on days 41-50 at ~40-50˚N and ~60-70 km, and is amplified and propagated into the polar lower atmosphere through the critical layer and positive refractive index action. The background wind at ~40-50˚N and ~60-70 km is stronger on days 25-34 than on days 41-50, but their instability is similar, indicating that stronger background winds might weaken E1 propagation and amplification at the mid-northern latitudes. Our results show that E1 absorbs adequate energy to be amplified under the background conditions during days 41-50, reflecting stronger temperature amplitude (see Figures 9a, 9b).

For E2, the spectra are at ~59.2 km and ~60-70°N on days 25-30 and 69-74 when the eastward wavenumber -2 signal with the period ~36 h and ~53 h (as shown in Figures 10a, 10b). The corresponding temperature spatial structures of these E2 (i.e., ~36 h and ~53 h) are presented in Figures 10c, 10d. The temperature spatial structure of E2 demonstrates an obvious amplitude bimodal structure at ~60-70˚N and ~60 km, and ~60-70˚N and ~70 km, with the maximum at ~60-70˚N and ~60 km. The maximum temperature amplitude of E2 occurs at ~60-70˚N and ~60 km with an amplitude of ~5 K on days 25-30, and the other peak is ~4 K (~60-70˚N and ~70 km). The temperature amplitude of ~9 K occurs on days 69-74 at ~60˚S and ~60 km, and the other peaks are ~7 K (~60-70˚N and ~70 km), ~5 K (~60-70˚N and ~50 km). The corresponding spatial structures of zonal wind and meridional wind of these E2 are shown in Figures 10e, 10f, 10g and 10h. The zonal wind spatial structure of E2 shows an obvious amplitude bimodal structure at ~60-70˚N and ~60 km, and ~40-50˚N and ~60 km, with the maximum at ~40-50˚N and ~60 km. The maximum zonal wind amplitude of E2 appears at ~60-70˚N and ~60 km (~40-50˚N and ~60 km) with an amplitude of ~6 m/s on days 25-30. Zonal wind amplitude occurs at ~40-50˚N and ~60 km with an amplitude of ~18 m/s on days 41-50, and the other peak is ~16 K (~60-70˚N and ~60km). The amplitude of E2 meridional wind reaches ~7 m/s at ~60-70˚N and ~70 km (days 25-30) and ~18 m/s at ~60-70˚N and ~60 km (days 41-50), respectively.

The diagnostic analysis of E2 on days 25-30 and 69-74 are shown in Figures 10i and 10j, respectively. Apparently, E2 is significantly amplified by the mean flow instabilities at the middle-high latitudes between ~40 km and ~70 km, with EP flux propagating into the polar lower atmosphere, and EP flux eventually propagate toward the equator at ~50 km. E2 is amplified and propagated by the wave-mean flow interaction near the critical layers (~36 h, ~53 h), and the positive refractive index region provides the promoting effect. The weak instability and strong background wind at ~50-60˚N and ~60-70 km provide the energy for the propagation and amplification of EP flux into the polar lower atmosphere during days 25-30. Moreover, E2 obtains sufficient energy from strong instability and suitable background wind at ~50-60˚N and ~60-70 km on days 69-74, and it is amplified and propagated into the polar lower atmosphere. The background wind at ~50-60˚N and ~60-70 km on days 127-130 is similar to on days 213-216, and the instability at ~50-60˚S and ~60-70 km is stronger on days 127-30 than on days 213-216. Although the background wind at ~50-60˚N and ~60-70 km is stronger on days 25-30 than on days 69-74, the instability at ~50-60˚N and ~60-70 km is stronger on days 69-74 than on days 25-30. The temperature amplitude results indicate that E2 absorbs sufficient energy to be amplified under the background conditions on days 69-74, with stronger temperature amplitude on days 69-74 (Figures 10a, 10b).

Figures 11a and 11b show the observed spectra of E3 at ~59.2km and ~60-70°N on days 35-38 and 53-56, and the wave periods of locked wavenumber -3 are ~29 h and ~27 h, respectively. The corresponding temperature spatial structures of these E3 (i.e., ~29 h and ~27 h) are shown in Figures 11c, 11d. The temperature spatial structure of E3 shows an obvious amplitude bimodal structure at ~50-60°N and ~60 km, and ~50-60°N and ~70 km, with the maximum at ~50-60°N and ~60 km. The strongest temperature amplitude of E3 occurs at ~60 km and ~50-60°N with an amplitude of ~6 K on the days 35-38, and the other peak is ~5 K (~50-60°N and ~70 km). The temperature amplitude of ~4 K occurs at ~60 km (~70 km) and ~50-60°N during days 53-56. The corresponding spatial structures of zonal wind and meridional wind of these E3 are illustrated in Figures 6e, 6f, 6g and 6h. The zonal wind spatial structure of E3 shows an obvious amplitude bimodal structure at ~40-50°N and ~70 km, and ~60-70°N and ~70 km. The zonal wind amplitudes of E3 occur at ~40-50°N and ~70 km with an amplitude of ~15 m/s on days 35-38, and ~12 m/s at ~60-70°N and ~70 km. The maximum zonal wind amplitude of E3 appears at ~40-50°N and ~70 km (~60-70°N and ~70 km) with an amplitude of ~7 m/s (~6 m/s) on days 53-56. The amplitude of E3 meridional wind reaches ~22 m/s at ~50-60°N and ~70 km (days 35-38) and ~12 m/s at ~60-70°N and ~70 km (days 53-56), respectively.

Obviously, the instability and appropriate background wind at the mid-latitudes between ~50 km and ~70 km and the interaction near the critical layers (~29 h, ~27 h) dramatically amplify the propagation of E3 (see Figures 11i and 11j). The background wind is similar on days 35-38 and 53-56, and the former is relatively unstable. This finding indicates that the E3 in propagation is more likely to gather sufficient energy to be amplified on days 35-38. The instability and appropriate background wind at the mid-high latitudes between ~50 km and ~70 km drastically amplify the propagation of E3, which is enhanced by the interaction near the critical layers (~29 h, ~27 h) and the positive refractive index region (Figures 11i, 11j). In particular, the strong instability and weak background wind at ~50-60°N and ~60-70 km on days 35-38 generate sufficient energy for the propagation and amplification of EP flux into the lower atmosphere, and ultimately point toward the equator at 50 km. The EP flux propagates to the lower atmosphere during days 35-38, and it is amplified by interactions at the critical layer (~29 h). In addition, weak instability and weak background winds on days 53-56 at ~50-60°N and ~60-70 km provide the energy to amplify E3 propagation. Combine with Figures 11c, 11d, the stronger the instability at ~50-60°N and ~60-70 km, the stronger the temperature amplitude of E3. The results show that the instability on days 35-38 at ~50-60°N and ~60-70 km are the primary reasons for the propagation and amplification of EP flux into the lower atmosphere.

3.3 Comparison between SH and NH

The observed latitude and maximum temperature amplitude for eastward planetary waves (i.e., E1, E2, E3, E4) decrease and weaken with increasing zonal wavenumber in the SH, reaching ~70-80˚S, ~60-70˚S, ~60-70˚S and ~50-60˚S, and ~10 K, ~9 K, ~6 K, and ~3 K, respectively. In addition, the occurrence date gets earlier with increasing zonal wavenumber. The temperature spatial structure demonstrates a bimodal-peak structure (~50 and ~60 km), mainly located at ~50 km. The maximum zonal wind amplitudes of E1 and E2, E3 and E4 are almost the same, which are ~20 m/s and ~10 m/s, respectively. The maximum meridional wind amplitudes of E1, E2, E3 and E4 are ~17 m/s, ~27 m/s, ~16 m/s and ~11 m/s, respectively. The wave period of E1 tends to get shorter from 5 to 3 days; while E2 and E3 are close to ~40 h and ~30 h; and E4 remains at ~24 h. E1, E2, E3 and E4 are more favorable to propagation in the SH winter and are abruptly amplified by the mean flow instabilities at the middle latitudes between ~40 km and ~70 km. With the propagation of EP flux into the lower atmosphere, and it finally propagates toward the equator at ~50 km. In addition, the propagation of EP flux for E1 to the upper atmosphere might be influenced by the instability and background wind at the Antarctic ~50km.

The observed latitudes of E1, E2 (E3) decrease with increasing wavenumber in the NH, which are ~70-80˚N, ~60-70˚N and ~60-70˚N. With bimodal-peak structure located at ~70 km, the temperature spatial structures of E1, E2 and E3 reach ~10 K, ~9 K and ~6 K, respectively.

The maximum zonal wind amplitude for E1, E2 and E3 occur at ~50-80˚N and ~70 km, and their amplitude are almost equal to ~18 m/s. The maximum meridional winds of E1, E2 and E3 occur at ~50-80˚N and ~70 km with amplitudes of ~22 m/s, ~18 m/s and ~22 m/s, respectively. The wave period of E1 tends to be shorter from 5-3 days; and E2 and E3 are close to ~48 h and ~30 h. In addition, E1, E2 and E3 are more favorable to propagation in the NH winter and are dramatically amplified by the mean flow instabilities at the middle latitudes between ~40 km and ~70 km, with the propagation of EP flux into the lower atmosphere and then toward the equator at ~50 km.

4 Summary and Conclusions

Based on the MERRA-2 temperature and wind observations in 2019, we present for the first time an extensive study of the global variation for eastward planetary wave activity, including zonal wave numbers of -1 (E1), -2 (E2), -3 (E3), -4 (E4) in the stratosphere and mesosphere. The temperature and wind amplitude and wave periods of each event were determined using 2-D least-squares fitting. Our study covered the spatial and temporal patterns of the eastward planetary waves in both hemispheres with a comprehensive diagnostic analysis on their propagation and amplification. The key findings of this study are summarized below:

1. The latitudes for the maximum (temperature, zonal and meridional

wind) amplitudes of E1, E2, E3 and E4 decrease with increasing wavenumber in the SH and NH. The E1, E2, E3 and E4 events occur earlier with increasing zonal wavenumber in the SH. In addition, eastward wave modes exist during summer periods with westward background wind in both hemispheres.

2. The temperature spatial structures of E1, E2, E3 and E4 present a double-peak structure, which is located at ~50 km and ~60 km in SH, ~60 km and ~70 km in SH. Furthermore, the lower peak is usually larger than the higher one.

3. The maximum (temperature, zonal and meridional wind) amplitude of E1, E2 and E3 decline with rising zonal wavenumber in the SH and NH. The maximum temperature amplitude in the SH are slightly larger and lie lower than those in the NH. In addition, the meridional wind amplitude are slightly larger than the zonal wind in the SH and NH.

4. The wave period of the E1 mode ranges 3-5 days in both hemispheres, while the period of E2 mode is slightly longer in the NH (~48 h) than in the SH (~40 h). The periods of E3 in both SH and NH are ~30 h, while the period of E4 is ~24 h.

5. The eastward planetary wave is more favorable to propagate in the winter hemisphere and is drastically amplified by the mean flow instabilities and appropriate background winds at polar region and the middle latitudes between ~40 km and ~80 km. Furthermore, the

amplification of planetary waves through wave-mean flow interaction occurs easily close to its critical layer. In addition, the direction of EP flux ultimately points towards the equator.

6. The strong instability and appropriate background wind in the lower layer of the Antarctic region might generate adequate energy to promote the E1 propagation and amplification to the upper atmosphere.

Overall, this study demonstrated how the background zonal wind in the polar middle atmosphere affects the dynamics of eastward planetary waves in the polar middle atmosphere.

Data availability. MERRA-2 data are available at http://disc.gsfc.nasa.gov.

Code availability. Code is available at http://hdl.pid21.cn/21.86116.7/04.99.01293.

Author contributions. LT carried out the data processing and analysis and wrote the manuscript. SYG and XKD contributed to reviewing the article.

Competing interests. The authors declare that they have no conflict of interest.

Acknowledgements. This work was performed in the framework of the Space Physics Research (SPR). The authors thank NASA for free online access to the MERRA-2 temperature reanalysis.

Financial support. This research work was supported by the National Natural Science Foundation of China (41704153, 41874181, and 41831071).

References

Alexander, S. P. and Shepherd, M. G.: Planetary wave activity in the polar lower stratosphere, Atmos. Chem. Phys., 10, 707-718, 10.5194/acp-10-707-2010, 2010.

Andrews, D., Holton, J., and Leovy, C.: Middle Atmosphere Dynamics, 489 pp.1987.

Bali, K., Dey, S., Ganguly, D., and Smith, K. R.: Space-time variability of ambient PM2.5 diurnal pattern over India from 18-years (2000–2017) of MERRA-2 reanalysis data, Atmos. Chem. Phys. Discuss., 2019, 1-23, 10.5194/acp-2019-731, 2019.

Coy, L., Štajner, I., DaSilva, A. M., Joiner, J., Rood, R. B., Pawson, S., and Lin, S. J.: High-Frequency Planetary Waves in the Polar Middle Atmosphere as Seen in a Data Assimilation System, Journal of the Atmospheric Sciences, 60, 2975-2992, 10.1175/1520-0469(2003)060<2975:Hpwitp>2.0.Co;2, 2003.

Gu, S.-Y., Liu, H.-L., Dou, X., and Jia, M.: Ionospheric Variability Due to Tides and Quasi-Two Day Wave Interactions, Journal of Geophysical Research: Space Physics, 123, 1554-1565, https://doi.org/10.1002/2017JA025105, 2018a.

Gu, S.-Y., Dou, X., Pancheva, D., Yi, W., and Chen, T.: Investigation of the Abnormal Quasi 2-Day Wave Activities During the Sudden Stratospheric Warming Period of January 2006, Journal of Geophysical Research: Space Physics, 123, 6031-6041, https://doi.org/10.1029/2018JA025596, 2018b.

Gu, S.-Y., Liu, H.-L., Pedatella, N. M., Dou, X., and Liu, Y.: On the wave number 2 eastward propagating quasi 2 day wave at middle and high latitudes, Journal of Geophysical Research: Space Physics, 122, 4489-4499, https://doi.org/10.1002/2016JA023353, 2017.

Gu, S.-Y., Liu, H.-L., Pedatella, N. M., Dou, X., and Shu, Z.: The quasi-2 day wave activities during

2007 boreal summer period as revealed by Whole Atmosphere Community Climate Model, Journal of Geophysical Research: Space Physics, 121, 7256-7268, https://doi.org/10.1002/2016JA022867, 2016a.

Gu, S.-Y., Li, T., Dou, X., Wu, Q., Mlynczak, M. G., and Russell Iii, J. M.: Observations of Quasi-Two-Day wave by TIMED/SABER and TIMED/TIDI, Journal of Geophysical Research: Atmospheres, 118, 1624-1639, https://doi.org/10.1002/jgrd.50191, 2013.

Gu, S.-Y., Liu, H.-L., Pedatella, N. M., Dou, X., Li, T., and Chen, T.: The quasi 2 day wave activities during 2007 austral summer period as revealed by Whole Atmosphere Community Climate Model, Journal of Geophysical Research: Space Physics, 121, 2743-2754, https://doi.org/10.1002/2015JA022225, 2016b.

Gu, S.-Y., Ruan, H., Yang, C.-Y., Gan, Q., Dou, X., and Wang, N.: The Morphology of the 6-Day Wave in Both the Neutral Atmosphere and F Region Ionosphere Under Solar Minimum Conditions, Journal of Geophysical Research: Space Physics, 123, 4232-4240, https://doi.org/10.1029/2018JA025302, 2018c.

Gu, S.-Y., Dou, X.-K., Yang, C.-Y., Jia, M., Huang, K.-M., Huang, C.-M., and Zhang, S.-D.: Climatology and Anomaly of the Quasi-Two-Day Wave Behaviors During 2003–2018 Austral Summer Periods, Journal of Geophysical Research: Space Physics, 124, 544-556, https://doi.org/10.1029/2018JA026047, 2019.

Lainer, M., Hocke, K., and Kämpfer, N.: Long-term observation of midlatitude quasi 2-day waves by a water vapor radiometer, Atmos. Chem. Phys., 18, 12061-12074, 10.5194/acp-18-12061-2018, 2018.

Li, H., Pilch Kedzierski, R., and Matthes, K.: On the forcings of the unusual Quasi-Biennial

Oscillation structure in February 2016, Atmos. Chem. Phys., 20, 6541-6561, 10.5194/acp-20-6541-2020, 2020.

Lilienthal, F. and Jacobi, C.: Meteor radar quasi 2-day wave observations over 10 years at Collm (51.3° N, 13.0° E), Atmos. Chem. Phys., 15, 9917-9927, 10.5194/acp-15-9917-2015, 2015.

Limpasuvan, V. and Wu, D. L.: Anomalous two-day wave behavior during the 2006 austral summer, Geophysical Research Letters, 36, https://doi.org/10.1029/2008GL036387, 2009.

Liu, G., England, S. L., and Janches, D.: Quasi Two-, Three-, and Six-Day Planetary-Scale Wave Oscillations in the Upper Atmosphere Observed by TIMED/SABER Over ~17 Years During 2002–2018, Journal of Geophysical Research: Space Physics, 124, 9462-9474, https://doi.org/10.1029/2019JA026918, 2019.

Liu, H. L., Talaat, E. R., Roble, R. G., Lieberman, R. S., Riggin, D. M., and Yee, J. H.: The 6.5-day wave and its seasonal variability in the middle and upper atmosphere, Journal of Geophysical Research: Atmospheres, 109, https://doi.org/10.1029/2004JD004795, 2004.

Lu, X., Chu, X., Fuller-Rowell, T., Chang, L., Fong, W., and Yu, Z.: Eastward propagating planetary waves with periods of 1–5 days in the winter Antarctic stratosphere as revealed by MERRA and lidar, Journal of Geophysical Research: Atmospheres, 118, 9565-9578, https://doi.org/10.1002/jgrd.50717, 2013.

Manney, G. L. and Randel, W. J.: Instability at the Winter Stratopause: A Mechanism for the 4-Day Wave, Journal of Atmospheric Sciences, 50, 3928-3938, 10.1175/1520-0469(1993)050<3928:IATWSA>2.0.CO;2, 1993.

Matthias, V. and Ern, M.: On the origin of the mesospheric quasi-stationary planetary waves in the unusual Arctic winter 2015/2016, Atmospheric Chemistry and Physics, 18, 4803-4815,

10.5194/acp-18-4803-2018, 2018.

Meek, C. E., Manson, A. H., Franke, S. J., Singer, W., Hoffmann, P., Clark, R. R., Tsuda, T., Nakamura, T., Tsutsumi, M., Hagan, M., Fritts, D. C., Isler, J., and I. Portnyagin, Y.: Global study of northern hemisphere quasi-2-day wave events in recent summers near 90 km altitude, Journal of Atmospheric and Terrestrial Physics, 58, 1401-1411, https://doi.org/10.1016/0021-9169(95)00120-4, 1996.

Merzlyakov, E. G. and Pancheva, D. V.: The 1.5–5-day eastward waves in the upper stratosphere–mesosphere as observed by the Esrange meteor radar and the SABER instrument, Journal of Atmospheric and Solar-Terrestrial Physics, 69, 2102-2117, https://doi.org/10.1016/j.jastp.2007.07.002, 2007.

Molod, A., Takacs, L., Suarez, M., and Bacmeister, J.: Development of the GEOS-5 atmospheric general circulation model: evolution from MERRA to MERRA2, Geoscientific Model Development Discussions, 7, 10.5194/gmdd-7-7575-2014, 2014.

Molod, A., Takacs, L., Suarez, M., Bacmeister, J., Song, I. S., and Eichmann, A.: The GEOS-5 Atmospheric General Circulation Model: Mean Climate and Development from MERRA to Fortuna, 2012.

Palo, S. E., Roble, R. G., and Hagan, M. E.: Middle atmosphere effects of the quasi-two-day wave determined from a General Circulation Model, Earth, Planets and Space, 51, 629-647, 10.1186/BF03353221, 1999.

Palo, S. E., Forbes, J. M., Zhang, X., Russell Iii, J. M., and Mlynczak, M. G.: An eastward propagating two-day wave: Evidence for nonlinear planetary wave and tidal coupling in the mesosphere and lower thermosphere, Geophysical Research Letters, 34,

https://doi.org/10.1029/2006GL027728, 2007.

Pancheva, D., Mukhtarov, P., Siskind, D. E., and Smith, A. K.: Global distribution and variability of quasi 2 day waves based on the NOGAPS-ALPHA reanalysis model, Journal of Geophysical Research: Space Physics, 121, 11,422-411,449, https://doi.org/10.1002/2016JA023381, 2016.

Rao, N. V., Ratnam, M. V., Vedavathi, C., Tsuda, T., Murthy, B. V. K., Sathishkumar, S., Gurubaran, S., Kumar, K. K., Subrahmanyam, K. V., and Rao, S. V. B.: Seasonal, inter-annual and solar cycle variability of the quasi two day wave in the low-latitude mesosphere and lower thermosphere, Journal of Atmospheric and Solar-Terrestrial Physics, 152-153, 20-29, https://doi.org/10.1016/j.jastp.2016.11.005, 2017.

Salby, M. L.: The 2-day wave in the middle atmosphere: Observations and theory, Journal of Geophysical Research: Oceans, 86, 9654-9660, https://doi.org/10.1029/JC086iC10p09654, 1981.

Sandford, D. J., Schwartz, M. J., and Mitchell, N. J.: The wintertime two-day wave in the polar stratosphere, mesosphere and lower thermosphere, Atmos. Chem. Phys., 8, 749-755, 10.5194/acp-8-749-2008, 2008.

Stray, N. H., Orsolini, Y. J., Espy, P. J., Limpasuvan, V., and Hibbins, R. E.: Observations of planetary waves in the mesosphere-lower thermosphere during stratospheric warming events, Atmos. Chem. Phys., 15, 4997-5005, 10.5194/acp-15-4997-2015, 2015.

Sun, J., Veefkind, J. P., van Velthoven, P., Tilstra, L. G., Chimot, J., Nanda, S., and Levelt, P. F.: Defining aerosol layer height for UVAI interpretation using aerosol vertical distributions characterized by MERRA-2, Atmos. Chem. Phys. Discuss., 2020, 1-36, 10.5194/acp-2020-39, 2020.

Tunbridge, V. M., Sandford, D. J., and Mitchell, N. J.: Zonal wave numbers of the summertime 2 day planetary wave observed in the mesosphere by EOS Aura Microwave Limb Sounder, Journal of Geophysical Research: Atmospheres, 116, https://doi.org/10.1029/2010JD014567, 2011.

Ukhov, A., Mostamandi, S., da Silva, A., Flemming, J., Alshehri, Y., Shevchenko, I., and Stenchikov, G.: Assessment of natural and anthropogenic aerosol air pollution in the Middle East using MERRA-2, CAMS data assimilation products, and high-resolution WRF-Chem model simulations, Atmospheric Chemistry and Physics, 20, 9281-9310, 10.5194/acp-20-9281-2020, 2020.

Venne, D. E. and Stanford, J. L.: Observation of a 4–Day Temperature Wave in the Polar Winter Stratosphere, Journal of the Atmospheric Sciences, 36, 2016-2019, 10.1175/1520-0469(1979)036<2016:Ooatwi>2.0.Co;2, 1979.

Wang, J. C., Chang, L. C., Yue, J., Wang, W., and Siskind, D. E.: The quasi 2 day wave response in TIME-GCM nudged with NOGAPS-ALPHA, Journal of Geophysical Research: Space Physics, 122, 5709-5732, https://doi.org/10.1002/2016JA023745, 2017.

Wu, W.-S., Purser, R. J., and Parrish, D. F.: Three-Dimensional Variational Analysis with Spatially Inhomogeneous Covariances, Monthly Weather Review, 130, 2905-2916, 10.1175/1520-0493(2002)130<2905:TDVAWS>2.0.CO;2, 2002.

Xiong, J., Wan, W., Ding, F., Liu, L., Hu, L., and Yan, C.: Two Day Wave Traveling Westward With Wave Number 1 During the Sudden Stratospheric Warming in January 2017, Journal of Geophysical Research: Space Physics, 123, 3005-3013, https://doi.org/10.1002/2017JA025171, 2018.

Yadav, S., Vineeth, C., Kumar, K. K., Choudhary, R. K., Pant, T. K., and Sunda, S.: Role of the phase of Quasi-Biennial Oscillation in modulating the influence of SSW on Equatorial Ionosphere, 2019 URSI Asia-Pacific Radio Science Conference (AP-RASC), 9-15 March 2019, 1-4, 10.23919/URSIAP-RASC.2019.8738274,

Yamazaki, K., Nakamura, T., Ukita, J., and Hoshi, K.: A tropospheric pathway of the stratospheric quasi-biennial oscillation (QBO) impact on the boreal winter polar vortex, Atmos. Chem. Phys., 20, 5111-5127, 10.5194/acp-20-5111-2020, 2020.

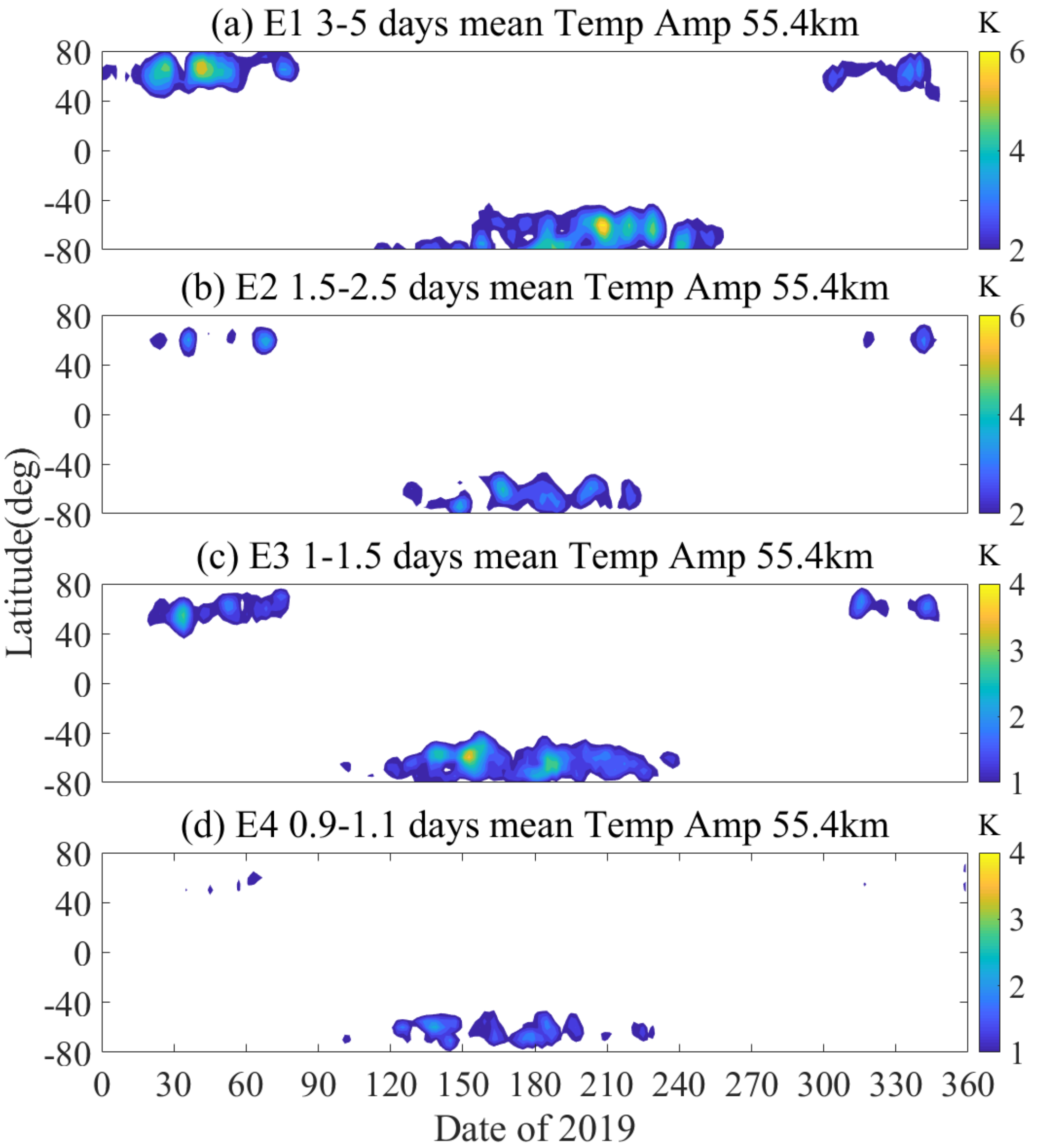

Figure 1. The global latitude-temporal variation structures of the (a) E1, (b) E2, (c) E3 and (d) E4 planetary waves during 2019. White areas represent small amplitude data (corresponds to the right color bar).

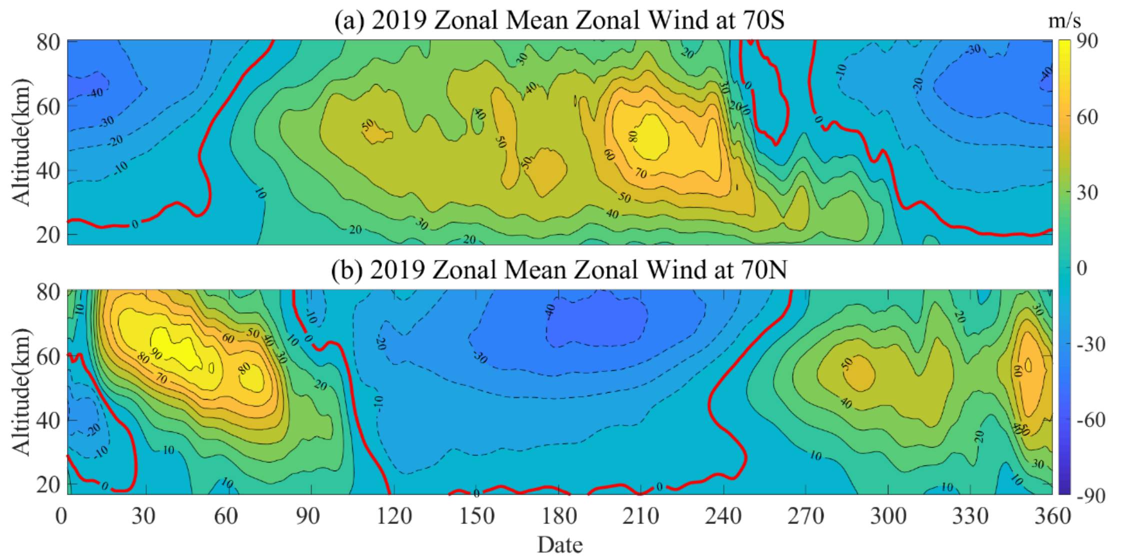

Figure 2. The zonal mean zonal wind variations of (a) 70°S and (b) 70°N during 2019. The dotted line represents eastward wind, the solid line represents westward wind, and the red solid line is 0 m/s.

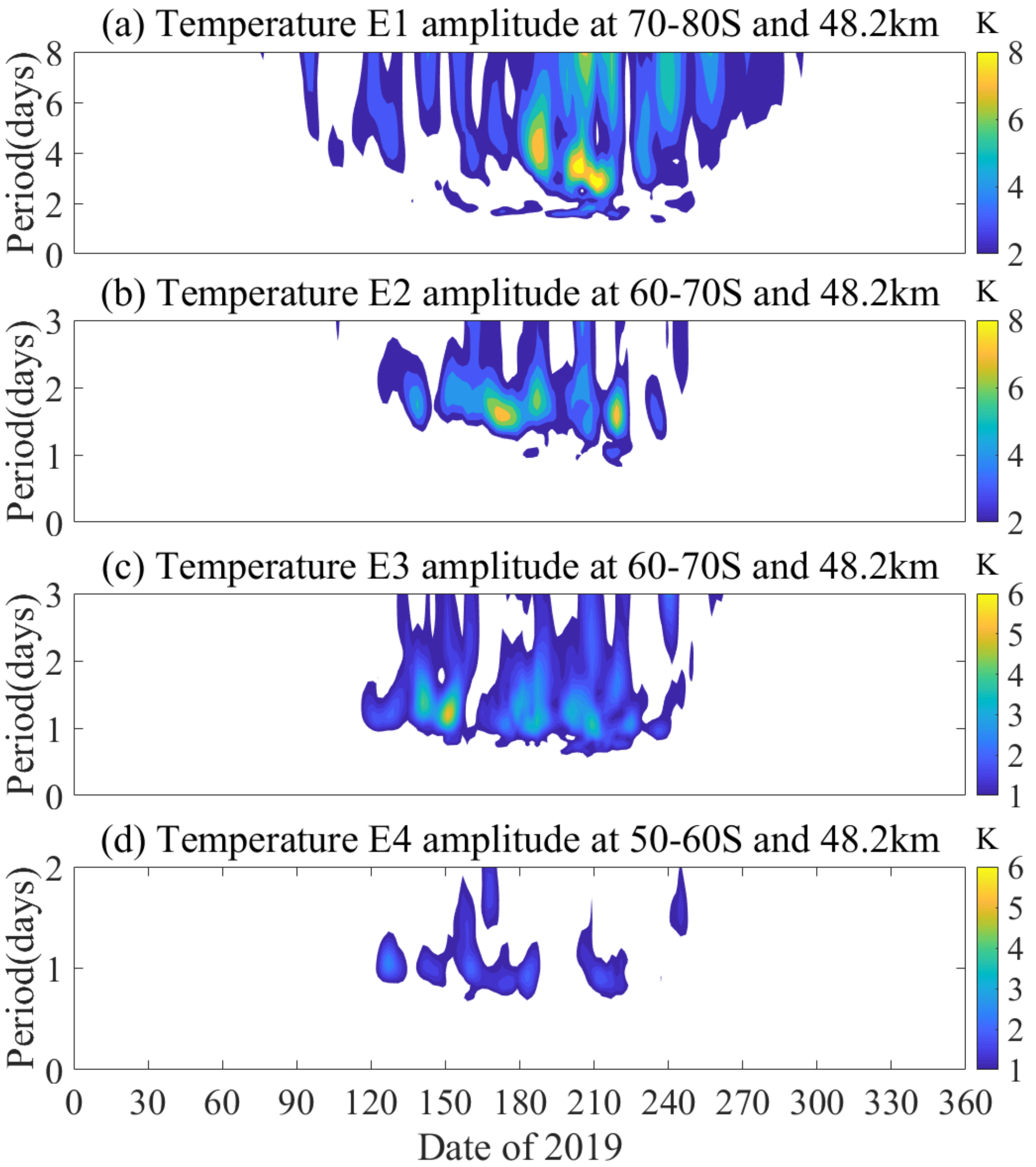

Figure 3. The temporal variations of (a) E1, (b) E2, (c) E3 and (d) E4 QTDWs during 2019 austral winter period.

823

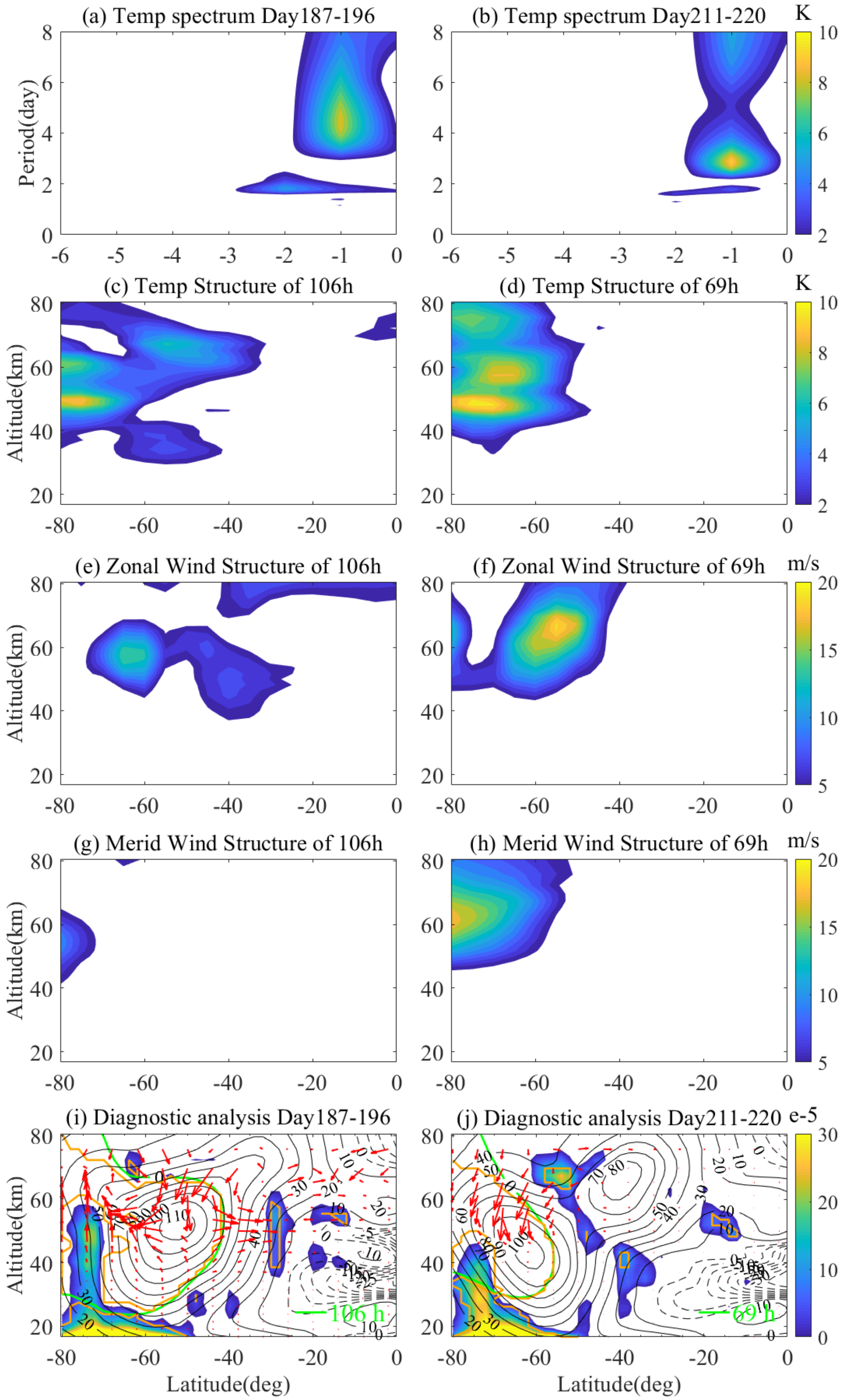

(a) Temp spectrum Day187-196
(b) Temp spectrum Day211-220
Period(day)
K
(c) Temp Structure of 106h
(d) Temp Structure of 69h
Altitude(km)
(e) Zonal Wind Structure of 106h
(f) Zonal Wind Structure of 69h
m/s
(g) Merid Wind Structure of 106h
(h) Merid Wind Structure of 69h
(i) Diagnostic analysis Day187-196
(j) Diagnostic analysis Day211-220
e-5
106 h
69 h
Latitude(deg)

Figure 4. The (a, b) spectra, (c, d) temperature spatial structures, (e, f) zonal wind spatial structures, (g, h) meridional wind spatial structures, and (i, j) diagnostic analysis of the E1 typical events during 2019 austral winter period. The MERRA-2 temperature data observations at 48.2 km and 70-80°S during days 187–196 (Figure 4a), 211–220 (Figure 4d) are utilized, respectively. In the diagnostic analysis of E1 events, the blue shaded region is instability, the red arrow is EP flux, and the green line is critical layer. The green line represents critical layers of E1 with the natural period. Regions enclosed by orange solid lines are characterized by the positive refractive index for the E1.

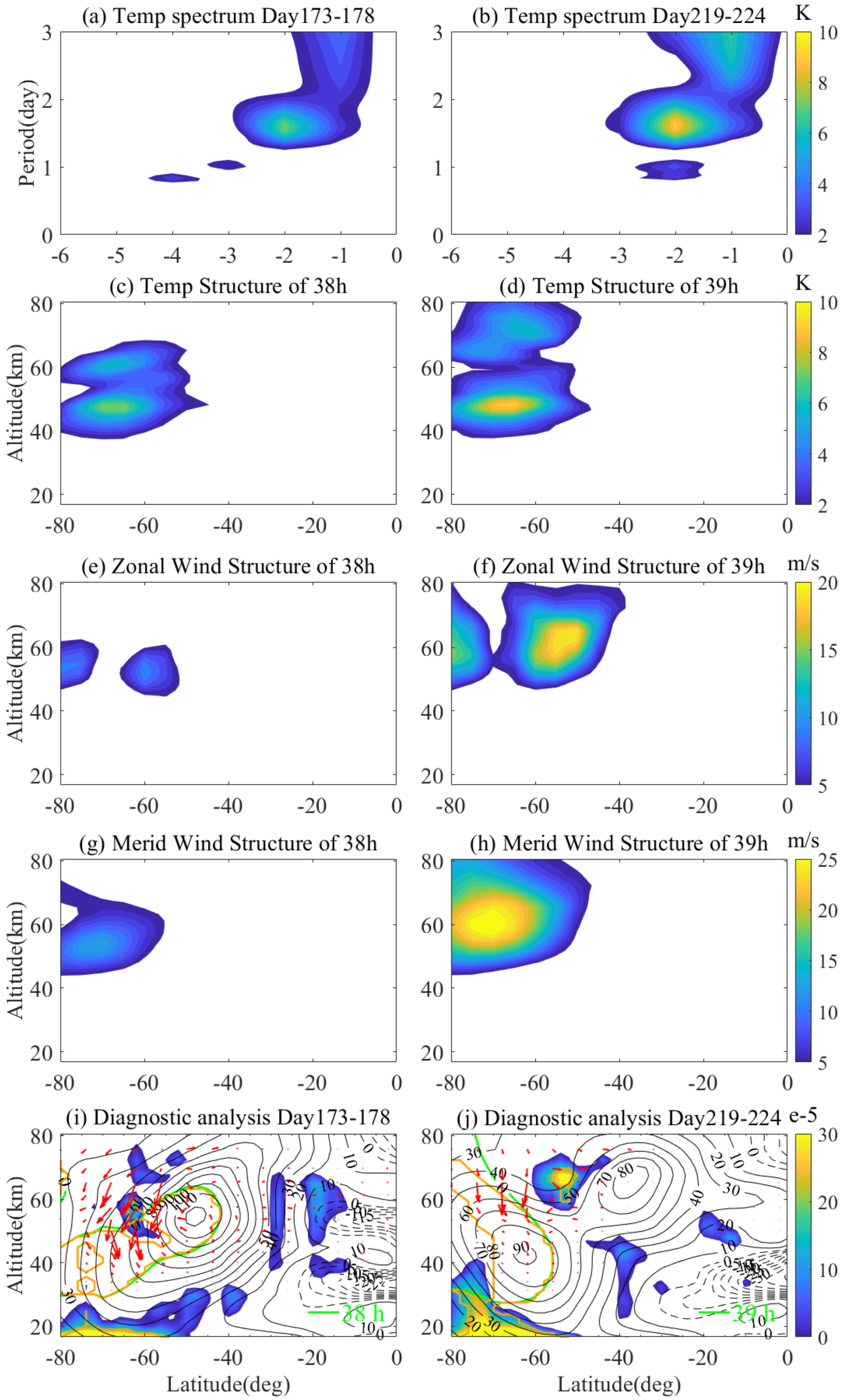

(a) Temp spectrum Day173-178
(b) Temp spectrum Day219-224
Period(day)
K
(c) Temp Structure of 38h
(d) Temp Structure of 39h
Altitude(km)
(e) Zonal Wind Structure of 38h
(f) Zonal Wind Structure of 39h
m/s
(g) Merid Wind Structure of 38h
(h) Merid Wind Structure of 39h
(i) Diagnostic analysis Day173-178
(j) Diagnostic analysis Day219-224
e-5
38 h
39 h
Latitude(deg)

833

Figure 5. Same as Figure 4 but for E2 during the 2019 austral winter period.

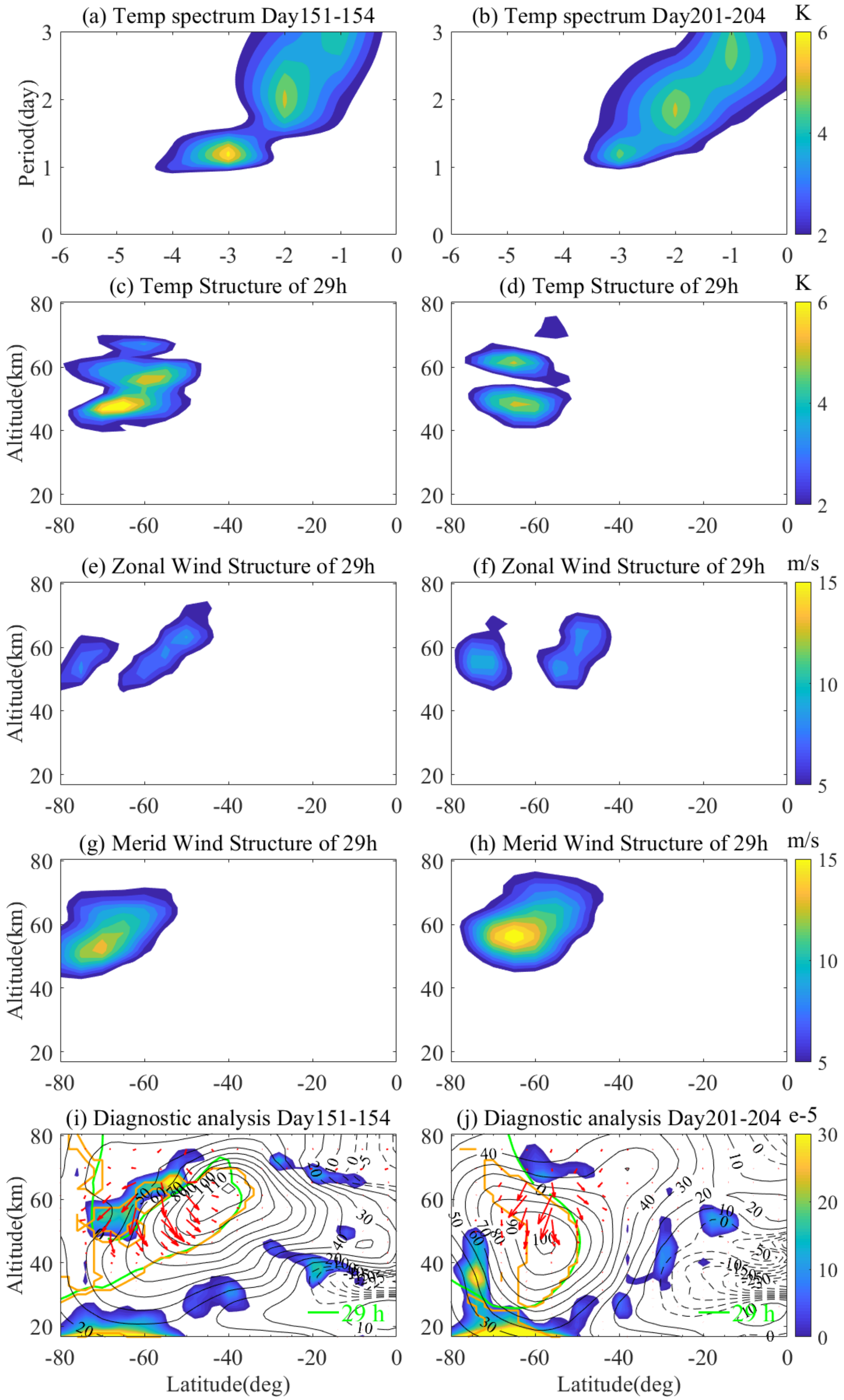
(a) Temp spectrum Day151-154
(b) Temp spectrum Day201-204
Period(day)
K
(c) Temp Structure of 29h
(d) Temp Structure of 29h
(e) Zonal Wind Structure of 29h
(f) Zonal Wind Structure of 29h
m/s
(g) Merid Wind Structure of 29h
(h) Merid Wind Structure of 29h
(i) Diagnostic analysis Day151-154
(j) Diagnostic analysis Day201-204
e-5
29 h
Altitude(km)
Latitude(deg)

835

Figure 6. Same as Figure 4 but for E3 during the 2019 austral winter period.

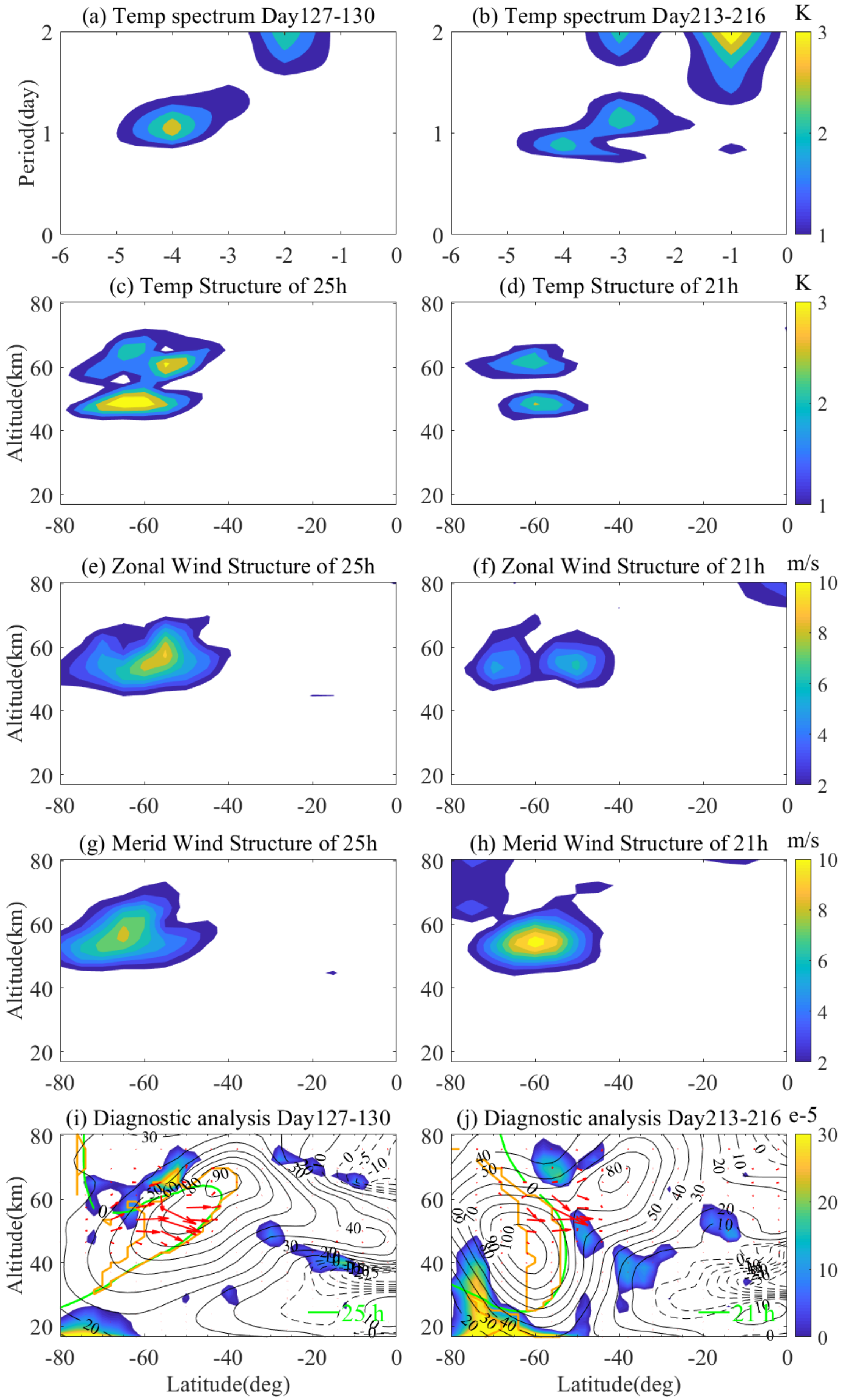

(a) Temp spectrum Day127-130
(b) Temp spectrum Day213-216
K
Period(day)
(c) Temp Structure of 25h
(d) Temp Structure of 21h
K
Altitude(km)
(e) Zonal Wind Structure of 25h
(f) Zonal Wind Structure of 21h
m/s
(g) Merid Wind Structure of 25h
(h) Merid Wind Structure of 21h
m/s
(i) Diagnostic analysis Day127-130
(j) Diagnostic analysis Day213-216
e-5
25h
21h
Latitude(deg)

837

Figure 7. Same as Figure 4 but for E4 during the 2019 austral winter period.

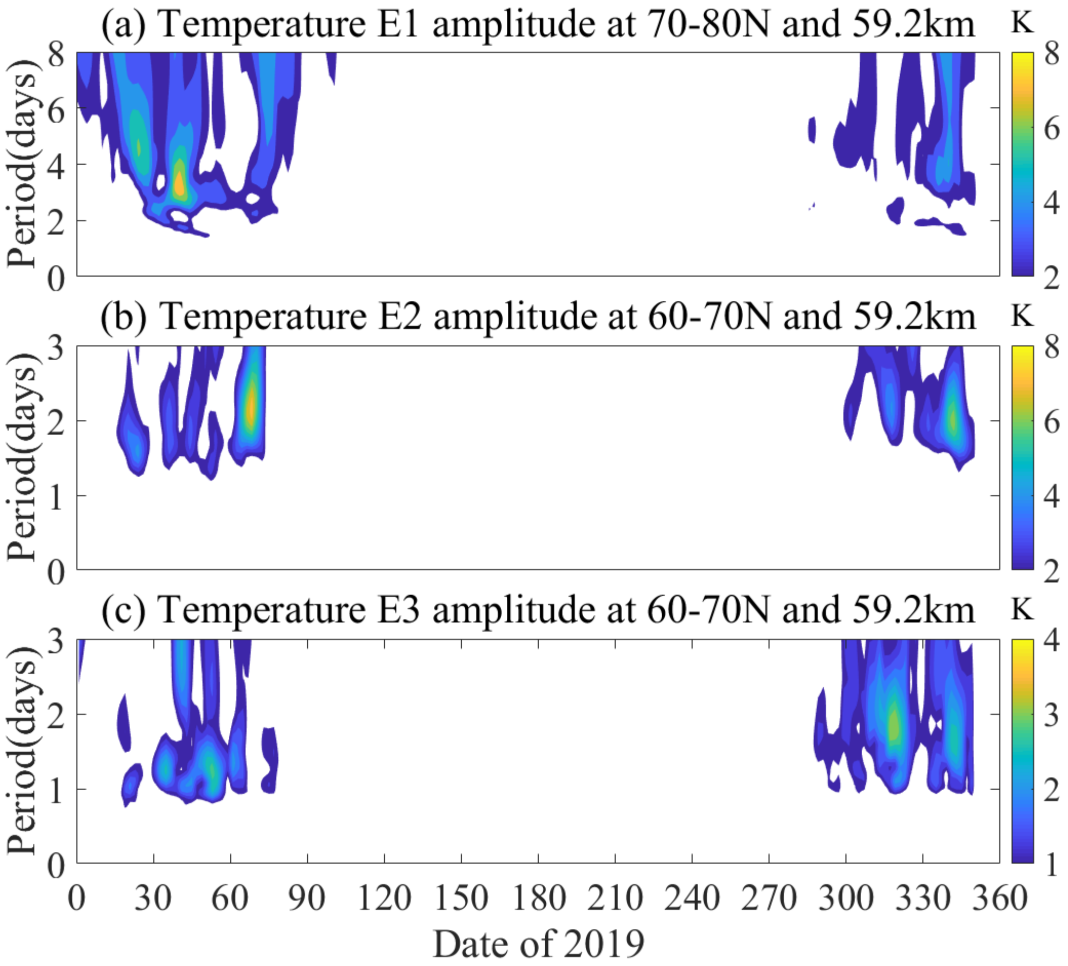

Figure 8. The temporal variations of (a) E1, (b) E2 and (c) E3 QTDWs during the 2019 boreal winter period.

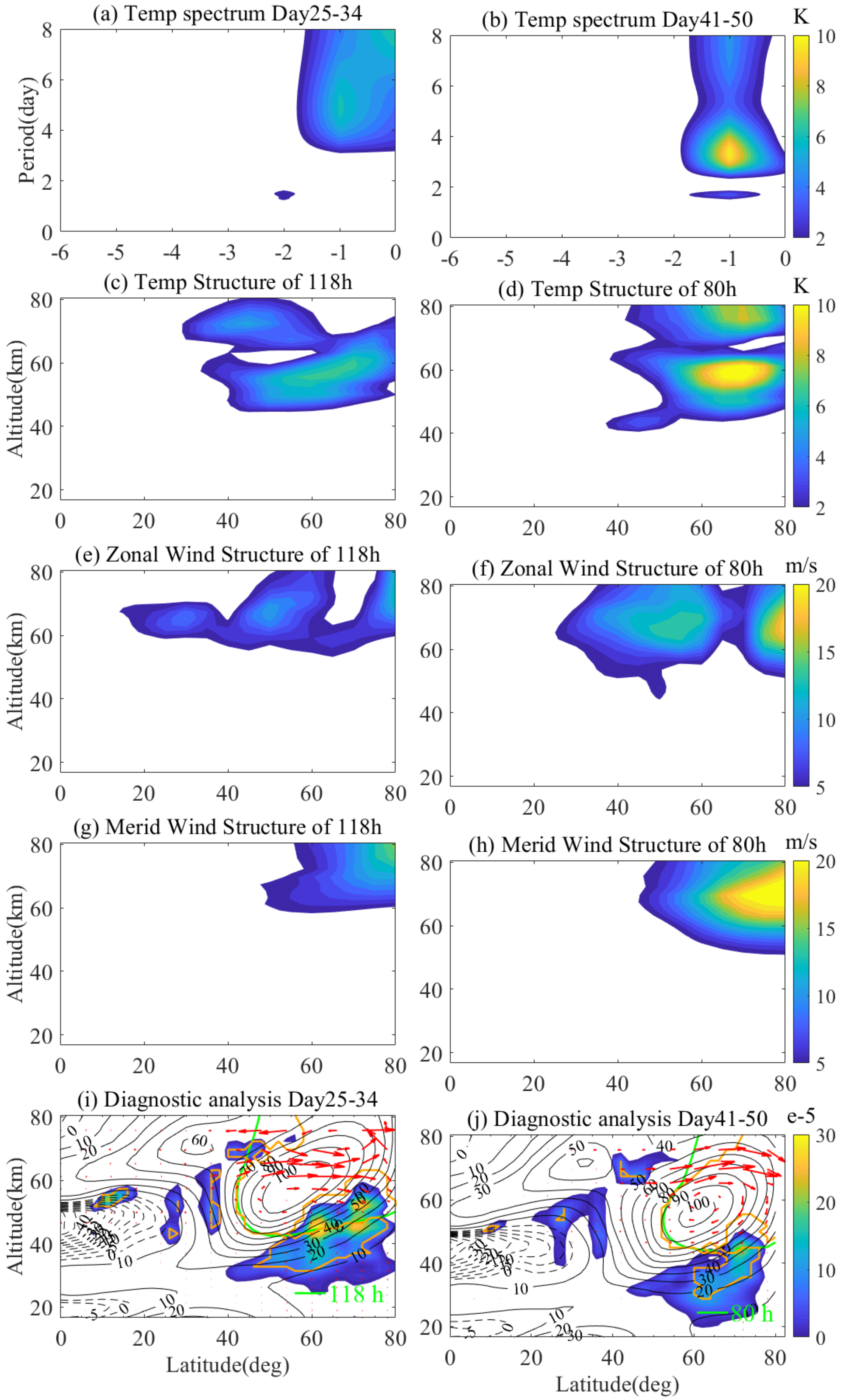
(a) Temp spectrum Day25-34
(b) Temp spectrum Day41-50
Period(day)
K
(c) Temp Structure of 118h
(d) Temp Structure of 80h
(e) Zonal Wind Structure of 118h
(f) Zonal Wind Structure of 80h
(g) Merid Wind Structure of 118h
(h) Merid Wind Structure of 80h
m/s
Altitude(km)
(i) Diagnostic analysis Day25-34
(j) Diagnostic analysis Day41-50
e-5
118 h
80 h
Latitude(deg)

Figure 9. The (a, b) spectra, (c, d) temperature spatial structures, (e, f) zonal wind spatial structures, (g, h) meridional wind spatial structures and (i, j) diagnostic analysis of the E1 typical events during 2019 boreal winter period. The E1 events at 48.2 km and 70-80°N were obtained from the MERRA-2 reanalysis.

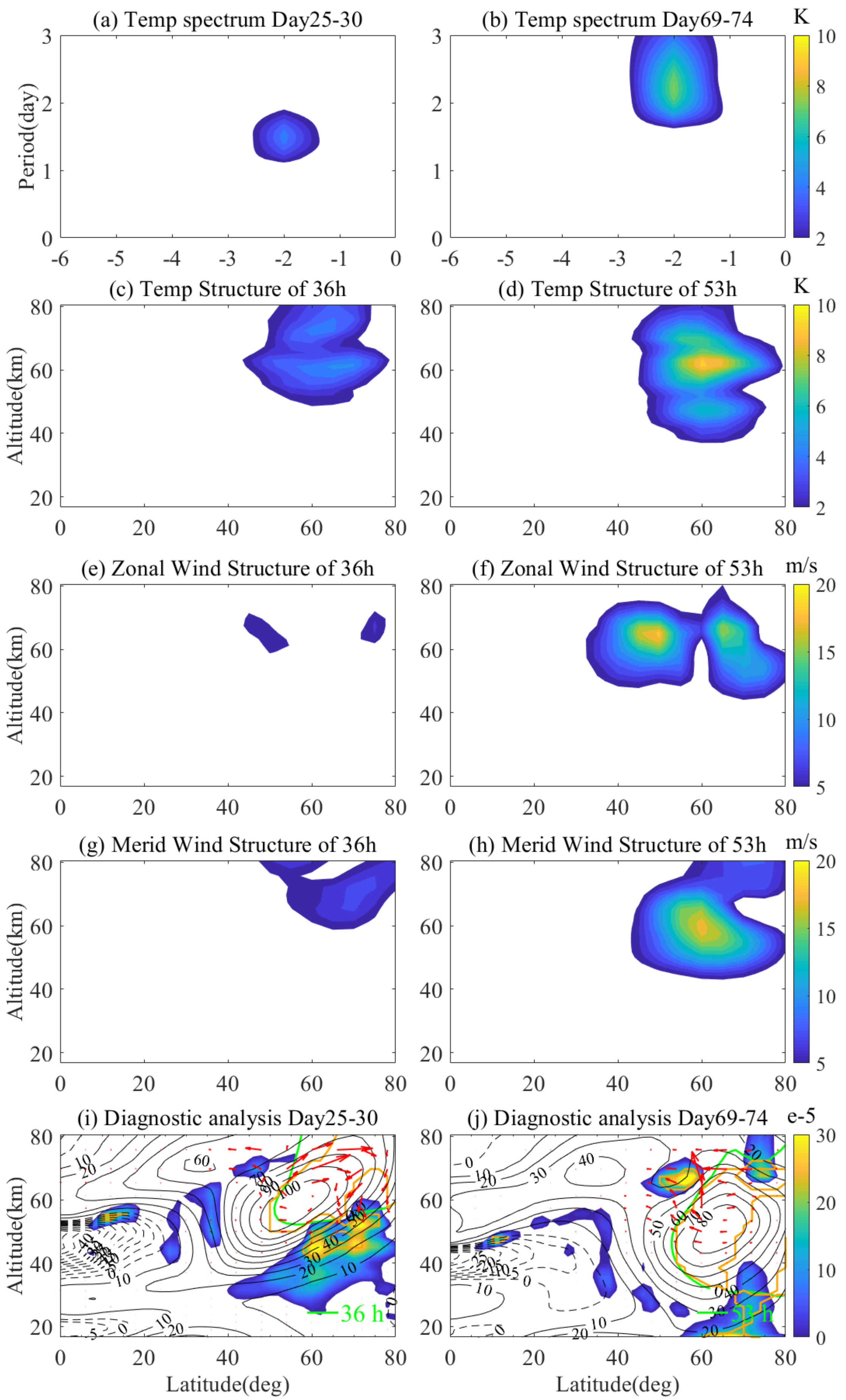

(a) Temp spectrum Day25-30
(b) Temp spectrum Day69-74
K
Period(day)
(c) Temp Structure of 36h
(d) Temp Structure of 53h
K
Altitude(km)
(e) Zonal Wind Structure of 36h
(f) Zonal Wind Structure of 53h
m/s
(g) Merid Wind Structure of 36h
(h) Merid Wind Structure of 53h
m/s
(i) Diagnostic analysis Day25-30
(j) Diagnostic analysis Day69-74
e-5
36 h
53 h
Latitude(deg)
Latitude(deg)

Figure 10. Same as Figure 9 but for E2 during the 2019 boreal winter period.

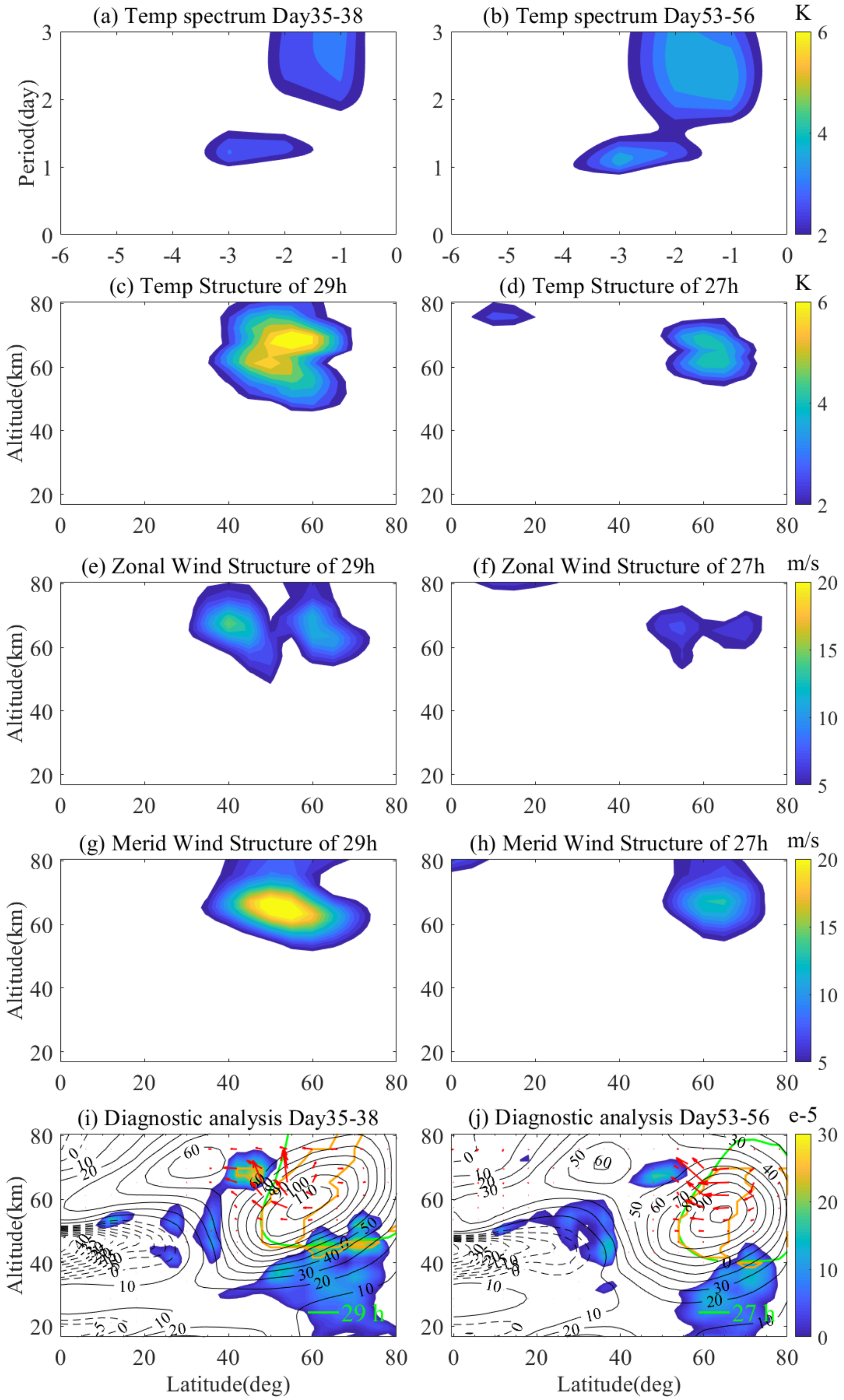
(a) Temp spectrum Day35-38
(b) Temp spectrum Day53-56
K
Period(day)
(c) Temp Structure of 29h
(d) Temp Structure of 27h
K
(e) Zonal Wind Structure of 29h
(f) Zonal Wind Structure of 27h
m/s
(g) Merid Wind Structure of 29h
(h) Merid Wind Structure of 27h
m/s
(i) Diagnostic analysis Day35-38
(j) Diagnostic analysis Day53-56
e-5
29 h
27 h
Altitude(km)
Latitude(deg)

Figure 11. Same as Figure 9 but for E3 during the 2019 boreal winter period.